California Board of Forestry and Fire Protection

Cellulose Nanocrystals as a Value-Based Additive for Low Carbon Footprint Concrete with Limestone

<mark>Draft Final Report</mark>

Authors:

Krishna Siva Teja Chopperla, Postdoctoral Scholar, Oregon State University, Corvallis, OR
Sivakumar Ramanathan, Postdoctoral Scholar, Oregon State University, Corvallis, OR
Keshav Bharadwaj Ravi, Postdoctoral Scholar, Oregon State University, Corvallis, OR
Angel Mateos, Research Engineer, University of California Pavement Research Center, Berkeley, CA
John Harvey, Professor, University of California, Davis, CA
Somayeh Nassiri, Associate Professor, University of California, Davis, CA
Jeffrey Alan Buscheck, Lab Manager, University of California Pavement Research Center, Berkeley, CA
Sabbie Miller, Assistant Professor, University of California, Davis, CA
O. Burkan Isgor, PI, Oregon State University, Corvallis, OR
W. Jason Weiss, PI, Oregon State University, Corvallis, OR

Draft November 1st, 2022

Table of Contents

List of Tables

List of Figures

vii

1. Executive Summary

This project evaluated cellulose nanocrystals (CNCs) as an additive that can aid in concrete mixture modifications in an effort to reduce concrete's carbon footprint. This project explored the use of CNCs in cementitious materials containing various amounts of limestone (LS). The heat of hydration, porosity, flexural strength, and drying shrinkage were measured. The binders were also evaluated for their resistance to ion transport by measuring their electrical resistivity. The scope was extended to also study binders that include supplementary cementitious materials (SCMs) and CNCs. The SCM mixtures studied were (i) 50% slag, (ii) 25% fly ash and 25% slag, and (iii) 20% fly ash and 5% silica fume. In addition, full-scale field trials were done at the University of California at Davis to demonstrate CNCs use with Ordinary Portland Cement (OPC) and Portland-Limestone Cement (PLC) in the field. An embodied carbon calculator was used to evaluate the benefits of utilizing CNCs.

In general, the following observations were made from the evaluation of the performance of the mixtures with CNCs and limestone:

- Lower dosages of CNC (up to 0.5% CNCs) to OPC-LS mixtures resulted in an increased degree of hydration of binder at all ages. At early ages, the increase in the degree of hydration of cement clinker was attributed to the combined effect of LS and CNCs. At a later age, the increased degree of hydration of cement clinker was primarily attributed to the CNCs.
- CNCs addition did not have a significant impact on the overall porosity and flexural strength of the paste samples.
- CNCs addition did not have a statistically significant impact on the drying shrinkage of mortar samples with limestone.
- The addition of CNCs to OPC-LS mixtures resulted in up to 38% increase in the 28-day bulk resistivity mainly due to increase clinker hydration and reduction in pore connectivity. It was observed that a mixture for which 22% of the OPC was replaced with LS and containing 0.2% CNC had an equivalent performance in terms of transport properties compared to the 100% OPC system.
- The addition of 20% LS and 0.2% CNCs together resulted in mixtures with ~19% reduced GHG emissions with comparable mechanical and transport properties to the conventional 100% OPC mixture.

From the evaluation of the performance of the OPC-SCM and PLC-SCM mixtures with CNCs, the following observations were made:

- CNCs addition did not have a significant impact on the 7-day heat release values for most SCM mixtures. Future research includes understanding the mechanism of CNCs effect on the hydration of SCM mixtures.

37   •   CNCs addition did not have a significant impact on the overall porosity, and the B3B
38   flexural strengths of majority of the SCM mixtures with CNCs were within $\pm$15% of the
39   flexural strength of mixtures without CNCs.
40   •   CNCs addition to the SCM mixtures resulted in an increase in the overall pore connectivity
41   and a reduction in the bulk resistivity when measured at 28 and 56 days, however the bulk
42   resistivity of the SCM mixtures are significantly higher than the reference OPC mixture.
43   The observed trend may be due to the agglomeration of CNCs, changes in the pore structure
44   due to delayed early age hydration when CNCs are used, and adsorption of CNCs on SCMs
45   resulting in slightly altering the reaction kinetics of SCMs. Further research is needed to
46   understand the mechanisms behind the effect of CNCs on the pore structure characteristics
47   and transport properties of the SCM mixtures.

48   The use of CNC with PLC was successfully used in field trials in California. The PLC mixtures
49   with and without CNCs had similar fresh concrete properties including slump, air content, set time
50   and unit weight. Hardened properties such as strength, modulus of elasticity, resistivity, and
51   shrinkage were also similar for both mixtures.

2. CHAPTER 1: Background

Cellulose nanomaterials (CNMs) are non-toxic, non-petroleum-based materials that may be used as concrete additives [1-3]. CNMs are derived from bio-degradable carbon-neutral sources [1-5] and include cellulose nanofibers (CNFs) and cellulose nanocrystals (CNCs). CNFs are fibrillated and are typically ~500-2000 nm long and 4-20 nm wide. CNCs are rod shaped crystals that are typically made using acid hydrolysis (though different processing approaches may be used) and are 50-500 nm in length and 3-20 nm in width [1, 6]. CNCs have been used in cementitious mixtures and have shown potential to improve mechanical properties of concrete [2, 3, 7-13] Similarly, it was shown that the addition of CNFs could improve concrete performance by promoting crack bridging and improving the post peak behavior of concrete [3, 9, 14-16].

Past work showed that the addition of CNCs improve the hydration of cementitious mixtures containing ordinary portland cement (OPC) [17]. This was attributed to two mechanisms – steric stabilization and short circuit diffusion (SCD) [17, 18]. Steric stabilization[1] contribute to property improvement at lower CNC dosages (up to 0.3% by binder volume), presumably due to a dispersing effect on the particles [17, 19]. It was also hypothesized that the adsorption of CNCs on cement grains resulted in the formation of preferential pathways for water to ingress through the C-S-H layer around the cement grains (i.e., short circuit diffusion), which increased the hydration of cement. This observation of improved hydration was confirmed by other researchers for mixtures containing up to 0.5% CNCs [3, 17, 18, 20-22].

Moon et al. [2] showed that modifying the CNC production process and cellulose source produces CNCs with different surface charges and attached functional groups. To study the effect of CNC type, Fu et al. [23] evaluated Type I/II and Type V OPC mixtures with CNCs derived from different sources and produced using different processing methods. It was reported that in addition to the CNC type, the chemistry of the cement also plays a role in material performance. Fu et al. [23] observed that the aluminate phases might influence early age hydration due to their surface charge, which results in preferential adsorption of CNCs on C_3A rather than the C_3S clinker phases. The preferential adsorption of CNCs on C_3A implied that the degree of reaction of the clinker of Type V OPC was higher when compared to Type I/II OPC. The literature also reported that while early-age cement hydration may be retarded due to CNC addition (probably due to the CNC blocking the surface of the cement), this retardation generally occurs before 20 hours after mixing. After approximately 30-40 hours, the rate of hydration increases with CNC. This accelerated hydration also results in an increase in the ultimate degree of hydration (up to 8%) compared to a mixture with no added CNCs [17, 23]. (This 8% increase refers to the mixture with 1% CNCs which had a degree of hydration of ~63 % at 7 days compared to a mixture without CNCs which had a degree of hydration of ~55% at the same age).

---

[1] Dispersion of cement grains due to adsorption on CNCs on their surfaces

87 The addition of CNCs was shown to improve the mechanical properties of the cementitious
88 mixtures. Some of the previous studies on the addition of CNCs showed a 20-30% increase in
89 compressive strengths and 11-20% increase in flexural strengths [19-21]. On the other hand, there
90 are studies that also show that CNC addition did not have any statistically significant effect on
91 strength [16]. The increase in strength when it occurred was attributed to both the increase in the
92 degree of cement hydration and an increase in pore filling and refinement [14, 20-22, 24, 25]. In
93 addition, improvement in the elastic modulus of C-S-H due to CNC addition was reported [17, 19,
94 21, 23, 26].

95 CNCs were also reported to refine pores in cementitious mixtures by reducing the pore size
96 distribution, improving the transport properties of the hardened mixtures [22, 27, 28]. Various
97 researchers have reported a decrease in the porosity of cementitious mixtures containing CNCs.
98 The tortuosity of the cementitious matrix was also reported to increase with the addition of CNCs
99 [26]. It was shown in literature that the addition of CNCs resulted in the improvement of electrical
100 resistivity of the cementitious mixtures [3, 24, 26, 29]. The increase in bulk resistivity indicates
101 that the transport properties of mixtures could be improved by CNC addition [24, 30].

102 In addition to the research work done in the laboratory, CNCs have been used in the field for
103 construction of a parking lot pavement in Greenville, South Carolina in 2018. Also, CNCs have
104 recently been produced and placed commercially in a bridge in Yreka, California in 2020 [31, 32]
105 to demonstrate the feasibility of using CNCs in large-scale concrete structures in the field. It was
106 reported that the concrete with CNCs had similar or slightly better 28-day compressive strength
107 compared to concrete with no added CNCs.

108 While CNCs may improve the mechanical and transport properties of cementitious materials, steps
109 have not been taken to demonstrate potential reductions in clinker and greenhouse gas (GHG) or
110 CO_2 emissions. This project discusses the potential of using CNCs to reduce the clinker content in
111 the concrete and thus reducing GHG emissions [33-35]. In this work, CNCs were used in
112 conjunction with the use of limestone to replace OPC.

113 Portland limestone cements (PLCs) are a viable alternative to OPCs [36-41]. Mixtures made using
114 PLC (ASTM C595 cement) have similar performance to mixtures made using OPC [41, 42].
115 Similar studies were performed using added limestone [36, 38, 43-45]. It was shown that the size
116 of the limestone can play a critical role due nucleation, particle packing, and dilution [38, 42, 44-
117 46]. PLCs could reduce up to 15% of the emissions associated with the production phase of cement
118 [47]. Therefore, this research was conducted to determine whether LS and CNCs can be used
119 synergistically to lower GHG emissions while not compromising on performance.

120 2.1. Computational Modeling Framework

121 A thermodynamic and pore partitioning model for concrete (PPMC) modeling framework is used
122 in this study to predict the performance of concrete [48-51]. The details of this modeling

123 framework will not be repeated here for brevity and interested readers are pointed to reading the
124 cited documents. Briefly, the chemical composition of the OPC and SCM, and the maximum
125 degree of reactivity (DOR*; measured using the Pozzolanic Reactivity Test [52-54]) of the SCM
126 are used as inputs to a kinetic [55] model and thermodynamic modeling [56] framework. The
127 GEMS3K software [57, 58] in conjunction with the CemData v18.01 thermodynamic database
128 [59] is used to perform thermodynamic calculations to predict the reaction products that form when
129 OPC and OPC+SCM binders react [56, 59-66]. The volumes of gel pores (<5nm in size) and
130 capillary pores (>5nm) in the hydrated cementitious paste is calculated from the reaction products
131 using a Pore Partitioning Model [67, 68]. The pore volumes are scaled to concrete using the PPMC,
132 which is then used to predict the performance of concrete [49, 50]. This modeling framework has
133 been shown to accurately predict the porosity, formation factor, and compressive strength of
134 concrete made with OPCs, PLCs, and SCMs [48-50, 69-71].

2.2. Organization and Contents of the Report

136 This report is composed of five chapters. The first chapter (section 2) consists of background on
137 CNCs research, introduction of the work performed, and the list of main research objectives. It
138 also briefs the computational modeling framework used in the study to predict the performance of
139 the mixtures such as porosity. The background section of this chapter gives a brief description of
140 CNCs and literature review of CNCs use in cementitious materials. The authors of this chapter are
141 S. Ramanathan, K.S.T. Chopperla, K. Bharadwaj, O.B. Isgor, and W.J. Weiss.

142 The second chapter (section 3) presents the research findings observed from evaluating the OPC-
143 LS-CNC mixtures performance. Chapter 2 briefs material characterization and the experimental
144 procedures used. Chapter 2 also includes the discussion on the results of the mixtures tested for
145 heat of hydration, non-evaporable water content, flexural strength, porosity, pore connectivity,
146 electrical resistivity, and drying shrinkage. The majority of the results and findings in the chapter
147 are published in ACI Materials Journal [72]. The authors of this chapter are S. Ramanathan, K.S.T.
148 Chopperla, O.B. Isgor, and W.J. Weiss.

149 The third chapter (section 4) presents the research findings from evaluating the performance of the
150 mixtures with SCMs and CNCs. The extended goal of this project is to evaluate the performance
151 of CNCs in mixtures with SCMs as using SCMs can enable further reducing the GHG emissions.
152 Chapter 3 includes the discussion of the results of the mixtures tested for heat of hydration, flexural
153 strength, porosity, pore connectivity, and electrical resistivity. Ongoing work is evaluating the
154 interactions between CNCs and SCMs, and the role of CNCs in improving the performance of the
155 mixtures with SCMs. The authors of this chapter are K.S.T. Chopperla, S. Ramanathan, O.B. Isgor,
156 and W.J. Weiss.

157 The fourth chapter (section 5) includes the details of the full-scale field trials done in California
158 using mixtures with OPC, PLC, and CNCs. The chapter includes details of the test sections

159   preparation and construction, fresh and hardened concrete properties, and hydrothermal
160   deformation of the slabs. Chapter 4 is authored by A. Mateos, J. Harvey, S. Nassiri, J.A. Buscheck,
161   and S. Miller. The final chapter summarizes the studies and their findings and includes the overall
162   conclusions.

163   2.3. Research Objectives

164   The main objectives of the project are:

165   • To evaluate whether an OPC-LS-CNC can be designed to have a similar performance to
166   the conventional OPC mixture to lower GHG emissions
167   • To calculate the GHG emissions of the mixtures used and determine the optimum CNC
168   dosage needed to lower carbon footprint
169   • To demonstrate the use of LS and CNCs in full scale field trails in slabs and to monitor
170   their performance

171

3. CHAPTER 2: Reducing GHG Emissions using CNCs, OPC, and Limestone

This chapter focuses on the objective of examining whether OPC in a concrete mixture can be replaced with LS and CNC to create a system with similar performance and a lower embodied carbon content (greenhouse gas emissions).

3.1. Constituent Materials and Characterization Procedures

Commercially available Type II OPC and LS (96% purity) were used in this study. Four LS replacement levels were used (0%, 10%, 20%, and 30% by mass of OPC). This is in addition to the LS already present in OPC. CNCs that were obtained in the form of suspension with 11% w/w CNC solids were used. The CNCs were manufactured by Forest Products Laboratory using sulfuric acid hydrolysis process. Four CNC concentrations used were 0%, 0.2%, 0.5%, and 1.0% solid volume by volume of binder (i.e., OPC+LS). CNC concentration was measured in terms of the volume of binder to be consistent with the previous studies [3, 17].

The CNC suspension and ASTM type II deionized (DI) water were chilled to 5 °C before the dispersion process. Chilled water (5°C) was used for dispersion to compensate the heat generated from dispersion [73], The CNC suspension was batched in the bowl of a high shear blender (Waring Commercial CB15VP blender) along with chilled DI water based on the procedure adapted from specification 10A of the American Petroleum Institute (API). Shear mixing was carried out for a total of 60 seconds at 4000 rpm in two sessions. After the first 30 seconds, the sides and bottom of the mixing bowl were scraped using a silicone spatula to release any adhered / agglomerated CNCs for about 15 seconds. The temperature of the solution was approximately 23 °C after the dispersion at the time of mixing. The water was adjusted to maintain a constant water-to-binder ratio (w/b) was 0.40. Shear blending using a high shear mixer was chosen for CNC dispersion as mechanical methods have been effective in dispersing agglomerates of nanomaterials [73, 74].

The chemical composition and physical properties of the OPC and LS are shown in Table 1. The chemical composition was determined using X-ray fluorescence (XRF) from which the oxide composition was determined using the fused bead process according to ASTM C114-18 [41, 75, 76]. The loss on ignition (LOI) of the cementitious powders was determined by igniting approximately 5 g of material in a ceramic crucible up to 1000 °C for three hours and measuring the mass after ignition. The fused beads were prepared by combining 1 g of the ignited powder with 5 g flux (for OPC) and 0.55 g powder with 5.5 g flux (for LS). The flux composed of 49.75% lithium metaborate, 49.75% lithium tetraborate, and 0.50% lithium iodide was mixed gently in a platinum crucible and fused in a furnace (Claisse LeNeo fluxer) for approximately 25 minutes at 1450 °C.

206   Table 1. Chemical composition (in wt%) and physical properties of the OPC and LS

Material	Na$_2$O	MgO	Al$_2$O$_3$	SiO$_2$	SO$_3$	K$_2$O	CaO	Fe$_2$O$_3$	LOI	d$_{50}$ (µm)	G
OPC	0.21	1.43	3.95	19.95	2.55	0.48	63.32	2.28	2.71	13.9	3.15
Limestone	0.14	5.74	0.79	2.93	0.13	0.12	86.50	0.41	42.27	15.2	2.71

207

208   Particle size distribution was obtained using laser diffraction (Horiba LA-920) [41]. The powder
209   was dispersed in isopropyl alcohol in front of a laser lamp assembly. Approximately 3-5 g of
210   material was added slowly in 0.5 g increments, and the solution was sonicated and circulated to
211   prevent the agglomeration of particles. Median particle size (d50) and specific gravity (G) values
212   of the SCMs are presented in Table 1 and are measured as an average of five runs. The specific
213   gravity of OPC and LS powder are also presented in Table 1. No other chemical admixture was
214   added to the mixture to avoid conflicting influences of CNCs and chemical admixtures.

215   A locally sources fine aggregate was used for making drying shrinkage samples. The oven dry
216   specific gravity of the fine aggregate was 2.39 and absorption capacity was 2.59%.

217   3.2. Mixing Procedures

218   3.2.1. Paste mixing

219   The cementitious materials were dry mixed for 90 s using a vacuum mixer at 400 rpm and 70%
220   vacuum. The CNC dispersed mix water was placed in a mixing bowl, and the dry mixed
221   cementitious materials were added, and mixed using a vacuum mixer (Renfert Inc. model
222   18281000) for 90 s at 400 rpm and a 70% vacuum level. The mixing cup was scraped using a
223   silicone spatula for 15 s, and vacuum mixing was carried out for an additional 90 s. A similar
224   mixing procedure was followed for cementitious paste mixing in literature [42].

225   3.2.2. Mortar mixing

226   Mortar samples having 0.40 water to binder ratio were prepared for drying shrinkage testing. The
227   prepared mortar samples consisted of 50% by volume of fine aggregate. Mortar was mixed in a
228   Hobart mixer as per ASTM C305-20. All the mixing water was placed in the bowl. The
229   cementitious material was added to water and then it was mixed at the slow speed (140 r/min) for
230   30 s. Over the next 30 s, the fine aggregate was added. The speed was changed to medium speed
231   (285 r/min) and mixed the mortar for 30 s. The mixer was stopped for 90 s, in this duration the
232   bowl and the paddle were scrapped down. Then the mixing was finished by mixing it for 60 s at
233   medium speed.

8

3.3. Tests on Cementitious Pastes

3.3.1. Isothermal calorimetry

Heat release was measured using isothermal calorimetry (TAM Air, TA Instruments) according to ASTM C1679-17. Cementitious pastes were mixed using a vacuum mixer as described in the mixing procedure. After mixing, 6-7 g of the cementitious paste was transferred to a glass ampoule and sealed. The glass ampoules were then lowered into the isothermal calorimeter which was pre-conditioned at 23 ± 0.05 °C. Data was not collected for the first 45 minutes. Heat flow and heat release were measured, and the data was collected for 7 days. Two replicates of all mixtures were tested for each mixture, and the average of the two replicates was reported [41, 77]. Replicate testing for all mixtures showed variability of less than 2% between the replicates.

3.3.2. Ball-on-three-ball (B3B) flexural strength

The cementitious paste mixture prepared was placed in 50 mm (diameter) × 100 mm (length) cylindrical molds in two layers and each layer was vibrated to ensure adequate compaction of the material. The molds were sealed, and the samples were placed on a roller for 24 hours to minimize the potential effect of bleeding. After 24 hours, the samples were removed from the roller and cured under sealed conditions at 23 ± 1 °C until sample preparation began for flexural strength testing.

Flexural strength testing was performed using the B3B test at 7 and 28 days according to ASTM C1904-20 [78]. A detailed procedure for B3B flexural strength testing can be found in the literature [78, 79]. At the age of testing, the cylinder was demolded, and the top and bottom of the cylinder were discarded to avoid end effects (approximately 20 mm from each end). The central portion of the cylinder was cut into disks that were 2.65 ± 0.15 mm thick. These samples were tested on a B3B testing frame [79]. The flexural strength was calculated based on the equation described in literature [79, 80]. The testing was carried out within 15 minutes of cutting the sample. At least six replicates were tested for all mixtures at each age of testing, and the coefficient of variation (COV) was less than 10% except in one mixture, whose COV was 12%.

3.3.3. Thermogravimetric analysis (TGA)

Immediately after flexural strength testing at 28 days, the central portion of each disk was obtained and ground into a fine powder using a mortar and pestle. The powdered sample was then sieved using a 75 μm sieve (#200 sieve). The samples were then immediately double sealed in plastic bags to minimize carbonation.

Calcium hydroxide and non-evaporable water content for the cementitious powders were obtained using thermogravimetric analysis (TGA). The testing consisted of placing approximately 30-50 mg of samples on a platinum pan, and the sample was then loaded into the TGA (TGA 5500, TA

268 Instruments). The TGA chamber was heated at the rate of 10°C/minute to 1000°C in a nitrogen
269 atmosphere. Calcium hydroxide content (normalized to per g of binder) and non-evaporable water
270 content (per g of binder) were calculated using equations 1 and 2a, respectively. The onset and end
271 temperatures were obtained using the tangential method described in Kim and Olek [81]. Replicate
272 testing for the mixtures showed that the variability was less than 2%.

273 $$m_{CH} = 4.11 \cdot \frac{m_{CH,start} - m_{CH,end}}{m_{init,anhyd}} + 0.74 \cdot \left(2.27 \cdot \frac{m_{Cc,start} - m_{Cc,end}}{m_{init}} - m_{Cc,init} \right) \qquad \text{(Eq. 1)}$$

274 where, m_{CH} is the mass of calcium hydroxide, $m_{CH,start}$ is the onset temperature of calcium
275 hydroxide mass decomposition, $m_{CH,end}$ is the end point of calcium hydroxide decomposition,
276 $m_{Cc,start}$ and $m_{Cc,end}$ are the onset and end points of calcium carbonate decomposition, $m_{Cc,init}$ is the
277 calcium carbonate present in the binder, $m_{init,anhyd}$ is the anhydrous sample mass in the TGA.

278 $$w_{ne} = \frac{A \cdot m_{105} - B \cdot m_{1000}}{m_{1000}} \qquad \text{(Eq. 2a)}$$

279 where, w_{ne} is the non-evaporable water content, m_{105} and m_{1000} are the sample masses at 105
280 °C and 1000 °C respectively obtained from the TGA, A and B are constants calculated from
281 equations 2b and 2c, respectively to account for the loss on ignition.

282 $$A = \left[(1 - r_{LS})(1 - LOI_{cem}) + \left(r_{SCM} \cdot (1 - LOI_{LS}) \right) + \left(D_{CNC} \cdot \rho_{CNC} \cdot k_{CNC} \cdot \left(\frac{1 - r_{LS}}{\rho_{cem}} - \frac{r_{LS}}{\rho_{LS}} \right) \right) \right]$$

283 $$\text{(Eq. 2b)}$$

284 $$B = \left[1 + D_{CNC} \cdot \rho_{CNC} \cdot k_{CNC} \cdot \left(\frac{1 - r_{LS}}{\rho_{cem}} + \frac{r_{LS}}{\rho_{LS}} \right) \right] \qquad \text{(Eq. 2c)}$$

285 LOI_{OPC} and LOI_{LS} are the loss on ignition for OPC and LS used in the study, r_{LS} is the LS
286 replacement level, D_{CNC} is the CNC suspension dosage by volume percentage of binder, ρ_{CNC}, ρ_{cem},
287 and ρ_{LS} are the specific gravities of CNCs, OPC, and LS respectively. k_{CNC} is the weight percentage
288 of the CNC solids (11% solids by weight).

289 3.3.4. Porosity and bulk resistivity of cementitious pastes

290 Porosity and bulk resistivity were measured using 50 mm × 100 mm cylinders at 7 and 28 days.
291 The cylinders were cured in sealed condition after casting until testing. The bulk resistivity was
292 measured on vacuum saturated samples in accordance with AASHTO TP 119-20 [82].

293 The demolded samples were placed under vacuum at 7 ± 2 Torr for 3 hours. After this, a simulated
294 pore solution containing 7.6 g/L of sodium hydroxide, 10.64 g/L of potassium hydroxide, and 2
295 g/L of calcium hydroxide was allowed to saturate the samples under vacuum for one hour.
296 Simulated pore solution was utilized to vacuum saturate the samples to maintain uniform pore
297 solution resistivity across all samples for formation factor calculations. After vacuum saturation,
298 the samples were stored in the simulated pore solution for 24 ± 4 hours at 23°C. The samples were
299 then measured for electrical impedance to calculate resistivity value. The bulk resistivity was
300 calculated according to equations 3a and 3b. Appropriate corrections for temperature and sample
301 geometry were applied as detailed in Ref. [83]. Two replicates of each mixture were tested and the
302 average data was reported.

303
$$\rho_{sat} = R_{sat} \frac{A}{L} \qquad \text{(Eq. 3a)}$$

304
$$\rho_{sat-corrected} = \rho_{sat} \cdot e^{\left[\frac{E_{A-cond}}{R} \left(\frac{1}{T} - \frac{1}{T_0} \right) \right]} \qquad \text{(Eq. 3b)}$$

305 where, $\rho_{sat-corrected}$ is the temperature corrected saturated bulk resistivity, ρ_{sat} is the saturated bulk
306 resistivity (in Ω-m), R_{sat} is the vacuum saturated resistance (in Ω), A is the cross-sectional area of
307 the sample (in m^2), L is the length of the sample, E_{A-cond} is the activation energy of conduction
308 (considered as 15 kJ/mol based on [84]), R is the universal gas constant (8.314 kJ/mol-K), T is
309 the sample temperature at the time of measurement (in K), and T_0 is the reference temperature
310 (298.15 K).

311 For the same cylinders, the saturated weight and the apparent weight were obtained immediately
312 after the bulk resistivity measurement. The cylinders were then dried at 105 °C until a constant
313 mass was achieved (i.e., the difference between two successive mass measurements is less than
314 0.1%) [85]. The porosity of the cylinders (in accordance with AASHTO TP 135) was calculated
315 according to equation 4 and reported as an average of two samples for all the mixtures.

316
$$\Phi_{paste} = \frac{w_{sat} - w_{dry}}{w_{sat} - w_{app}} \qquad \text{(Eq. 4)}$$

317 where, Φ_{paste} is the porosity of the cementitious paste, w_{sat} is the vacuum saturated sample mass,
318 w_{dry} is the constant mass obtained after drying the samples at 105 °C, w_{app} is the apparent mass of
319 the samples.

320 The saturated formation factor (F_{sat}) of the mixtures was calculated according to equation 5

321
$$F_{sat} = \frac{\rho_{sat-corrected}}{\rho_{ps}} \qquad \text{(Eq. 5)}$$

322 where, $\rho_{sat\text{-}corrected}$ is the temperature corrected saturated bulk resistivity and ρ_{ps} is the resistivity of
323 the simulated pore solution (0.127 Ω-m). Since the samples were vacuum saturated and stored in
324 simulated pore solution, it is assumed that the pore solution resistivity is uniform for all samples.

325 The pore connectivity (a combination of tortuosity and constriction), β of the paste samples is
326 calculated from equation 6.

327
$$\beta = \frac{\rho_{ps}}{\phi_{paste} \cdot \rho_{sat-corrected}}$$
(Eq. 6)

328 where, ρ_{ps} is the resistivity of the simulated pore solution (0.127 Ω-m).

329 3.3.5. Dynamic vapor sorption (DVS)

330 Dynamic vapor sorption (DVS) measurements were made on two samples (LS20-CNC0.0 and
331 LS20-CNC0.2) that were seal cured for 28 days to determine if CNCs have an effect on the pore
332 size distribution of paste samples. The samples were demolded at 28 days, broken into small
333 chunks that weigh ~70-80 mg. These chunks were vacuum saturated with limewater. They were
334 placed under vacuum for 3 hours, and saturated calcium hydroxide solution for an hour under
335 vacuum. The samples were then placed under the solution for three days in a 23 °C chamber to
336 allow for the sample chunks to get completely saturated. At three days, an assumption of full
337 saturation (i.e. degree of saturation of 100%) is made due to the small sample size.

338 DVS measurements were carried out using a Q5000 vapor sorption equipment (TA Instruments)
339 in an inert nitrogen atmosphere. The steps for ramping down the relative humidity to 0% is as
340 follows:

341 1. The saturated sample was equilibrated at 23.00 °C
342 2. The relative humidity was set to 97.50 % and held for 2880 minutes
343 3. The relative humidity was ramped down to 90%, 80%, 50%, 11%, and 0% in consecutive
344 steps over a duration of 5880 minutes for each step.
345 4. Each step was maintained until the mass change recorded was <0.001% for 15 minutes.
346 5. After reaching 0% RH, the sample was held at isothermal condition for 1440.00 min to
347 equilibrate

348 The pore radius at each RH was calculated using equation 7 and 8. The pore radius is assumed to
349 be the sum of Kelvin radius and thickness of water adsorbed film [86]. Kelvin radius can be
350 determined using equation 7 and t-curve can be determined using equation 8 [87, 88].

351
$$r_k = -\frac{2\gamma V_m}{RT ln(RH)}$$
(Eq. 7)

352
$$t = \left(\frac{AV_m}{6\pi RT(RH)}\right)^{1/3}$$
(Eq. 8)

353 where, r_k is Kelvin radius (m), t is thickness of water adsorbed film, γ is surface tension of the pore
354 solution (= 72×10^{-3} N/m), Vm is the molar volume of the pore solution, R is the ideal gas constant
355 with a value of 8.314 J/(mol.K), T is the absolute temperature (K), and A is Hamaker constant for
356 the interaction of solid-liquid-gas (considered to be -19×10^{-20} J). The degree of saturation (DOS)
357 at each RH is calculated using equation 9.

358 $$DOS_{RH,x} = (M_{RH,x} - M_{RH,0})/(M_{RH,100}-M_{RH,0}) \qquad\qquad \text{(Eq. 9)}$$

359 where, $DOS_{RH,x}$ is the degree of saturation at x% RH, $M_{RH,x}$ is mass of the sample at x% RH, $M_{RH,0}$
360 is mass of the sample at 0% RH, and $M_{RH,100}$ is mass of the sample at 100% RH.

361 ## 3.4. Tests on Cementitious Mortars

362 ### 3.4.1. Drying shrinkage

363 Mortar samples of dimensions 25 mm (width) x 25 mm (height) x 285 mm (length) were prepared
364 for four different mixtures (OPC, OPC-0.2%CNC, LS30, LS30-0.2%CNC). The curing and drying
365 shrinkage measurement procedures for the mortar specimens were followed according to ASTM
366 C596-18. Three specimens were cast for each mixture, and the average and standard deviation of
367 the drying shrinkage strain measured over the drying period were reported.

368 ## 3.5. Experimental Results and Discussion

369 ### 3.5.1. Heat release

370 Figure 1 shows the variation of heat flow (the derivative of the heat release) for the first 24 hours
371 with a change in CNC dosage. At all LS replacement levels, the heat release was retarded by
372 approximately 2-3 hours (indicated by the curve shifting to the right) with the addition of CNCs.
373 This retardation causes a delay in the onset of the acceleration period, which was approximately
374 similar for 0.2% and 0.5% CNC dosages and higher for 1.0% CNC dosage in all cases. This trend
375 of retardation due to increased CNC dosage is consistent with literature. Based on the Parrot-Killoh
376 (PK) model [89], the heat flow curve can be divided into three phases, namely, the nucleation and
377 growth phase, the diffusion in three dimensions, and the reduction in transport of ionic species at
378 later ages, which was discussed in detail in [89, 90]. For mixtures with CNCs, the rate of reaction
379 of OPC-LS mixtures in the nucleation and growth phase (~6 hours) was slower compared to the
380 mixtures without CNCs. However, the diffusion phase occurs for a longer duration in mixtures
381 containing CNCs compared to the mixtures without added CNCs. This was evident from the higher
382 heat flow for mixtures with CNCs at all LS replacement levels. A similar trend of retardation with
383 CNC addition was observed by Fu et al. [23] and Cao et al. [17]. Cao et al. [17] attributed this
384 retardation to the adsorption of CNCs on the cement grains, resulting in fewer surfaces undergoing
385 hydration. A similar retardation effect was explained in the literature for superplasticizers and
386 other chemical admixtures interacting with cementitious mixtures [6, 17, 91].

387

(a)

388

389

(b)

390

14
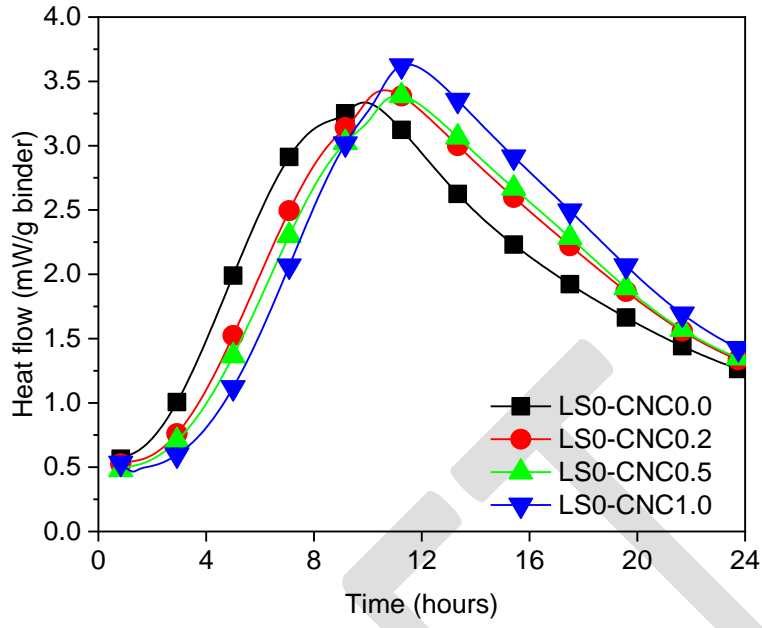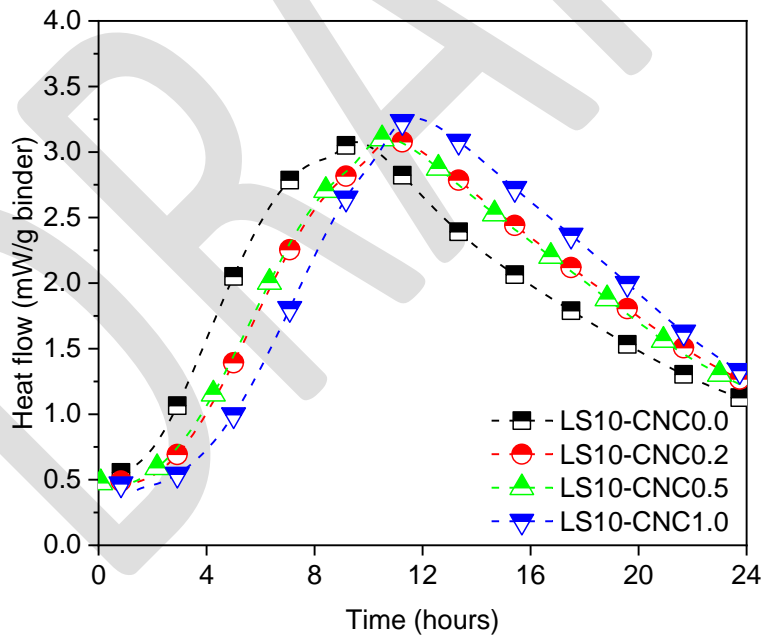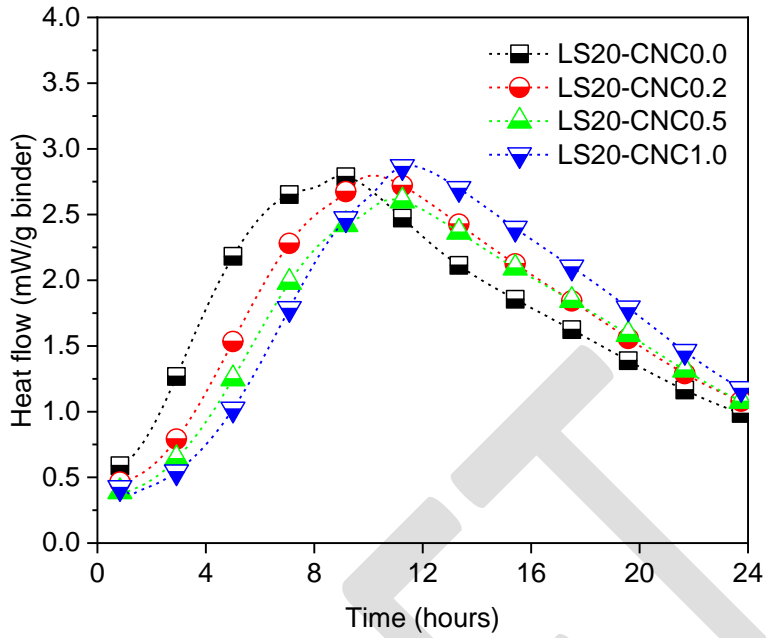
391

392   (c)

393
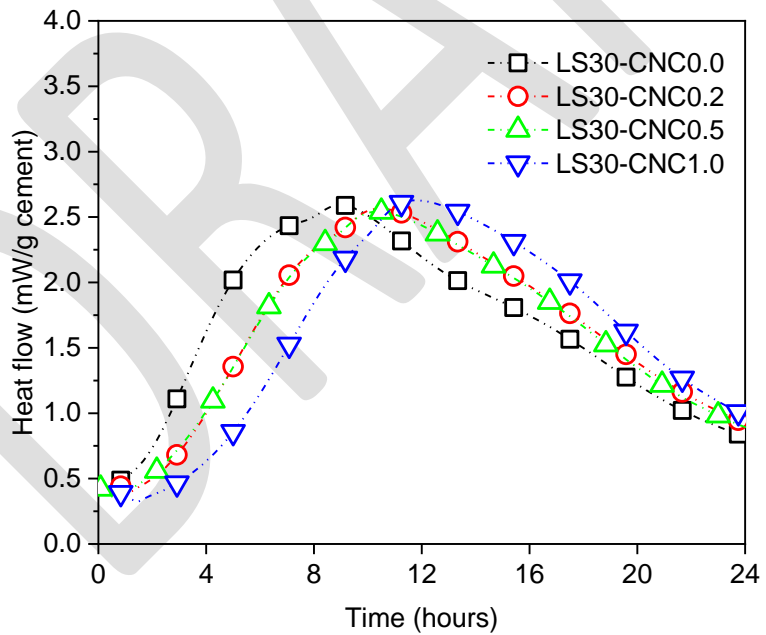
394   (d)

395   Figure 1. Change in heat flow with varying CNC dosage – (a) LS0 (b) LS10 (c) LS20 (d)
396   LS30

397 CNCs addition appeared to affect the heat flow peak associated with silicate hydration in the
398 mixture as well as the aluminate peak (or sulfate depletion peak), as shown in Figure 1. The heat
399 flow in the mixtures without CNCs (shown in black and square markers) was characterized by two
400 distinct peaks occurring at approximately 7 (LS30) to 8.25 (LS0) hours and approximately 8.5
401 (LS20) to 10 (LS0) hours, respectively for silicate and aluminate peaks. However, for the mixtures
402 containing CNCs, these peaks mostly overlap. The overlapping peaks likely correspond to silicate
403 and aluminate reactions occurring at approximately the same time, and as a result, the peak heat
404 flow rate appeared to be higher with added CNCs. Similar observations in peak overlap were made
405 by others in literature for cementitious mixtures containing fly ash [92, 93]. It was reported that
406 the optimal sulfate level in OPC-fly ash mixtures caused an offset between the C_3S hydration peak
407 and the aluminate peak [93]. In this case, the addition of CNCs to OPC-LS mixtures could have
408 an influence on the sulfate balance. The change in sulfate balance may be due to the adsorption of
409 sulfate ester end groups of CNCs on C_3A phase of OPC. However, additional studies are needed
410 to examine this. The higher rate of heat flow in the deceleration phase is likely due to short circuit
411 diffusion [17].

412 Figure 2 shows the 7-day heat release for the mixtures studied here. The heat release values ranged
413 from 302 J – 311 J/g binder (LS0), 285 J – 293 J/g of binder (LS10), 261 J – 274 J/g binder (LS20),
414 and 247 J – 252 J/g binder (LS30) for the various mixtures as in Fig. 2a-d. Up to the first 24 hours,
415 the heat release of the mixtures with CNCs lagged behind the mixtures without CNCs, indicating
416 the retardation due to CNC addition. After approximately 24 hours, there was a cross-over in the
417 heat release curves, indicating an increased rate of hydration for mixtures with CNCs due to short
418 circuit diffusion. For mixtures with no CNCs, dilution and filler effects can explain the results
419 [94]. However, with the addition of CNCs, there was a slight increase in the 7-day heat release.
420 For a given LS replacement level, the addition of CNCs resulted in 2-3% increase in heat release
421 per g of binder compared to mixtures with no added CNCs.

422

(a)

424
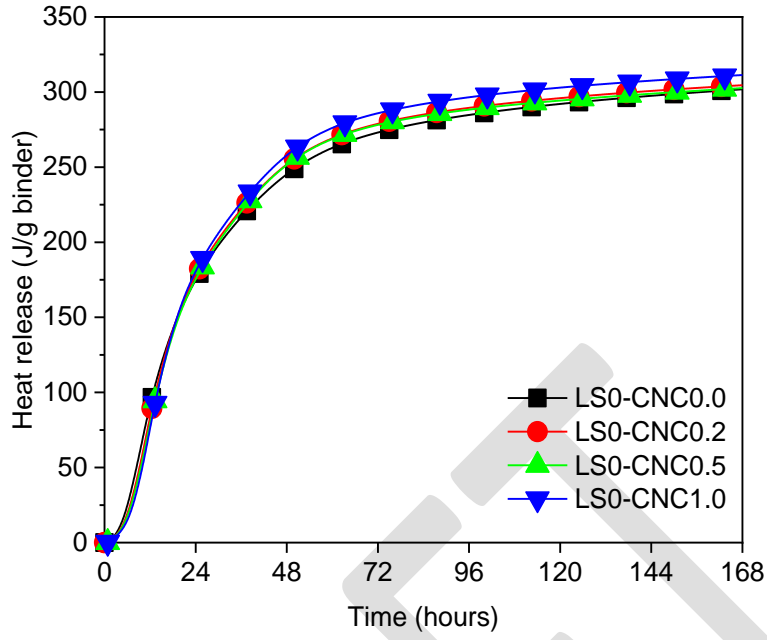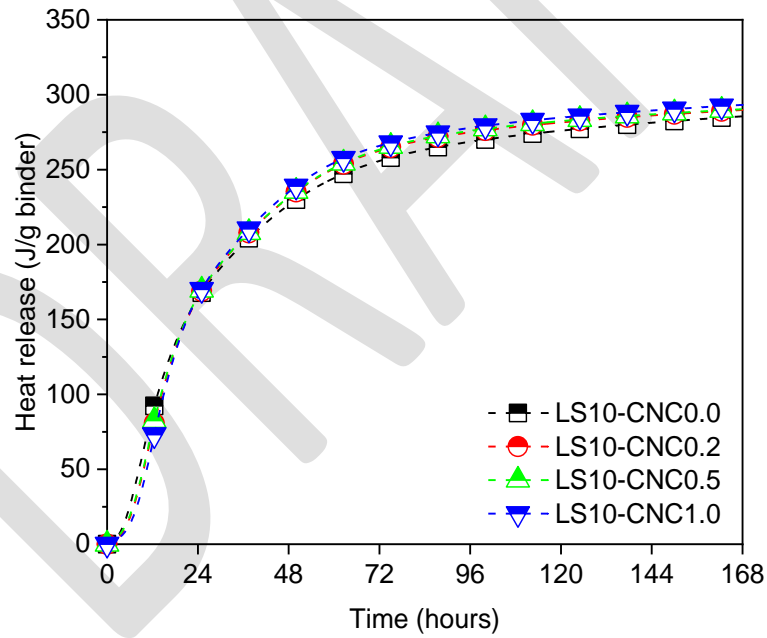
(b)
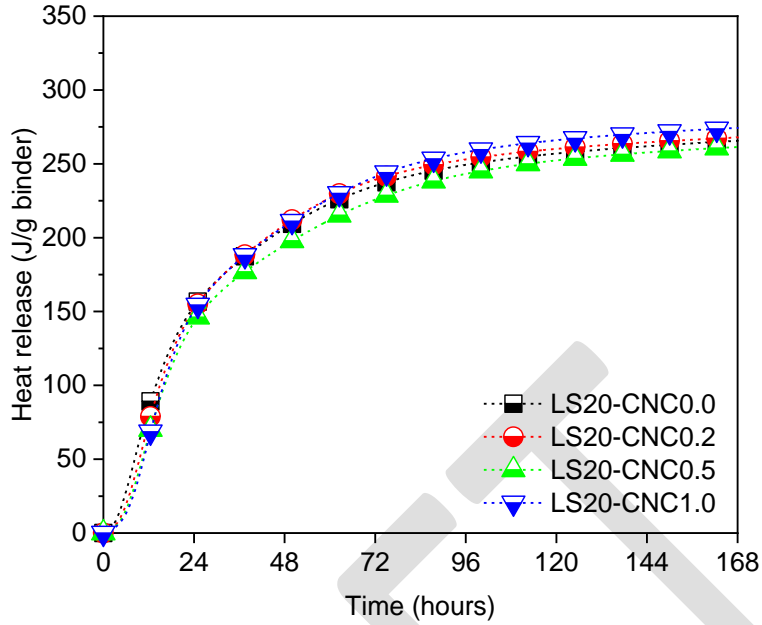
426

427   (c)

428
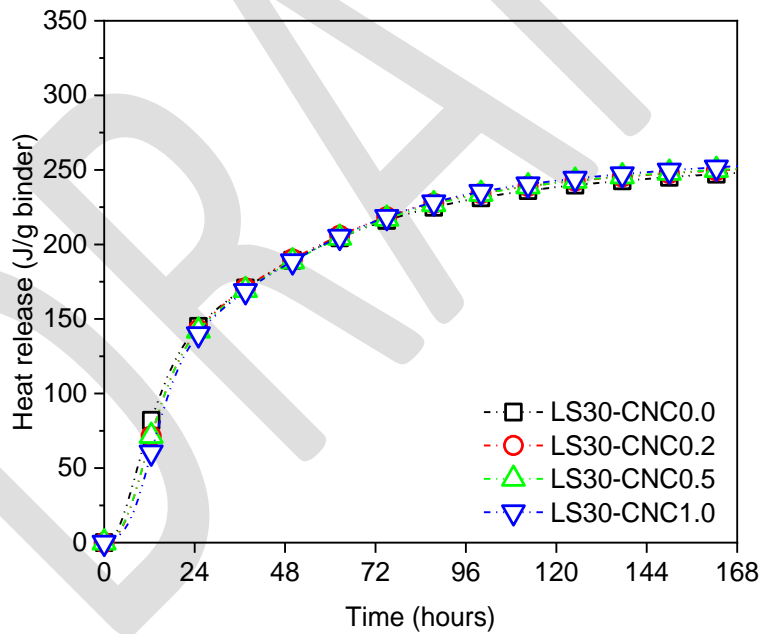
429   (d)

430   Figure 2. Representative 7-day heat release of mixtures at different CNC dosages for
431   LS30 mixtures

432   The replacement of OPC with LS in the mixtures causes a proportional decrease in the 7-day heat
433   release values due to the dilution effect. The dilution effects are offset by addition of LS and CNCs.

434 The combined effect of LS and CNCs was evident from Figure 3, where it was observed that the
435 7-day heat release of the mixtures with added CNCs and LS lie above the dilution line. This
436 increase in heat release was likely due to enhanced hydration of the cement clinker resulting from
437 a combination of short circuit diffusion (SCD) and nucleation effect due to the presence of CNCs
438 and LS, respectively [17, 44, 45]. This increase in hydration may also be due to other factors.
439 Some have speculated that this may be due to changes in pore solution chemistry; however, studies
440 [95] have evaluated the changes in pore solution chemistry and reported little change in ions during
441 the first 12 hours, and changes on the order of 20% or less after that (CNC having a slightly higher
442 Na^+, OH^- concentration and a slightly lower K^+, SO_3 concentration). Similar improvements in the
443 heat of hydration were observed in literature for OPC pastes with CNC addition. Fu et al. [23]
444 observed an approximately 5% increase in the degree of hydration of Type I/II clinker up to 7
445 days. It is likely that the use of clinkers with low C_3A contents could result in further enhancement
446 in the clinker hydration [6, 29, 96]. The formation of carboaluminate phases due to the added LS
447 [97] could also contribute to the increase in the heat release.
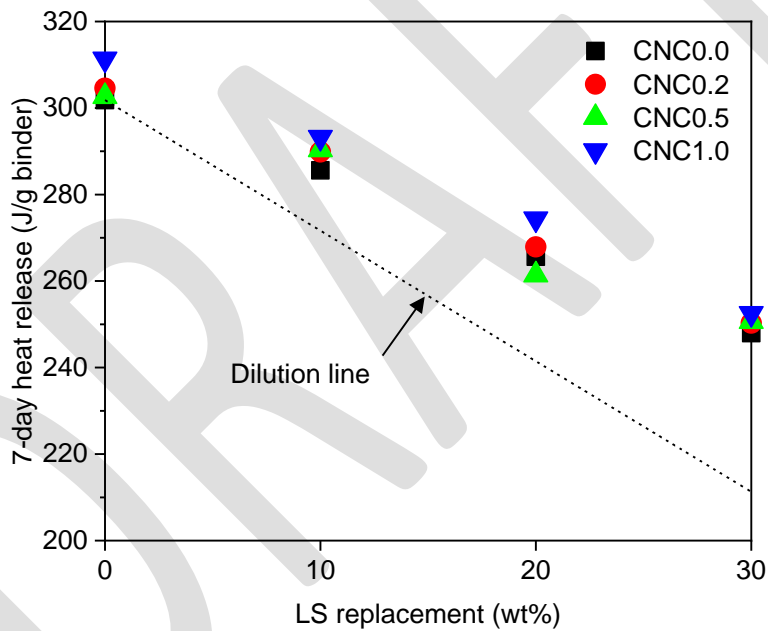
448

449 Figure 3. Effect of CNC dosage on 7-day heat release

450 3.5.2. Thermogravimetric analysis – calcium hydroxide and non-evaporable water content

451 The 28-day calcium hydroxide content of the mixtures is shown in Figure 4. The 28-day calcium
452 hydroxide content of the mixtures varied from 9.9 g - 11.7 g /100 g binder for CNC0.0 mixtures,
453 11.7 g – 13.7 g/100g binder for CNC0.2 mixtures, 11.9 g – 13.5 g/100g binder for CNC0.5
454 mixtures, and 10.3 g – 13.5 g / 100g binder for CNC1.0 mixtures. When CNCs were added (up to
455 0.5% by binder volume) to the mixture, there was an increase in the 28-day calcium hydroxide
456 content of the mixtures that can be explained by the increase in the clinker hydration. The average

457   increase in calcium hydroxide content at low CNC dosage (0.5% CNCs by volume) was ~36%
458   (LS0), ~17% (LS10), and ~1% (LS30). The increase in calcium hydroxide content on the addition
459   of low doses of CNCs is consistent with reported data in the literature [6, 15]. At lower CNC
460   dosages, steric stabilization may allow for greater diffusion of water through the matrix to the
461   cement grains, resulting in enhanced hydration of the clinker [6]. At 1.0% CNC dosages, however,
462   there was no significant influence of CNCs on the calcium hydroxide content of the OPC-LS
463   mixtures. This is probably due to the reduced impact of CNCs on cement hydration as CNCs tend
464   to agglomerate at higher CNC dosages [17, 19].
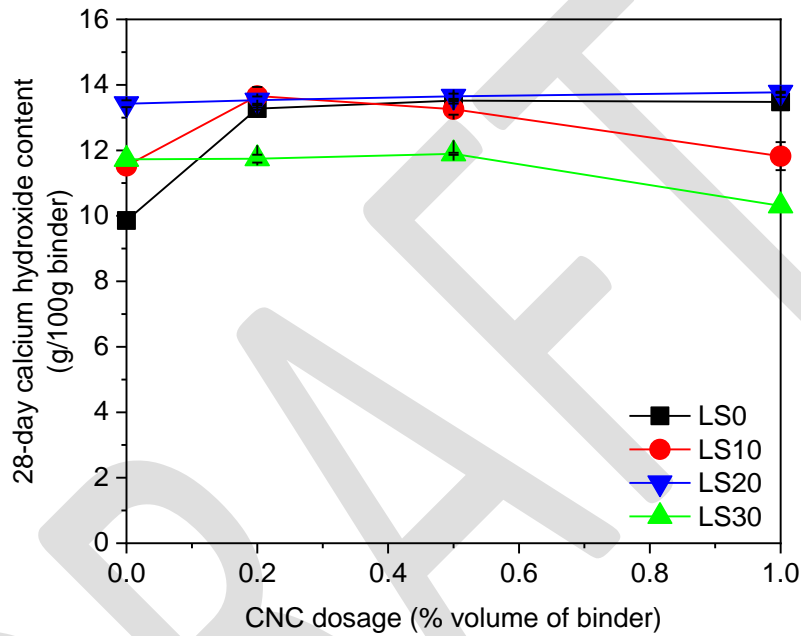
465

466   Figure 4. 28-day calcium hydroxide content of different mixtures

467   The later-age degree of hydration can be computed by calculating the non-evaporable water
468   content (w_n). It was observed that the increase in w_n from 7 to 28 days was generally higher for
469   mixtures containing CNCs compared to those without. Figure 5 shows the 28-day non-evaporable
470   water content of the different mixtures at different CNC dosages.
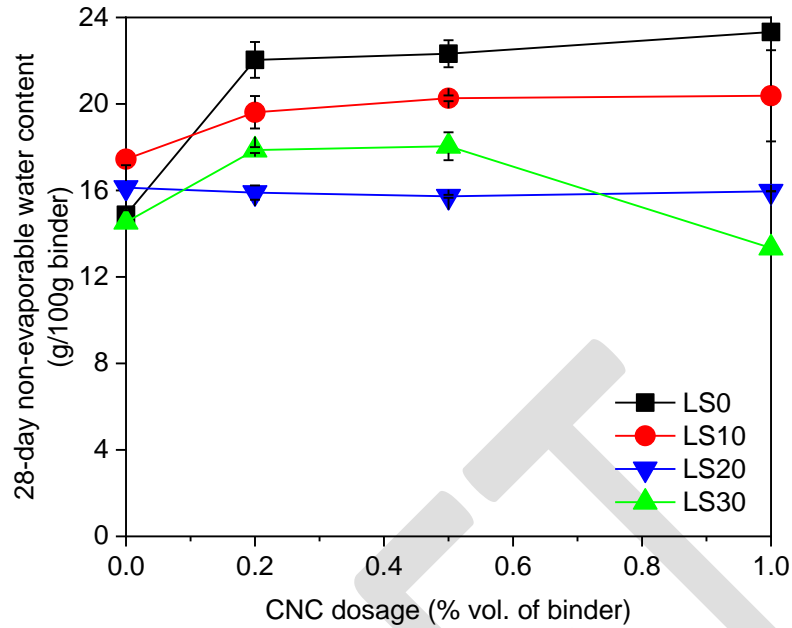
Figure 5. 28-day non-evaporable water content of the mixtures

It was evident that the addition of small amounts of CNCs (up to 0.5% by volume of binder) resulted in an increase in the non-evaporable water content when compared to the mixtures with no CNCs. The increase in w_n ranged from 14% (LS10) – 47% (LS0) and 16% (LS10) – 48% (LS0) with 0.2% and 0.5% CNC addition, respectively. LS10-CNC0.0 was observed to be an exception as the w_n was higher than LS0-CNC0.0 mixture. Increased bound water content for high LS mixtures up to 0.5% CNC dosage indicated a more "effective" clinker usage i.e., more cement participates in the hydration reaction. This indicated that CNCs could be added to OPC-LS mixtures to improve clinker efficiency while reducing the clinker content. Cao et al. [17, 18] reported similar increases in the non-evaporable water content of mixtures containing CNCs.

3.5.3. B3B flexural strength

Figure 6 shows a parity plot for the 7-day and 28-day B3B flexural strengths for the mixtures with and without CNCs. The 7-day B3B flexural strengths of mixtures range from 20.2 MPa (LS30) – 21.1 MPa (LS0), 15.9 MPa (LS30) – 21.2 MPa (LS0), and 16 MPa (LS30) – 20.6 MPa (LS10) at 0.2%, 0.5%, and 1.0% CNC dosage, respectively. It should be noted that the B3B flexural strengths indicate characteristic strength of the mixtures, and they are higher than flexural strength determined using conventional flexural strength testing due to the size effect. A detailed discussion of the size effect of samples on B3B flexural strength can be found in literature [79].

490

491

(a)

492

493

(b)
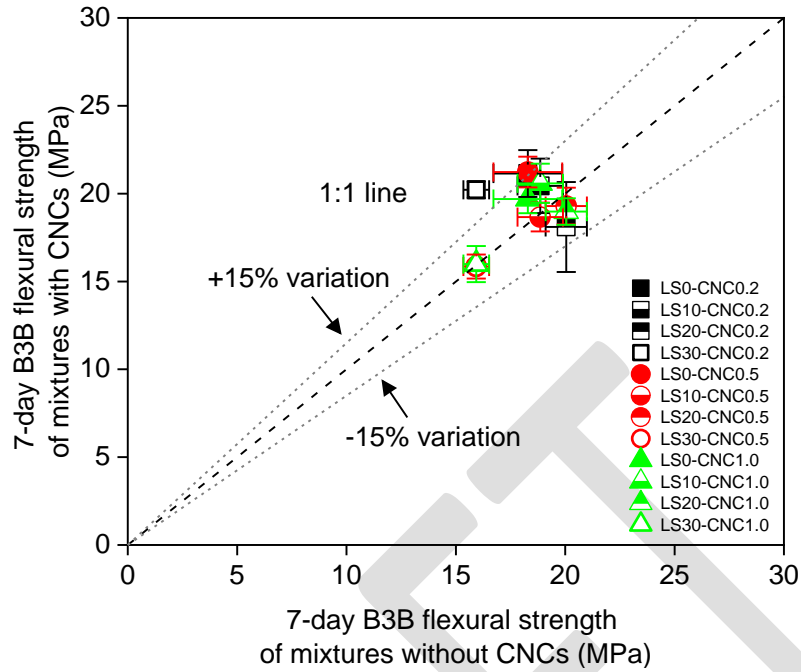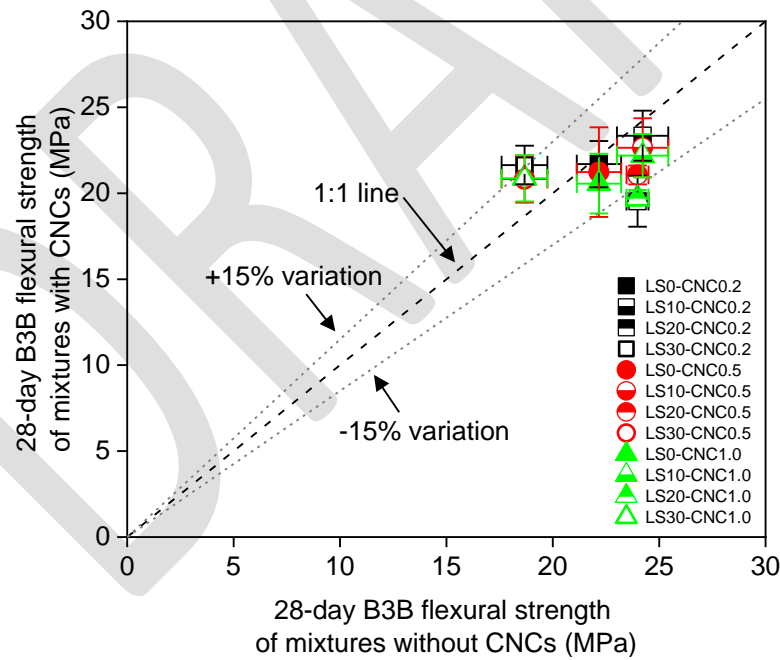
Figure 6. Effect of CNC dosage on B3B flexural strength – (a) 7 days (b) 28 days. A data point
on the 1:1 line indicates similar performance, and a data point above the 1:1 line indicates better
performance for mixtures with added CNCs (i.e., the measurement on the Y-axis). 1 MPa =
145.04 psi.

22

498   Comparing the mixtures with and without CNCs at 7 days, it was observed that CNCs do not have
499   adverse effects on early-age strength development. Clear effects of dilution due to high LS
500   replacement was seen in the early age flexural strength for mixtures without CNCs consistent with
501   the literature, where reduction in early age mechanical properties was seen with an increase in LS
502   replacement [46]. However, the addition of CNCs compensates for this dilution effect (along with
503   the nucleation effect of LS) and the increase in strength was generally within 15% of the mixtures
504   without CNCs with the exception of LS30-CNC0.2, which showed a 27% increase. A similar trend
505   was observed for 28-day B3B flexural strength; there were no adverse effects on the strength
506   development of mixtures due to CNC addition. The 28-day flexural strength of the mixtures with
507   CNCs was within 15% of the mixtures without CNCs.

508   3.5.4. Bulk resistivity and pore structure characteristics

509   The 7-day and 28-day bulk resistivity and saturated formation factor values of the mixtures with
510   different LS replacement levels is shown in Figure 7 and Figure 8 respectively. CNCs did not
511   substantially impact the 7-day bulk resistivity (and saturated formation factor) of the mixtures,
512   seen from Figure 7a and Figure 8a. Only dilution and filler effects on account of LS replacement
513   predominated at this age, which was consistent with literature for OPC-LS mixtures [46].

514

515   (a)

516

517   (b)
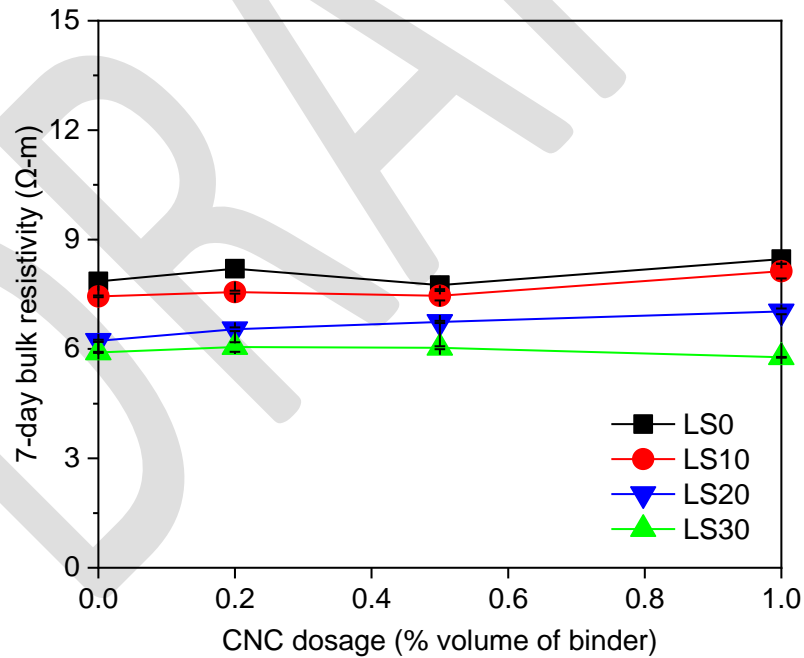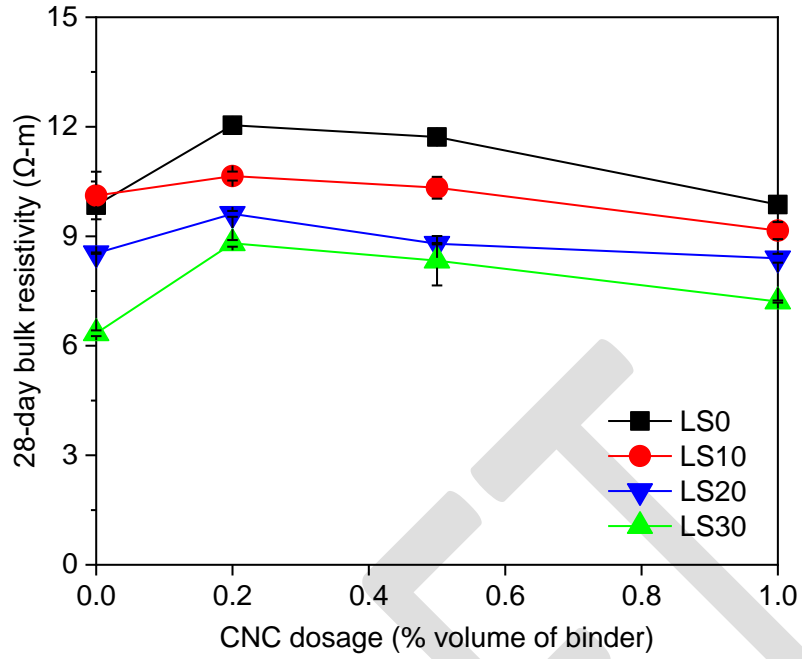
518   Figure 7. Effect of CNC dosage on saturated bulk resistivity (a) 7-days (b) 28-days

519

520

521   (a)

522

523   (b)
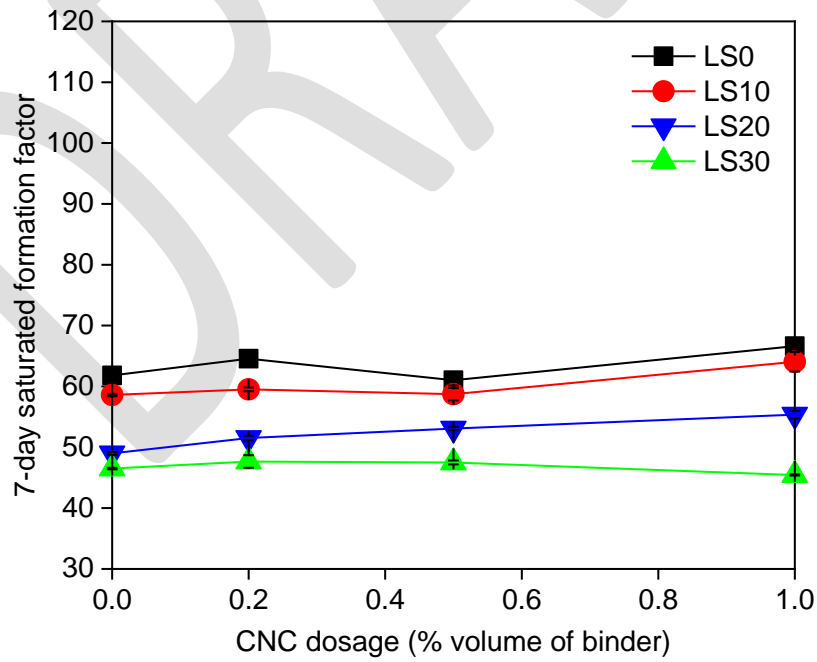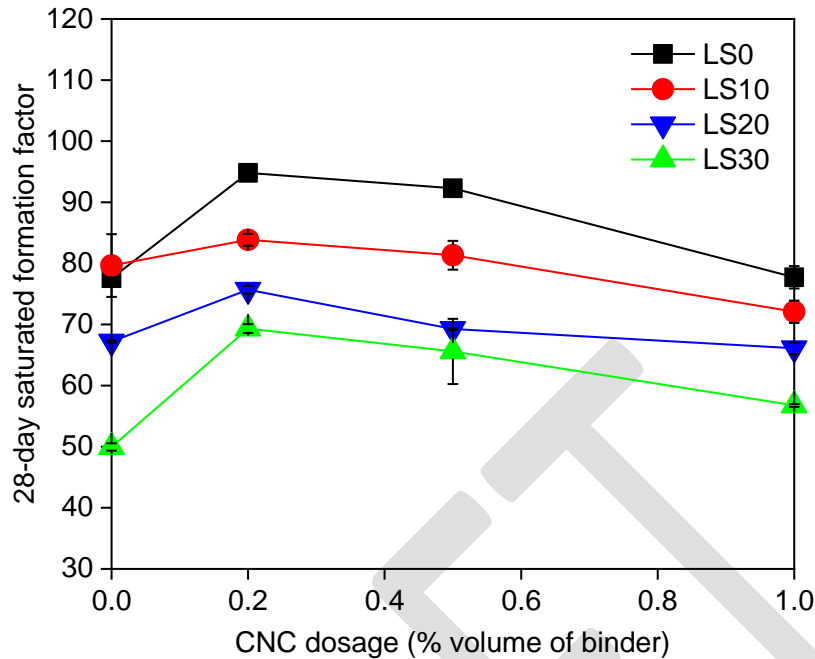
524   Figure 8. Effect of CNC dosage on saturated formation factor (a) 7-days (b) 28-days

525   The effect of CNC addition on the bulk resistivity (and saturated formation factor) of the different
526   mixtures was seen at 28 days (Figure 7b and Figure 8b). CNC dosages of up to 0.5% by binder
527   volume resulted in an increase in the 28-day saturated bulk resistivity compared to the mixtures
528   without CNCs for a given LS replacement level. The increase in bulk resistivity values ranged
529   from 5% (LS10) - 38% (LS30) and 2% (LS10) - 31% (LS30) at 0.2% and 0.5% CNC dosage by
530   binder volume, respectively. The dilution effect due to LS addition was compensated by a
531   combination of LS and CNC dosages up to 0.5% by binder volume. However, no such
532   compensation was observed at higher CNC dosage. When the CNC dosage was 1.0% by binder
533   volume, the effect was pure dilution, and the 28-day bulk resistivity was similar to mixtures with
534   no added CNCs.

535   The 28-day porosity data for the different mixtures with and without CNCs is shown in Figure 9.
536   A thermodynamic modeling approach [98] (briefed in Chapter 1) was used to provide an idea of
537   how porosity of mixtures varies with LS replacement. The porosity of CNC0.0 mixtures
538   determined from thermodynamic modeling [98] is shown in Figure 9 as a baseline to compare the
539   porosity of mixtures with and without CNCs. The experimental results were in good agreement
540   with the modeling results for CNC0.0 mixtures. At all CNC dosages, the porosity of the mixtures
541   was the lowest for LS0 mixtures and increased with increase in LS content. This was consistent
542   with literature for mixtures without CNCs [98, 99], where the porosity of mixtures decreased first
543   (up to 2% LS addition) and then increased with an increase in LS replacement. No significant

544 changes in total porosity of the samples were observed when CNCs were added and the variation
545 was less than 1% when compared to the corresponding mixtures without CNCs.

546
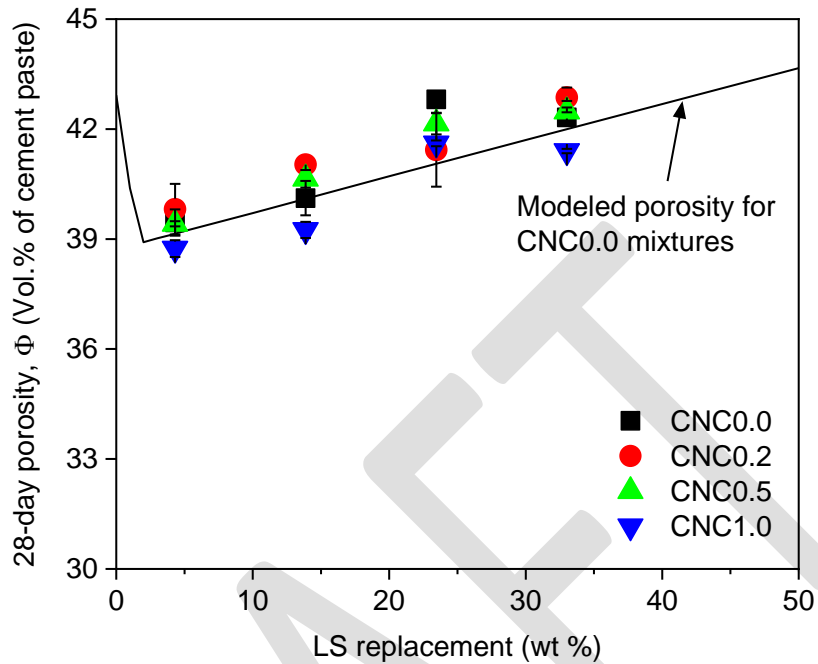
Figure 9. 28-day porosity of mixtures with and without CNCs. The ends of the error bars shown
here represent the measured values and the markers show the average value of the two samples.
The limestone replacement percentages also account for the limestone present in the cement
clinker (4.1% for this cement).

551 While the porosity of the mixtures did not significantly vary, differences were observed in the pore
552 connectivity (β) of the mixtures (shown in Figure 10). The pore connectivity of the mixtures
553 without CNCs generally increased with an increase in LS replacement level and ranged from 0.03
554 (LS0 and LS10) - 0.05 (LS30), consistent with literature [98]. It was seen that low dosages of
555 CNCs up to 0.5% by volume of binder caused a decrease in pore connectivity (indicating increased
556 performance), and the lowest pore connectivity was observed for mixtures with 0.2% CNCs by
557 volume of binder. For CNC0.2 and CNC0.5 mixtures, the decrease in pore connectivity ranged
558 from 7% (LS10) - 29% (LS30) and 3% (LS10) – 24% (LS30) respectively compared to the CNC0.0
559 mixtures with the same LS replacement levels. At 1.0% CNC dosage, only LS30 showed decreased
560 pore connectivity (compared to its 0% CNC counterpart i.e., LS30CNC0.0), whereas LS0, LS10,
561 and LS20 mixtures did not follow the trend (compared to LS0CNC0.0, LS10CNC0.0, and
562 LS20CNC0.0 respectively). This could be due to agglomeration of CNCs at higher CNC dosages
563 as discussed in the previous section on B3B flexural strength. This decrease in pore connectivity
564 with CNC addition was likely due to increased cement hydration resulting in pore filling and
565 consequently increasing the bulk resistivity of the mixtures [14, 17, 21, 100].
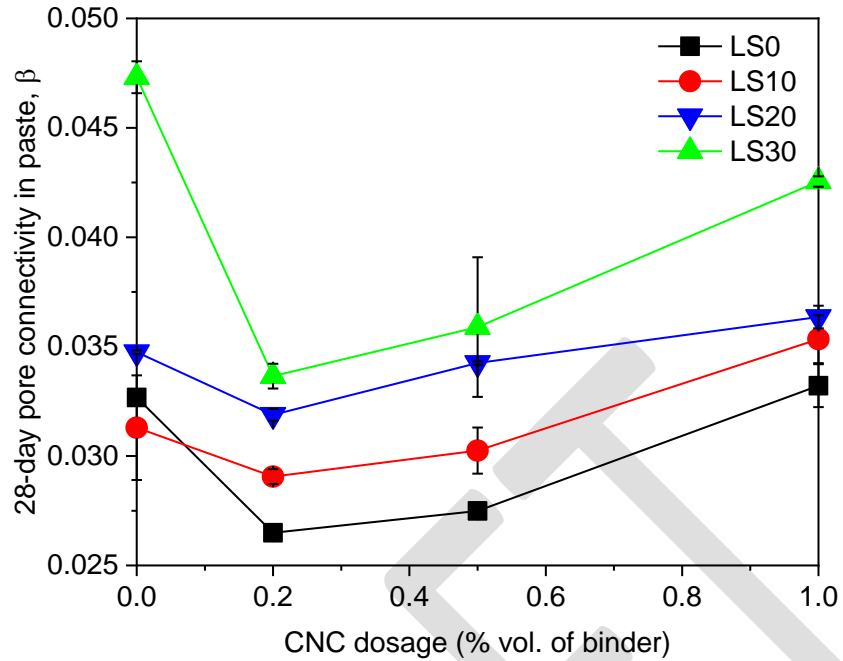
566

567　　　Figure 10. Pore connectivity in mixtures with and without CNCs at 28 days. The ends of the
568　　error bars shown here represent the measured values and the markers show the average value of
569　　　　　　　　　　　　　　　　　　the two samples.

570　　3.5.5. Drying shrinkage

571　　The drying shrinkage test results of the mixtures LS0-CNC0.0, LS0-CNC0.2, LS30-CNC0.0, and
572　　LS30-CNC0.2 are shown in Figure 11.
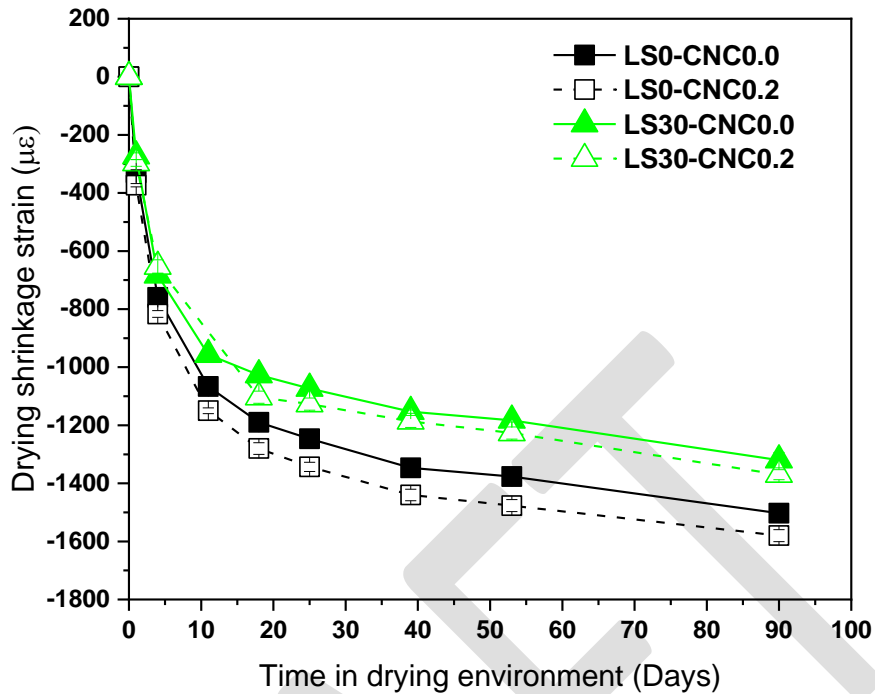
573

574   Figure 11. Drying shrinkage results of the mortar specimens

575 It was observed that LS0 mixtures with CNC had a slightly higher shrinkage strain than the mixture

576 without CNC. After 90 days of exposure to the drying environment, a maximum difference of 5%

577 of average shrinkage strain was observed between the LS0 mixtures with and without CNCs. The

578 observed slightly higher shrinkage strain could probably be due to higher clinker hydration with

579 the CNCs addition. For LS30 mixtures, there was no statistically significant difference in drying

580 shrinkage strain between the mixtures with and without CNCs.

581 3.5.6. Dynamic vapor sorption

582 Figure 12 shows the cumulative pore volume determined for the LS20 paste samples with and

583 without CNC. It was observed that the cumulative pore volumes are similar for the LS20 samples

584 and not affected by the CNC addition. Figure 13 shows the pore size distribution of LS20 samples

585 with and without CNC.

28

586
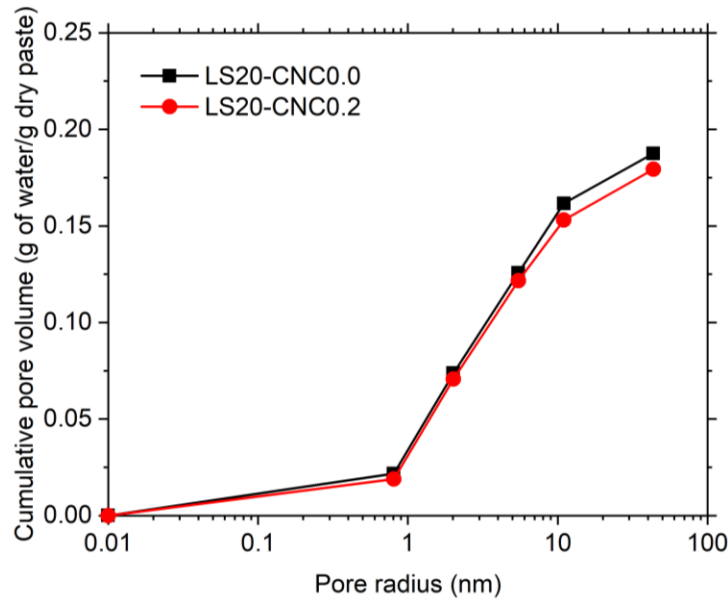
587

588   Figure 12. Cumulative pore volume of LS20 paste samples with and without CNC
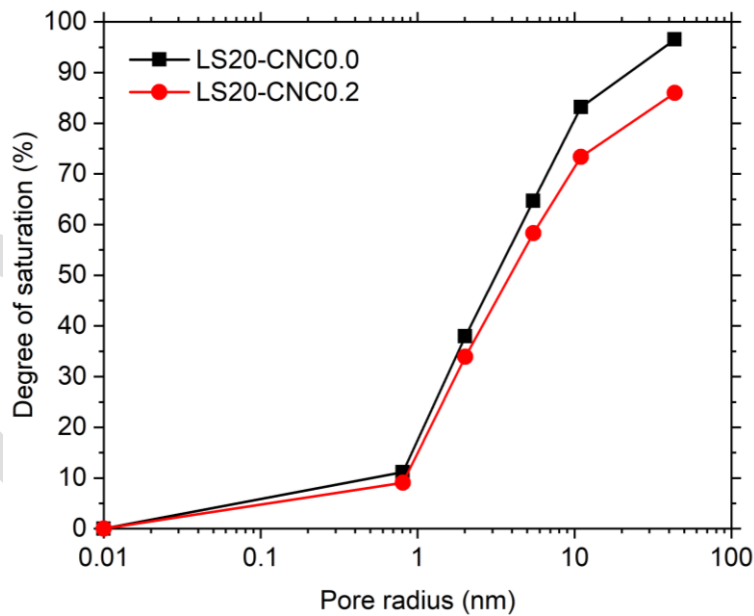
589

590   Figure 13. Pore size distribution of LS20 paste samples with and without CNC

591   The pores in the sample can be classified as capillary pores (with pore radius ≥ 5 nm) and gel pores

592   (with pore radius < 5 nm) [86]. From Figure 13, it was observed that the degree of saturation of

593   LS20-CNC0.2 mixture is slightly lower than LS20-CNC0.0 mixture indicating higher fraction of

594   capillary pores (and any entrapped air voids) in the LS20-CNC0.2 mixture. Despite the higher

595 fraction of capillary pores in LS20-CNC0.2 when compared to LS20-CNC0.0, it should be noted
596 that the pore connectivity (β) in LS20-CNC0.2 mixture was 8% lower than LS20-CNC0.0 mixture.

597 3.5.7. Thoughts on developing "greener" mixtures with CNCs

598 The approach studied here has two components with respect to making concrete greener. The first
599 component is to replace a part of OPC in the mixture by LS as it would reduce the GHG emissions.
600 The second component is to add CNCs to the mixture to augment the properties of mixtures with
601 LS. Replacing OPC with LS (>15%) can result in a decrease in bulk resistivity at high replacement
602 levels due to dilution effects (45). However, with CNC addition, an increase in bulk resistivity was
603 observed and compensated for the dilution effects. The following assumptions are made to
604 calculate the GHG emissions using the life cycle inventory (LCI) calculation tool developed by
605 Miller et al [41, 101]:

606 • The transportation distances for ingredients were assumed based on previous research
607 conducted [41, 101].
608 • All mixtures contain the same quantities of aggregates and chemical admixtures.
609 • A cradle-to-gate option (A1 to A3) was considered for evaluating emissions associated.
610 Only the emissions associated with raw material transport, manufacturing, batching, and
611 end of life were included here. In terms of life cycle assessment (LCA) modules, for the
612 raw materials and concrete production stage, LCA modules A1-A3 were considered.
613 Batching raw materials for concrete was considered the boundary for this phase.
614 Additionally, for end-of-life emissions associated, LCA modules C1-C4 was considered.
615 The emissions associated with the "in use" phase of concrete (i.e. B1-B7) and recycling
616 (i.e. LCA module D) was not considered here. LCA modules A4 and A5, associated with
617 the use phase of concrete were not considered here.
618 • Since CNCs are derived from carbon neutral sources, it was assumed that CNCs have
619 negligible CO_2 emissions. It is acknowledged that CNC manufacturing and CNC
620 dispersion in the construction phase (LCA modules A4 and A5) contributes to minor CO_2
621 emissions. The emissions associated with CNCs in a full-scale production environment
622 will depend on the distance of the plant from the raw materials, type of raw materials, and
623 the processing used to manufacture the CNC [102]. Additional research is needed on the
624 LCA of CNC when commercially produced. Work is in progress to evaluate the full LCA
625 of CNCs; however, it is anticipated as lab and pilot plants move to full scale the full LCA
626 of these materials will become more clearly understood. It should be noted that in this paper
627 refrigeration is used to limit fungal growth in the CNCs over the duration of the research
628 project. However, refrigeration is not necessary for full scale applications.
629

630 Figure 14 shows the plot of 28-day bulk resistivity as a function of GHG emissions. A general
631 form of the linear equation is shown in equation 10 and the parameters m and b for the different
632 CNC dosages is shown in Table 2.

$$\rho_{28-day} = m_i(f, CNC).GHG + b_i(f, CNC) \qquad \text{(Eq. 10)}$$

634 where, ρ_{28-day} is the saturated bulk resistivity at 28 days, m is the slope, GHG is the % GHG
635 emissions reduced, and b is the intercept on the Y-axis.

636
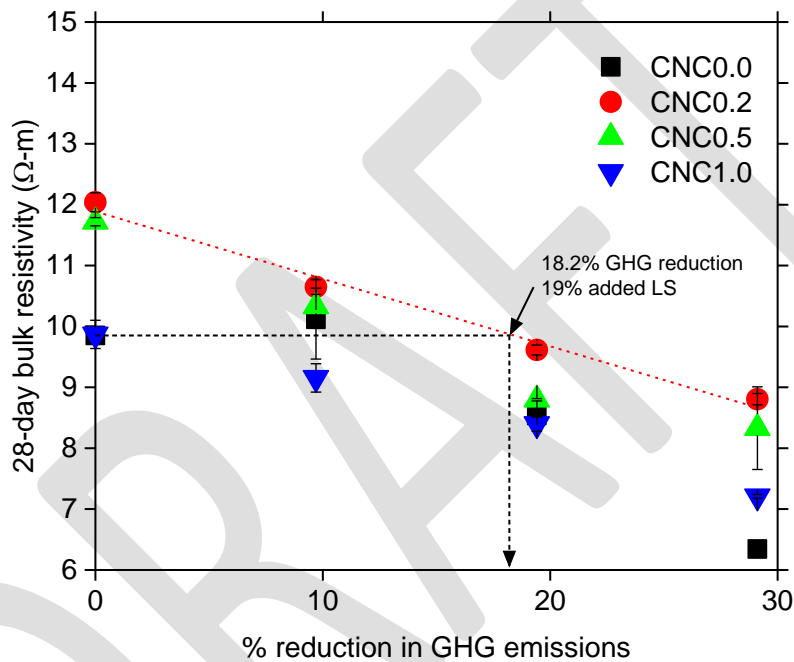
638 Figure 14. 28-day saturated bulk resistivity versus GHG emissions for OPC-LS mixtures with
639 and without CNCs. The ends of the error bars shown here represent the measured values and the
640 markers show the average value of the two samples.

641 Maximum reduction in GHG emissions possible with optimal LS and CNC contents was calculated
642 based on m and b from Table 2. It was found that equivalent performance (in terms of resistivity)
643 could be achieved by 19% LS addition (22% total LS) with 0.2% dosage of CNCs and this
644 corresponded to 18.2% reduction in GHG emissions compared to the LS0-CNC0.0 mixture.
645 Therefore, 20% LS addition with 0.2% CNC dosage was considered, which corresponded to a
646 19.4% decrease in GHG emissions. A comparison of the other cementitious paste properties is
647 shown in Table 3, where it was seen that LS20 mixtures with 0.2% CNC addition had similar
648 performance compared to a 100% OPC mixture with no added CNCs. Further reduction in GHG
649 emissions (~29%) can be achieved by adding 30% LS and 0.2% CNCs with similar 28-day B3B
650 flexural strength and slightly lower (~10.6%) 28-day saturated bulk resistivity compared to 100%
651 OPC mixture. It should be noted that single-operator variability of bulk resistivity measurement

652 according to ASTM C1876-19 should be within 12%, implying that the reduction in bulk resistivity
653 due to 30% LS and 0.2% CNC addition is not significant compared to 100% OPC mixture.

654 Table 2. Slope (m_i) and intercept (b_i) values for best fit lines

i	CNC dosage (% volume of binder)	m_i	b_i
1	0.0	-0.12	10.53
2	0.2	-0.11	11.89
3	0.5	-0.12	11.55
4	1.0	-0.09	9.97

655 Table 3. Comparison of properties between LS20-CNC0.2 and LS0-CNC0.0 mixtures

Property evaluated	Testing age	LS0-CNC0.0	LS20-CNC0.2	% change
Heat of hydration of clinker (J/g cement)	7 days	301.84	334.86	+10.9%
Non-evaporable water content (g/100g binder)	28 days	14.87 ± 0.00	15.79 ± 0.32	+6.2%
B3B flexural strength (MPa)	28 days	22.17 ± 1.04	19.56 ± 1.48	-11.7%
Saturated formation factor, F_{sat}	28 days	77.57 ± 0.00	75.70 ± 0.63	-2.4%
Overall porosity, Φ	28 days	$39.45 \pm 0.36\%$	$43.30 \pm 0.00\%$	+3.8%
Pore connectivity, β	28 days	0.0327	0.0305	-6.7%

656

657 Past research showed that the performance of PLCs (confirming to ASTM C595) was similar to
658 OPC [37, 38, 42, 98] in terms of mechanical properties and durability and hence is an acceptable
659 substitute in the push towards sustainability in the concrete industry. The use of PLCs could result
660 in reducing the GHG emissions by ~10%. Any further LS replacement without added reactive
661 SCMs would result in a significant reduction in mechanical and transport properties rendering the
662 possibility of using high LS dosages unfeasible. The addition of CNCs to OPC-LS mixtures
663 resulted in improved transport properties (which would result in reduced diffusion of deleterious
664 species) without compromising mechanical properties. The increased degree of hydration at 28
665 days in OPC-LS mixtures with CNCs indicated that the OPC clinker is utilized more effectively.
666 Therefore, the addition of CNCs to mixtures containing higher amounts of LS (up to 22%,
667 including the LS content in OPC) could push this envelope further and pave way for ternary blends
668 and result in "greener" mixtures without compromising on the performance.

3.6. Conclusions

OPC-LS-CNC mixtures were studied as a possible method to reduce GHG emissions. The addition of up to 0.5% CNCs to OPC-LS mixtures resulted in an increased degree of hydration of binder at all ages. At early ages, the increase in degree of hydration was attributed to the combined effect of LS and CNCs. At later age, the increased degree of hydration was due to the CNCs.

The addition of low dosages of CNCs up to 0.5% resulted in a decrease in pore connectivity of the mixtures and an increase in bulk resistivity of up to 38%. CNCs addition did not have a significant impact on the overall porosity and B3B flexural strength of the mixtures at both 7 and 28 days. Also, the addition of CNCs did not have a significant impact on the drying shrinkage strain of the mortar specimens made with limestone. There was slightly higher (~5%) drying shrinkage strain after 90 days in drying environment for the mixture with OPC and CNC when compared to mixture without CNC, probably due to higher clinker reaction in the presence of CNCs.

The addition of 20% LS and 0.2% CNCs together resulted in mixtures with ~19% reduced GHG emissions with comparable mechanical and transport properties to the conventional 100% OPC mixture. Higher GHG emission reductions up to ~29% can be achieved by adding 30% LS and 0.2% CNCs resulting in mixtures with similar mechanical properties and slightly lower (~11%) bulk resistivity. These findings pave way to explore the use of CNCs to achieve further lower GHG emissions and develop "greener" mixtures.

4. CHAPTER 3: Performance of Mixtures with SCMs and CNCs

As shown in Chapter 2, CNCs can be used to improve the performance of mixtures with limestone by increasing the degree of hydration and providing a way to reduce GHG emissions. To further reduce the GHG emissions, this research also evaluated the use of SCMs to replace the cement along with using CNCs. Therefore, the extended goal of this project, and the objective of this chapter, is to evaluate the performance of CNCs in mixtures with SCMs.

4.1. Constituent Materials and Characterization Procedures

4.1.1. Materials

Commercially available Type II OPC and a PLC made using the same clinker as OPC were used for this study. SCMs considered in this study were fly ash (FA), slag (SL), and silica fume (SF). The chemical composition and particle size parameters of the OPC, PLC, and the SCMs are shown in Table 4. X-ray fluorescence was used to determine the chemical composition of the materials, LOI was determined using a furnace, and particle size parameters were determined using laser diffraction technique. The detailed procedures for the material characterization and testing were described in Chapter 2. CNCs that were obtained in the form of suspension with 11% w/w CNC solids were used. The CNCs were manufactured by Forest Products Laboratory using sulfuric acid hydrolysis process. Four CNC concentrations used were 0%, 0.2%, 0.5%, and 1.0% solid volume by volume of binder.

706 Table 4. Chemical composition and particle size parameters of the OPC, PLC, and SCMs (NA:
707 not applicable)

%	Cement		SCMs		
	OPC	PLC	Fly Ash (FA)	Slag (SL)	Silica Fume (SF)
SiO_2	19.95	18.38	51.86	31.58	95.88
Al_2O_3	3.95	3.62	21.70	12.13	0.69
Fe_2O_3	2.28	2.07	5.04	0.55	0.12
CaO	63.32	61.69	8.61	41.34	0.70
MgO	1.43	1.33	2.58	6.97	0.26
SO_3	2.55	2.48	0.78	3.75	0.15
LOI	2.71	6.42	1.42	0.00	4.30
Na_2O	0.21	0.22	2.58	0.24	0.16
K_2O	0.48	0.44	1.45	0.28	0.49
TiO_2	0.19	0.18	1.19	0.47	0.01
P_2O_5	0.10	0.10	0.23	0.00	0.05
ZnO	0.01	0.01	0.02	0.00	0.06
Mn_2O_3	0.07	0.07	0.03	0.19	0.04
Cl	0.003	0.003	0.01	0.00	0.01
Limestone	4.31	13.32	NA	NA	NA
d_{50} (µm)	10.52	15.70	13.01	29.08	4.96
d_{90} (µm)	27.89	59.18	44.62	87.81	11.28

708

709 Several binder combinations that are currently accepted by CALTRANS were used in this study.
710 The OPC and PLC were used with 50% SL, 20% FA + 5% SF, and 25% FA + 25% SL. All the
711 considered binder combinations were evaluated with and without CNCs.

712 **4.1.2. Paste mixing and sample preparation**

713 The cementitious materials were dry mixed for 90 s using a vacuum mixer at 400 rpm and 70%
714 vacuum. The CNC dispersed mix water was placed in a mixing bowl, and the dry mixed
715 cementitious materials were added, and mixed using a vacuum mixer (Renfert Inc. model
716 18281000) for 90 s at 400 rpm and a 70% vacuum level. The mixing cup was scraped using a
717 silicone spatula for 15 s, and vacuum mixing was carried out for an additional 90 s. Pastes were
718 prepared at a water to binder ratio of 0.40. The prepared pastes were cast in 50 mm diameter and
719 100 mm length cylinder molds. The cylinder molds with the fresh pastes were rotated on a roller
720 at 60 rpm for 12 hours to prevent any bleeding and they were kept sealed until testing.

721 **4.1.3. Tests on cementitious pastes**

722 All the paste mixtures were tested for heat release (and heat flow), B3B flexural strength, porosity,
723 and saturated bulk resistivity. Heat release (and heat flow) were measured using isothermal
724 calorimetry for seven days. The samples were tested for B3B flexural strength at 28 and 56 days.
725 Samples were tested for porosity and bulk resistivity at 28 and 56 days. All samples were sealed
726 after casting until the age of testing. The detailed procedures for testing the samples were reported
727 in Chapter 2 and not repeated here for brevity.

728 ## 4.2. Experimental Results and Discussion

729 **4.2.1. Heat flow**

730 Figure 15a-f shows the heat flow (rate of heat release) for the OPC-SCM and PLC-SCM mixtures
731 up to first 40 hours. For all the SCM mixtures, CNC addition resulted in a slight retardation
732 (indicated by the curve shifting to the right) compared to mixtures without CNC. This retardation
733 causes a delay in the set time and the onset of the acceleration period. A higher CNC dosage
734 caused a longer retardation. Similar observation was made in Chapter 2 where CNCs were used
735 along with OPC and limestone. The heat flow peak intensity of the PLC-SCM mixtures is lower
736 compared to OPC-SCM mixtures because of additional reduction of clinker from LS replacement.
737 A secondary peak after approximately 24 hours was observed that requires further study.

738
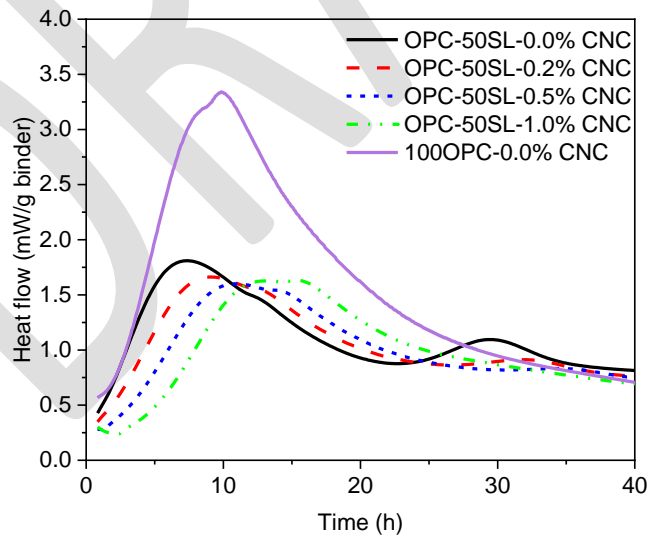
739

740   (a)

741

742

(b)

743

744

(c)

37

745

746

(d)

747

748

(e)

749

38

750

751   (f)
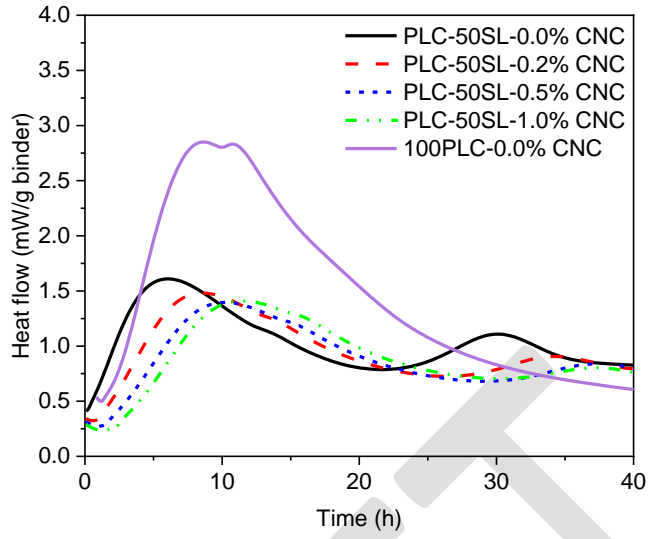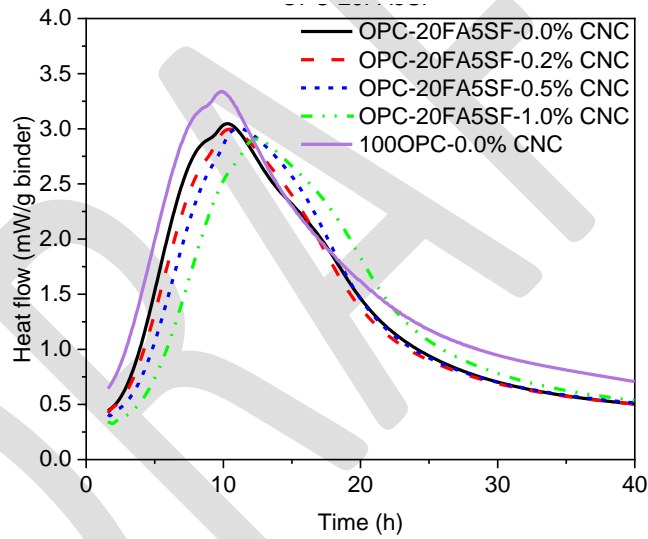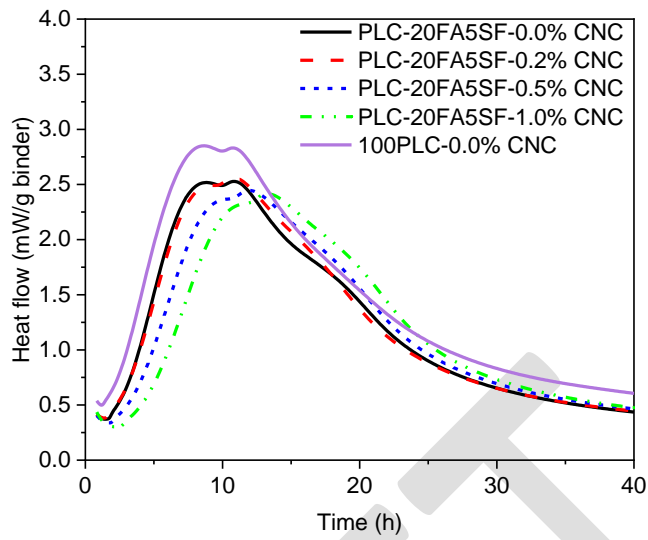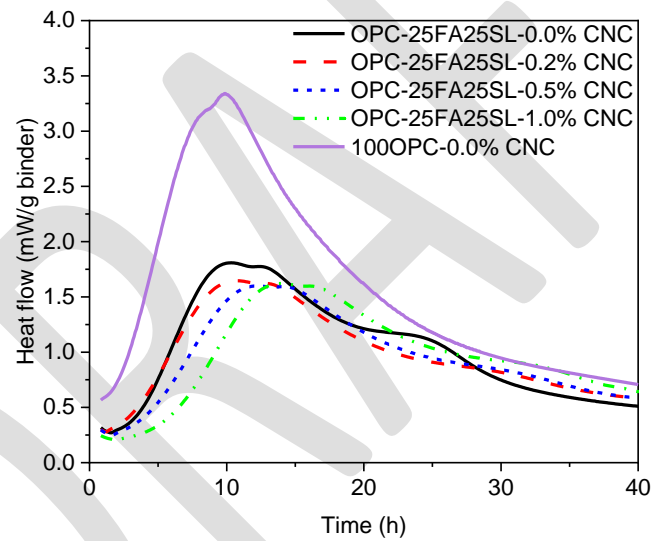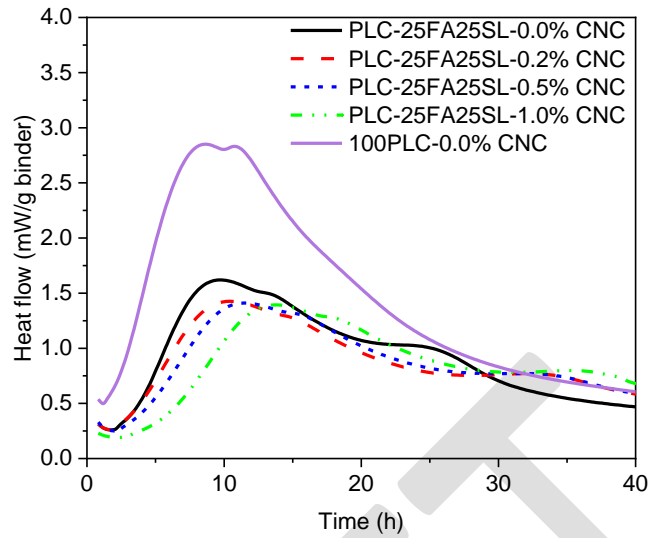
752   Figure 15. Change in heat flow with varying CNC dosage – (a) OPC-50SL (b) PLC-50SL (c)
753   OPC-20FA5SF (d) PLC-20FA5SF (e) OPC-25FA25SL (f) PLC-25FA25SL

754   In case of OPC-SL50 mixture (Figure 15a), the shift in the silicate peak ranged from 1.5 hours
755   (0% CNC) to 6.5 hours (1% CNC). In case of PLC-SL50 mixtures (Figure 15b), the filler effect
756   of LS in the PLC caused an acceleration in the 0% CNC mixture (compared to the 100OPC-
757   CNC0.0 mixture), but with increase in CNC dosage, the peak shifted with CNC content to later
758   ages (i.e., from 2 hours (0% CNC) to 5 hours (1% CNC)). In both OPC-SL50 and PLC-SL50
759   mixtures, the slag hydration peak, characterized by the third peak (after approximately 24 hours)
760   had lower intensity with CNC addition. For instance, in OPC-SL50-0.0% CNC mixture the slag
761   hydration peak intensity was 1.2 mW/g binder occurring at 30 hours, whereas for the mixtures
762   with CNC, the peak was shifted to 35 hours with a lower heat flow intensity of 1 mW/g binder. A
763   similar trend was observed for PLC-SL50. It appears that addition of CNCs to OPC/PLC-SL
764   mixtures resulted in retardation of slag hydration.

765   For OPC-20FA-5SF (Figure 15c) and PLC-20FA-5SF (Figure 15d) mixtures, the observed trends
766   are similar. Any retardation in the pastes due to the presence of fly ash is compensated by the
767   presence of SF in 0% CNC mixtures. In case of mixtures with CNC, there appears to be a
768   retardation by 3 hours (OPC mixtures) and 5 hours (PLC mixtures). For mixtures with OPC-25FA-
769   25SL (Figure 29e) and PLC-25FA-25SL (Figure 29f), similar trends are observed; with increase
770   in CNC dosage, there is a shift in the silicate hydration peak to the right by a maximum of three
771   hours. However, a much longer retardation (as long as 10 hours) of the peak associated with the
772   slag hydration was observed at higher CNC dosage.

773   In all cases, the aluminate peak (or the sulfate depletion peak) for the mixtures with CNC had a
774   higher intensity compared to mixtures without CNCs. In case of FA mixtures, the silicate and the

775 aluminate peaks overlapped, indicating that CNC addition may be close to causing a sulfate
776 imbalance like conditions, similar to the observations made for mixtures with LS and CNCs.

777 Figure 16 shows the 7-day heat release for the mixtures studied here. The 7-day heat release values
778 for OPC-SCM ranged from 302 – 311 J/g binder for OPC mixtures, 268 – 275 J/g binder for OPC-
779 50SL mixtures, 251 – 259 J/g binder for OPC-25FA25SL mixtures, and 268 – 274 J/g binder for
780 OPC-20FA5SF mixtures when CNC dosages were varied from 0 – 1% by volume of binder. The
781 7-day heat release values for the PLC-SCM mixtures ranged from 285 – 287 J/g binder for PLC
782 mixtures, 247 – 258 J/g binder for PLC-50SL mixtures, 233 – 241 J/g binder for PLC-25FA25SL
783 mixtures, and 248 – 251 J/g binder for PLC-20FA5SF mixtures when CNC dosages varied from 0
784 – 1% by volume of binder.

785

786

787   (a)

788

789

40

790

791   (b)
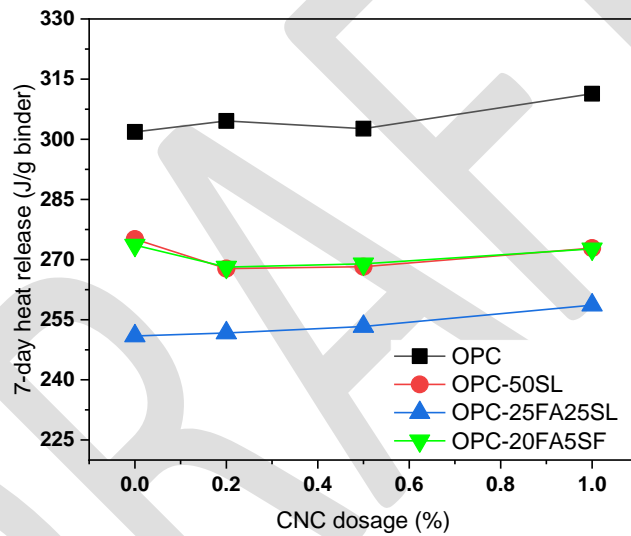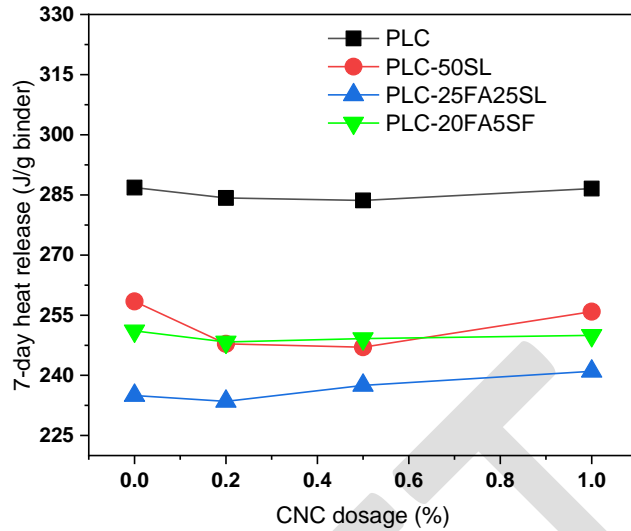
792   Figure 16. Effect of CNC dosage on 7-heat release (a) OPC mixtures (b) PLC mixtures

793   It was observed that overall, the CNCs addition did not significantly affect the 7-day heat release
794   value of the mixtures with SCMs. The 7-day heat release values of the mixtures with CNCs were
795   usually within $\pm$2% of the 7-day heat release values of the respective mixtures without CNCs.
796   When CNCs were added at low dosages of 0.2 and 0.5% to PLC-50SL mixture, it was observed
797   that the 7-day heat release was reduced by 4.1 and 4.4%, respectively, and this needs to be further
798   investigated. When CNCs were added at 1.0% dosage to OPC-25FA25SL and PLC-25FA25SL
799   mixture, the 7-day heat release values were increased by 3.1 and 2.6%, respectively. The
800   adsorption behavior of CNCs on SCMs is not known, and it could be playing an important role in
801   terms of reaction rate of SCMs. More research work is needed to explain possible mechanisms for
802   the role of CNCs in hydration of SCM mixtures.

803   **4.2.2. B3B flexural strength**

804   Figure 17 shows a parity plot for the 28-day and 56-day B3B flexural strength for the mixtures
805   with and without CNCs. It should be noted that the B3B flexural strengths indicate characteristic
806   strength of the mixtures, and they are higher than flexural strength determined using conventional
807   flexural strength testing due to the size effect.

41

808

809

810

(a)

811

812

(b)
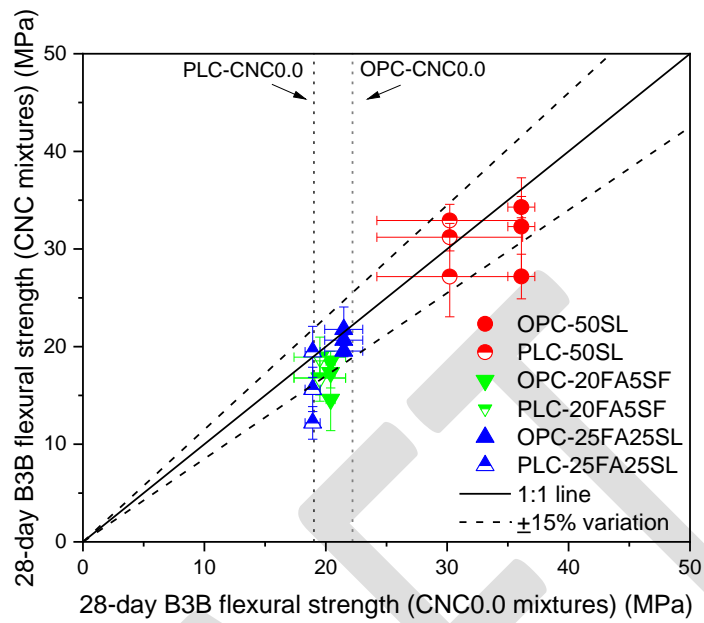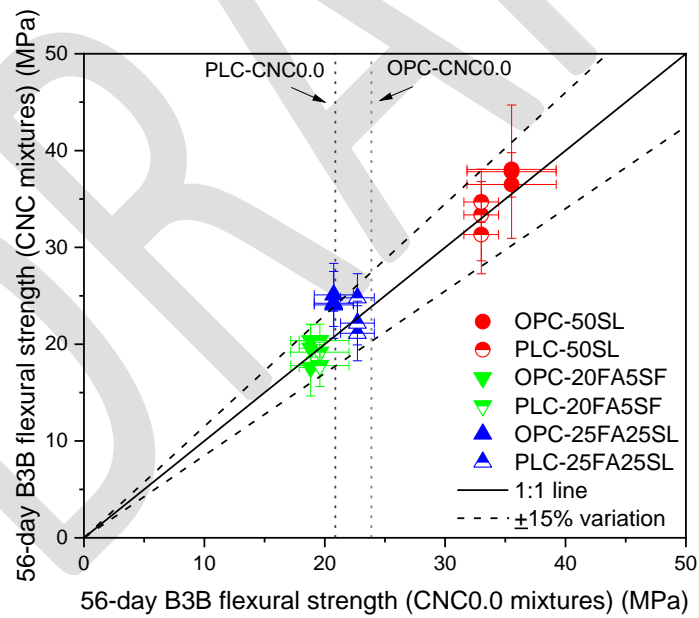
Figure 17. Effect of CNC dosage on B3B flexural strength – (a) 28 days (b) 56 days. A data
point on the 1:1 line indicates similar performance, and a data point above the 1:1 line indicates
better performance for mixtures with added CNCs (i.e., the measurement on the Y-axis).

816 With CNC addition, B3B flexural strength of the most mixtures were within 15% of the flexural
817 strength of the mixtures without CNC. The 28-day B3B flexural strengths of the mixtures that had
818 lower than 15% of the B3B flexural strengths of the mixtures without CNC were OPC-50SL-
819 CNC1.0, OPC-20FA5SF-CNC0.5, and PLC-25FA25SF-CNC0.5. With the exception of the three
820 mixtures, it can be said that the addition of CNCs did not have an adverse effect on the 28-day
821 flexural strengths of the mixtures with SCMs.

822 It was observed that the mixtures with PLC and SL, PLC-50SL and PLC-25FA25SL, had
823 improved strength from 28 days to 56 days. No adverse effects of adding CNCs in terms of flexural
824 strength was seen at 56 days, as none of the mixtures with CNCs had lower than 15% of the flexural
825 strength of the mixtures without CNCs. It was observed that 56-day B3B flexural strength of OPC-
826 25FA25SL mixtures with CNC had slightly higher (by 1 to 6%) than 15% of the B3B flexural
827 strength of the OPC-25FA25SL-CNC0.0.

828 **4.2.3. Bulk resistivity and pore structure characteristics**

829 The 28-day and 56-day saturated bulk resistivity values of the mixtures with OPC, PLC, and
830 different SCMs are shown in Figure 18. Bulk resistivities of the SCM mixtures with and without
831 CNCs were significantly higher than the OPC-CNC0.0 mixtures at both 28 and 56 days as seen in
832 Figure 18. Overall, the mixtures with 20FA5SF had the highest bulk resistivity among the mixtures
833 tested, likely due to the inclusion of finer material like silica fume that contributed to a reduction
834 in pore connectivity. At 28 days, the bulk resistivity of the SCM mixtures, except OPC-50SL,
835 decreased with the addition of CNCs at low dosages (0.2 and 0.5%) and increased at higher dosage
836 of 1.0% CNC. Only OPC-50SL and PLC-50SL had slightly higher 28-day resistivities (4.6 and
837 11.8%, respectively) at 1.0% CNC dosage when compared to the respective mixtures without
838 CNC. For OPC-50SL, the 28-day bulk resistivity of the mixtures were between 40.2 ohm.m and
839 47.4 ohm.m with varying CNC dosage.

840

841

842

843   (a)

844

845   (b)
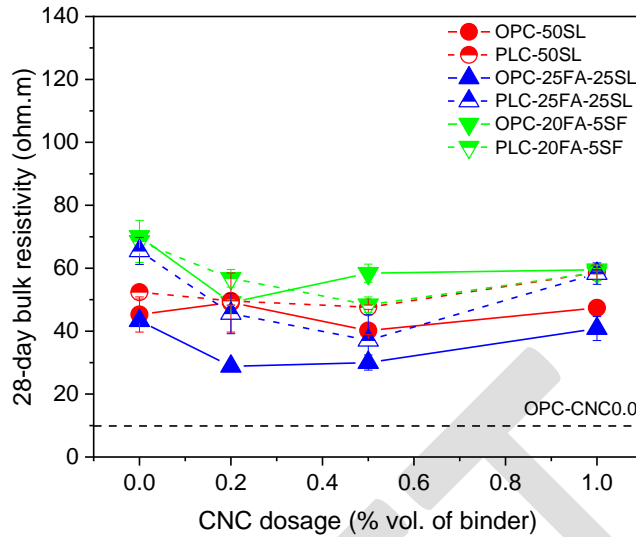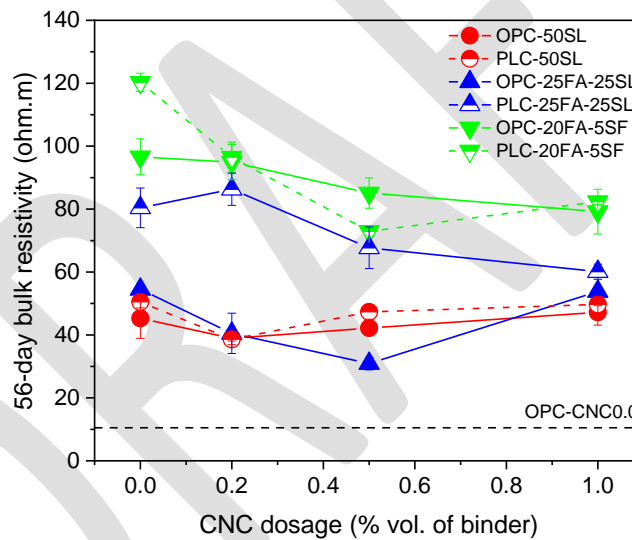
Figure 18. Effect of CNC addition on saturated bulk resistivity of the mixtures with SCMs (a) 28 days (b) 56 days.

At 56 days, it was observed that with the addition of CNCs, the bulk resistivities were decreased for most of the mixtures. The decrease in bulk resistivity with CNC addition ranged from 1.3% to 43.3%. The two mixtures that had higher bulk resistivity compared to their respective mixtures without CNC were OPC-50SL-CNC1.0 (higher by 4.2%) and PLC-25FA25SL-CNC0.2 (higher by 7.3%). The possible reasons for the overall trend of reduction in bulk resistivities with the addition of CNCs to the SCM mixtures include agglomeration of CNCs when SCMs are present and possible adsorption of CNCs on SCMs resulting in slower reaction of SCMs. A comparison

855 study is underway evaluating the long-term resistivity and chloride transport properties. The 28-
856 day and 56-day porosity data for the different mixtures with and without CNCs is shown in Figure
857 19. A thermodynamic modeling approach was used to provide an idea of how much porosity of
858 the samples would vary with different SCMs and SCM contents.

859

860
(a)

861

862
(b)
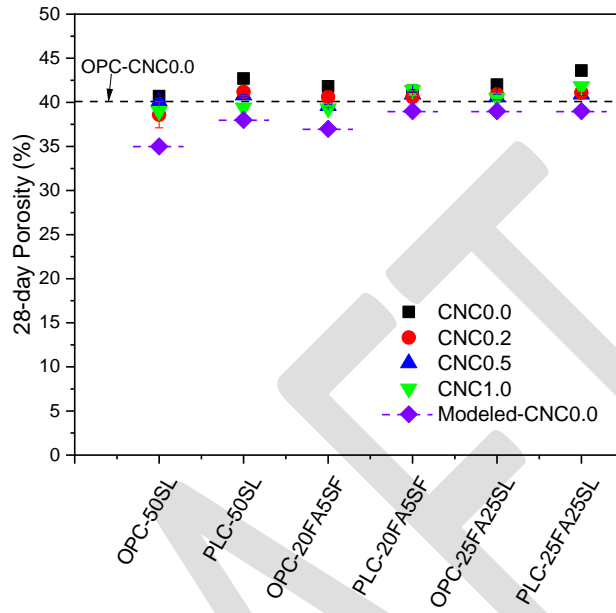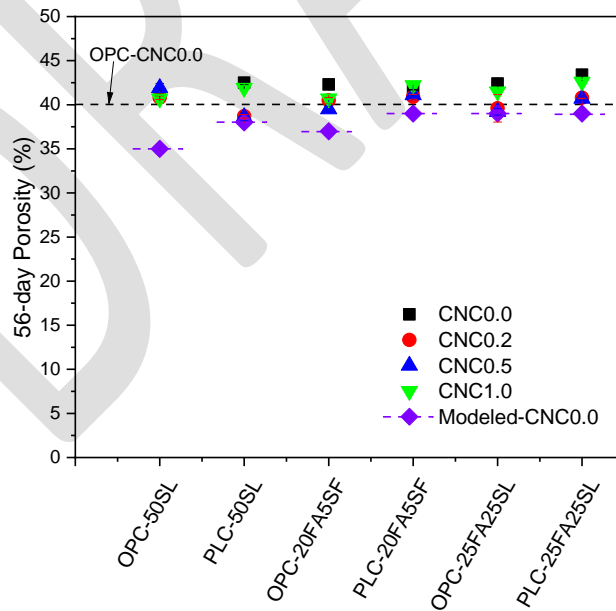
863
Figure 19. Porosity of the paste samples at (a) 28 days (b) 56 days

45

864 The porosity of CNC0.0 mixtures determined from thermodynamic modeling is shown in Figure
865 19 as a baseline to compare the porosity of mixtures with and without CNCs. The porosity of the
866 mixture OPC-CNC0.0 is also shown in Figure 19 as a reference. Minimal changes in total porosity
867 of the samples were observed when CNCs were added, and the variation was less than 3% for the
868 most mixtures and less than 4% for all the mixtures when compared to the corresponding mixtures
869 without CNCs. The mixtures that had more than 3% difference in porosity between the mixtures
870 with CNC and without CNC were PLC-50SL (CNC1.0 mixture at 28 days with 3.3% difference
871 and 56 days with 3.9% difference) and OPC-25FA25SL (CNC0.5 mixture at 56 days with 3.2%
872 difference).

873 The pore connectivity (β) of the mixtures determined at 28 days and 56 days are shown in Figure
874 20. It was observed that the pore connectivity of the SCM mixtures was significantly lower than
875 the OPC-CNC0.0 mixture as SCMs are known to improve the pore refinement. With the addition
876 of CNCs to the SCM mixtures, differences in the determined pore connectivity values were
877 observed. It was observed that the pore connectivity of the mixtures with CNCs were generally
878 higher than the respective mixtures without CNCs. Again, it is important to remember that SCMs
879 are even more effective at later ages so longer-term testing is still needed.

880
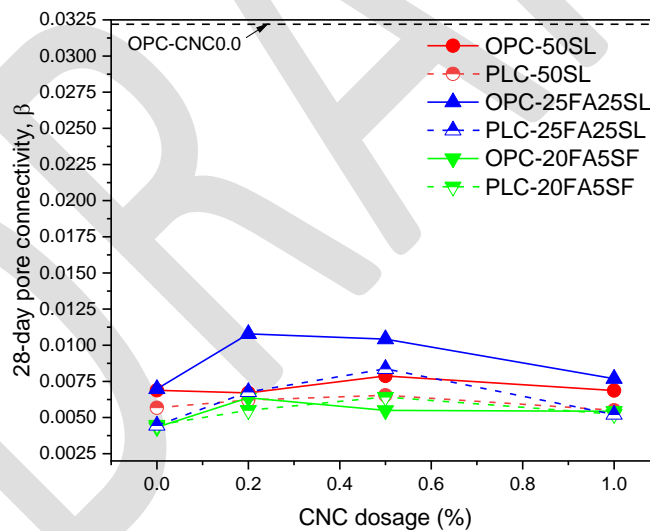
881

882   (a)
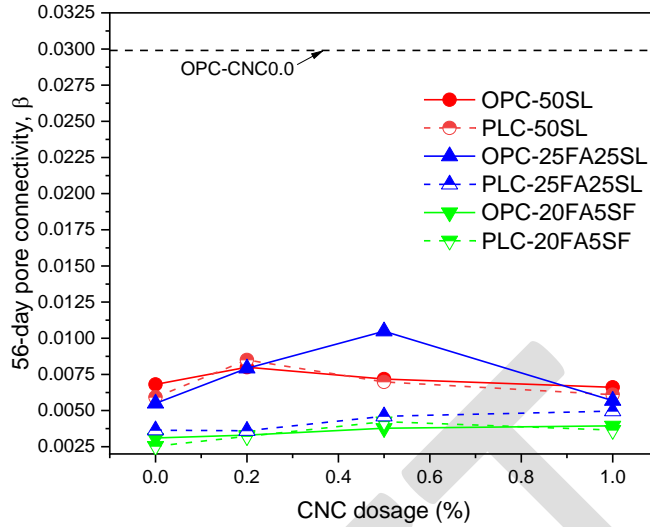
883

884   (b)

885   Figure 20. Effect of CNC dosage on pore connectivity (β) in the pastes (a) 28 days (b) 56 days

886   At 28 days, except the OPC-50SL mixture, the pore connectivity values peak at 0.2 or 0.5% CNC
887   dosage and reduce at 1.0% CNC dosage. In the case of OPC-50SL mixture, the 28-day pore
888   connectivity values were very similar at all CNC dosages except at 0.5% CNC dosage. Similar
889   trend was observed with 56-day pore connectivity values where it peaks at either 0.2 or 0.5% CNC
890   dosage and slightly reduces at 1.0% CNC dosage, with the exception of OPC-20FA5SF and PLC-
891   25FA25SL mixtures where the pore connectivity increased with increase in CNC dosage. The 28-
892   day pore connectivity values of the SCM mixtures ranged from 0.0045 to 0.0108, which are
893   significantly lower (by 66 - 86%) when compared to pore connectivity value (0.0322) of OPC-
894   CNC0.0 mixture. The 56-day pore connectivity values of the SCM mixtures ranged from 0.0025
895   to 0.0105, which are significantly lower (by 65 - 92%) when compared to pore connectivity value
896   (0.0299) of OPC-CNC0.0 mixture. The general increase in pore connectivity values with the CNC
897   dosage can explain the general decrease in saturated bulk resistivity of the SCM mixtures with
898   CNCs as the porosity did not significantly change with the CNC addition.

899   4.3. Conclusions

900   OPC-SCM-CNC and PLC-SCM-CNC mixtures were evaluated for CNCs use in the mixtures with
901   SCMs. Overall, CNCs addition to the SCM mixtures did not significantly affect the 7-day heat
902   release values, except the 25FA25SL mixtures where a reduction of up to 4.4% in 7-day heat
903   release at low CNC dosages. In the mixtures with 25FA25SL, there was up to 3.1% increase in 7-
904   day heat release at 1.0% CNC dosage. The interaction between CNCs and SCMs need to be
905   understood to clearly explain the effect of CNCs on the degree of hydration of the SCM mixtures,
906   and ongoing work is currently underway.

47

907 The 28- and 56-day B3B flexural strength of the majority of the SCM mixtures with CNC were
908 within +15% of the flexural strength of the respective mixtures without CNC. At 56 days, the
909 addition of CNCs improved the flexural strength of OPC-25FA25SL mixtures by 16 (at 1.0%
910 CNC) – 21% (at 0.5% CNC).

911 The addition of low dosages of CNCs up to 0.5% resulted in an overall increase in pore
912 connectivity of the SCM mixtures and reduction in bulk resistivity measured at 28 and 56 days. It
913 was noted that the 28-day pore connectivity values of the SCM mixtures ranged from 0.045 to
914 0.0108, which were significantly lower than the 28-day pore connectivity value of 0.0322 for OPC-
915 CNC0.0 mixture. The 56-day pore connectivity values of the SCM mixtures ranged from 0.025 to
916 0.0104, which were again significantly lower than the 56-day pore connectivity value of 0.0299
917 for OPC-CNC0.0 mixture. The 56-day saturated bulk resistivity values ranged from 30.9 to 120.3
918 ohm.m for the mixtures with SCMs depending on type of SCM and CNC dosage, which were
919 significantly higher than the 56-day bulk resistivity value of 10.5 ohm.m for OPC-CNC0.0
920 mixture.

921 The overall trend of reduction in bulk resistivities and increase in pore connectivity with the
922 addition of CNCs to the SCM mixtures could be due to the agglomeration of CNCs, alteration of
923 the pore structure due to delayed early hydration, and possible adsorption of CNCs on SCMs
924 resulting in lower reaction of SCMs. Further research is needed to understand the adsorption
925 behavior of CNCs on SCMs and evaluate the resulting effect on the performance of the SCM-CNC
926 mixtures. Future research shall also include studying the effect of reduction in pH of the pore
927 solution in the SCM mixtures on CNCs performance in the mixtures.

5. CHAPTER 4: Full Scale Field Trials of Slabs Placement using Mixtures with Limestone and CNCs at UC Davis Pavement Research Center

928
929

930 This chapter of the report summarizes the results of the implementation of the use of cellulose
931 nanocrystals (CNC) in portland cement concrete (PCC) pavement. In this experiment, the use of
932 CNC is evaluated in combination with portland-limestone cement (PLC) and compared with
933 ordinary portland cement (OPC) concrete in a set of pilot slabs built on the research site of the
934 University of California Pavement Research Center (UCPRC) in Davis, California.

5.1. Test Sections Preparation

935

936 Three test sections were built for three mixtures. The three mixtures were i) OPC mixture with
937 30% slag (labelled as OPC), ii) PLC mixture with 30% slag (labelled as PLC), and iii) PLC mixture
938 with 30% slag and 0.1% CNC (labelled as CNC). The location of the test sections is shown in
939 Figure 21 (picture taken after the application of the curing compound on the lean concrete base)
940 and Figure 22 (picture taken after the construction of the concrete slabs).

941

942 Figure 21. Location of test sections (white path at the bottom of the picture; picture taken after
943 the application of the curing compound on the lean concrete base).

944

945   Figure 22. Test sections (from picture bottom to top: PLC, CNC, and OPC)

946 **5.1.1. Test sections configuration**

947 The test sections were designed to study mixture constructability and mid-term (less than a year)
948 ambient environmental response. While mechanical and durability characteristics of the mixtures
949 are important as well, they do not constitute the main focus of the test sections experiment.
950 Mechanical properties were evaluated based on laboratory testing of specimens prepared from
951 mixtures sampled during the test sections construction. Limited durability laboratory testing was
952 conducted on specimens also prepared from the construction mixtures.

953 One of the goals of the experiment is to evaluate the ambient environmental response, focused on
954 moisture-related shrinkage and thermal deformations. To maximize those deformations, the
955 concrete slab thickness was set to a low value, 4 inches and slab width was set to 8 feet, rather than
956 the conventional 12 feet, so that the consolidation could be achieved with a vibrating rolling screed
957 while maintaining the 4 inch slump of the mixtures.

958 The location of the test sections was selected to build a walking path at the UCPRC site in Davis.
959 The total length of the walking path is approximately 70 feet, with an approximately 45 feet useful
960 length that is not affected by shading from nearby buildings so that uniform solar exposure could
961 be obtained. The three test sections, one per mixture type, were built along the useful length. Each
962 section consists of three 5 feet long slabs as shown in Figure 23.

PLC   CNC   OPC

5×8 ft

45 ft

⊗ Instrumented slabs | Full-depth joints (metal form)
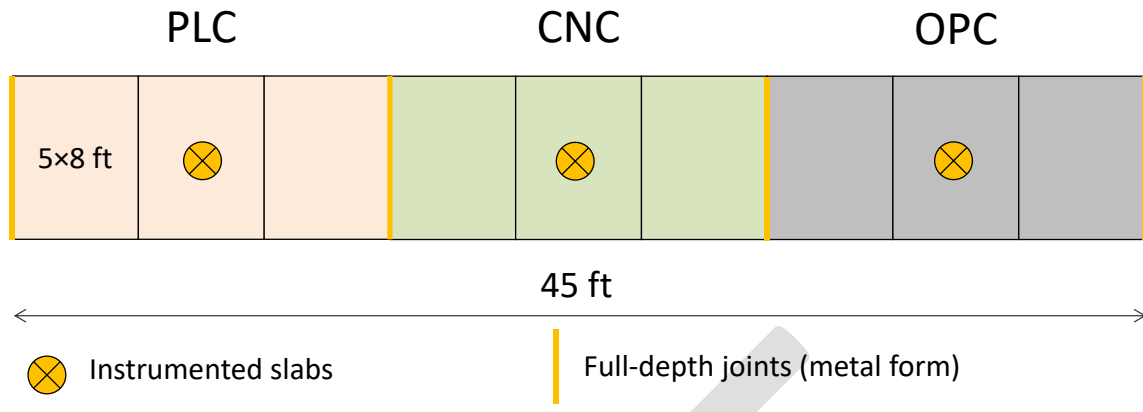
963

964   Figure 23. Test sections layout

965   Beneath the 5×8 ft (length × width) and 4 inch thick slabs is a lean concrete base that is 4 inch
966   thick, which in turn was placed on a 3 to 4 inch thick aggregate subbase (Figure 24). The subgrade
967   is clay. The shoulder was backfilled with loose aggregates after the construction of the concrete
968   slabs.

5×8 ft   10 ft

Sawcut (1.3 in.)   *Curing compound interlayer*

4 in.

4 in.   Lean Concrete Base
3-4 in.   Aggregate subbase
                                   Clay subgrade
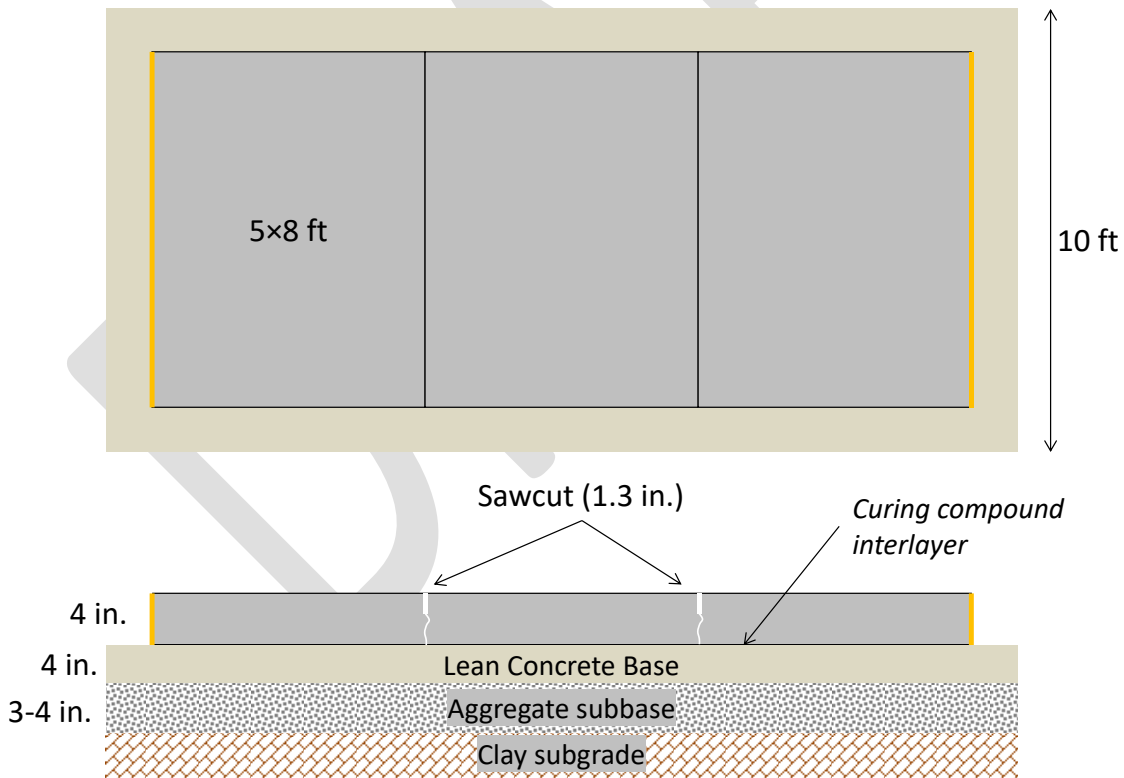
969

970   Figure 24. Test section configuration

51

5.1.2. Test section instrumentation

The instrumentation installed in each of the sections, shown in Figure 25, focuses on measuring the response to the ambient environment loading. The instrumentation of each section includes:

- Two thermocouples on rods for measuring temperature profile in the slabs and base.
- Two relative humidity (RH) sensors. The RH sensors are Sensirion SHT85, housed in a porous plastic tube.
- Two pairs of GeoKon 4200 vibrating wire strain gages (VWSGs), located at two of the slab corners, 10 in. from the shoulder edge of the slabs. Each pair includes a VWSG close to the top of the slab (0.8 in. from top) and another VWSG close to the bottom of the slab (0.8 in. from bottom).
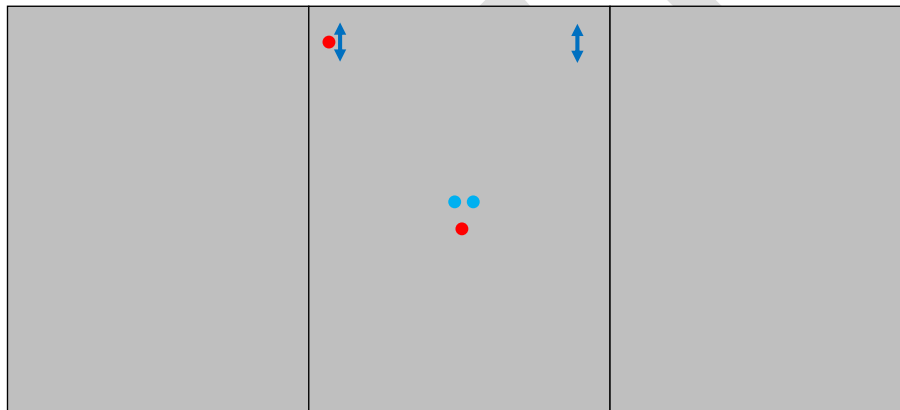
● Thermocouples rod; five depths: 0.2 in. / 0.8 in. / 2 in. / 4 in. (slab bottom) / 6 in. (lean concrete base)

● RH sensor (0.8 in. Depth)

↔ VWSGs; two depths: 0.8 in. / 3.2 in. (0.8 in. above slab bottom)

Figure 25. Test section instrumentation (Not to scale)

In addition to the instrumentation embedded in the test sections, three prisms per concrete mixture were fabricated and instrumented with a VWSG each (Figure 26 left). The prisms are 20×6×1.6 in. in size and they are referred as unrestrained shrinkage prisms (USP) in this report. The concrete for the prisms' fabrication was the same used for the construction of the slabs (sampled from the ready-mix trucks) although screened through 3/4 in. sieve to remove the largest aggregates. These prisms were cured the same as the slabs and left outdoors by the test sections so that they were subjected to the same ambient environmental conditions (Figure 26 right). These prisms measure the unrestrained deformations of the concrete as they are not bonded to any support.

992   Figure 26. Unrestrained shrinkage prisms

993   5.2. Materials and Mixtures

994   The chemical composition and fineness of OPC, PLC, and Ground granulated blast furnace slag
995   used are shown in Table 5. As expected, the PLC has higher fineness than OPC [38]. The mill
996   certificates of the cementitious materials are attached in the Appendix section. The three mixtures
997   were i) OPC mixture with 30% slag (OPC), ii) PLC mixture with 30% slag (PLC), and iii) PLC
998   mixture with 30% slag and 0.1% CNC (CNC).

999   Table 5. Chemical composition and fineness of OPC, PLC, and Slag used (NA: not available)

%	OPC	PLC	GGBFS
SiO_2	20.3	18.4	NA
Al_2O_3	4.1	3.5	17.5
Fe_2O_3	3.9	3.0	NA
CaO	62.4	58.4	NA
MgO	4.9	4.2	NA
SO_3	3.1	3.0	2.5
LOI	2.6	10	NA
Na_2O	0.19	0.24	0.45
K_2O	0.41	0.30	(Na_2O_e)
Limestone	3.4	14	NA
Blaine Fineness, cm^2/gm	4184	5470	4780

1000

1001   **5.2.1. OPC mixture**

1002   The OPC mixture design and materials were supplied by Cemex (Perkins plant, in Sacramento
1003   area). This mixture is used for concrete paving in regular applications where high early strength is

53

1004 not required. The mixture is designed to achieve the strength needed to open to traffic (550 psi
1005 flexural strength) in 10 days. The mixture design is shown in Table 6.

1006   Table 6. OPC mixture design (1 cy)

Material	Description	Design quantity
Coarse Aggregate	Gravel	1900 lb
Fine Aggregate	Sand	1313 lb
Cement	Type II/V ordinary portland cement (OPC), ASTM C150	413 lb
Ground granulated blast furnace slag (GGBFS)	Slag, Grade 120, ASTM C989	177 lb
Water reducer	Master Glenium 7500	4 oz/cwt
Water	-	34.0 gal

1007

1008 The Type II/V cement was produced by the Cemex Victorville plant (California). The slag was
1009 produced in Rizhao (China); slag content is 30% of total cementitious materials.

1010 For water-reducing admixture, the Master Glenium 7500 was selected after showing acceptable
1011 compatibility with the CNC suspension. The Master Glenium 7500 is a high-range water-reducing
1012 admixture, based on polycarboxylate technology, meeting ASTM C494 Types A and F
1013 specifications. The water-reducer content was based on trial batching conducted with the PLC
1014 mixture by UCPRC. All three mixtures were batched with 4 oz/cwt of Master Glenium 7500
1015 following the mix design.

1016 The water-reducer typically used by the supplier for this mixture, based on lignosulphonate
1017 technology, was assumed to be incompatible with a CNC slurry produced by sulfuric hydrolysis
1018 evaluated in the preliminary phase of this experiment.

1019 Some other properties of the OPC mixture are listed below:

1020   • Crushed alluvial aggregates, mainly siliceous
1021   • Water/total cementitious ratio is 0.481
1022   • Non-air-entrained concrete
1023   • Design slump: 4 inches

1024 **5.2.2. PLC mixture**

1025 The PLC mixture is the same as the OPC mixture except for replacement of the Type II/V cement
1026 with portland-limestone cement (Type IL, ASTM C595), on a one-to-one basis. The Type IL
1027 cement was produced by the Cemex Victorville plant (California). All other materials and
1028 quantities in Table 1 remain the same in the PLC mix

5.2.3. CNC mixture

The CNC mixture is the same as the PLC mixture except for the addition of the cellulose nanocrystals. The added CNC content is 0.1% (CNC solids by weight of total cementitious materials); this is 0.590 lb of CNC solids per cy of concrete.

The CNC was supplied by Forest Products Laboratory (FPL) and produced by sulfuric acid digestion (product name: 2022-FPL-CNC-213). According to FPL, from this production method, CNC has sulfuric half-esters on the surface. The CNC solids are rigid rods typically about 5 nm wide by 100-150 nm long. The product was supplied as a suspension with 10.4% CNC solids content.

5.3. Test Sections Construction

The subbase was prepared by the UCPRC team in April 2022. The lean concrete base (LCB) was supplied by Elite ready mix and placed and consolidated by Vanguard on May-6, 2022. The concrete was supplied by Cemex ready mix plant in Perkins, close to Sacramento, and placed, consolidated, and cured by UC Davis Facilities Construction team with support from UCPRC on June-27, 2022. The fresh concrete QC and specimen preparation were conducted by Twining with support from UCPRC team.

The timing of the construction of the slabs (June-27, 2022) is summarized below:
- Ready mix truck 1, CNC mixture: 12:50-12:55
- Ready mix truck 2, PLC mixture: 13:55-14:00
- Ready mix truck 3, OPC mixture: 14:45-14:50

The weather conditions during paving were dry and warm, with air maximum temperature and minimum relative humidity (RH) approximately 105°F (40°C) and 15%, respectively. Wind speed was below 2 mph and the sky was clear. Air minimum temperature and maximum RH, during the first nights after construction, were approximately 60°F (15°C) and 80%, respectively. Days following construction had similar weather conditions, typical of Davis during summer.

The concrete was consolidated with a vibrating rolling screed and finished with trowel. No surface texturing was applied. The curing was conducted with white pigmented, resign based, curing compound meeting ASTM C309 Type 2B specifications, applied at a nominal rate of 150 ft²/gal.

A few construction pictures are shown in Figure 27 - Figure 29. Figure 28a shows the test section after the preparation and before the concrete placement. Figure 28b shows the placement of PLC mixture. Figure 28c shows the use of vibrating rolling screed for the CNC mixture and Figure 28d shows finishing of OPC mixture.

1061

1062 Figure 27. Test section instrumentation; left: thermocouple rod and pair of VWSFs; right:
1063 thermocouple rod and two RH sensors

(a)　　　　　　　　　　　　　　　　(b)

(c)   (d)

Figure 28. Slabs construction pictures; (a) before concrete pouring; (b) placing PLC concrete; (c) consolidating CNC concrete; (d) finishing OPC concrete section

Figure 29. Trowel finishing of PLC section (bottom of photograph); CNC section already sprayed with curing compound (middle of photograph; note that white covering is from the curing compound and not the CNC effect); rolling screed consolidation of OPC concrete (middle-top of photograph).

5.3.1. Control of water content

The three mixtures (OPC, PLC, and CNC) all have a design water to cementitious materials ratio
of 0.481, equivalent to 34.0 gal of water per cubic yard of concrete. The following steps were
followed to ensure that the three mixtures would be produced with the same amount of mixing
water:

• The three mixtures were batched at the plant with a target of 31.0 gal of water/cy.

• The actual amount of water added at the plant (batch water plus any water added by the
truck driver) was noted in the truck dispatch.

• The remaining water (to match exactly 34.0 gal/cy) was added at the construction site
either directly from the truck tank or as part of the CNC suspension.

The water content of the fresh concrete was measured following AASHTO T 318. Three specimens
were tested per mixture type. The results are shown in Figure 30. The PLC and the CNC mixtures
had similar measured water contents. For the three mixtures, the measured water contents were
over the 8.9% theoretical water content (the theoretical water content is the same for the three
mixtures).
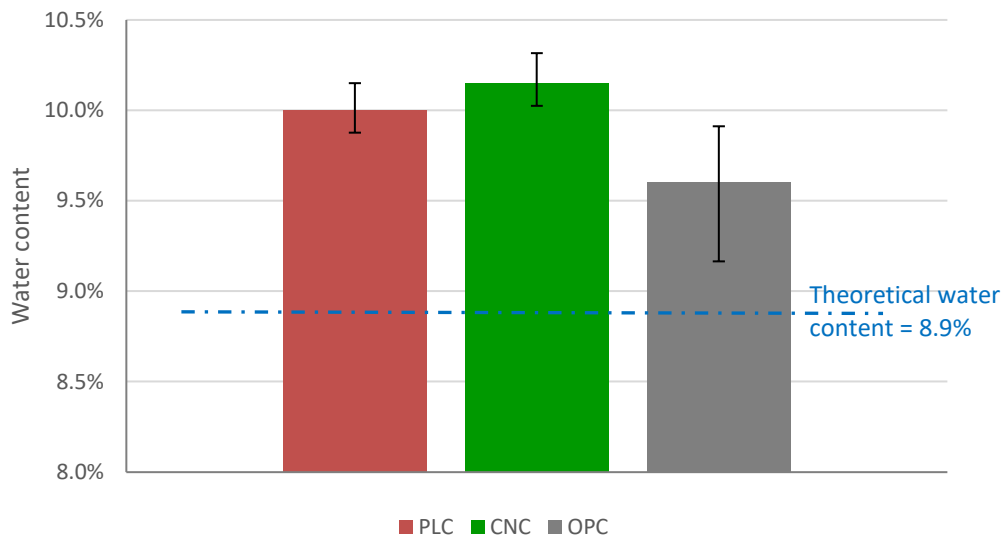
Figure 30. Measured water content (evaporable water / dry weight of mixture, AASHTO
T 318) (Note: The theoretical water content includes the design batch water plus the water
absorbed by the aggregates in the saturated surface-dry (SSD) condition.)

5.3.2. CNC addition

The CNC were dispersed in their water suspension 4-5 hours before mixing into concrete (CNC
solids content of the suspension was 3.33%). A high-shear blender (Waring CB15 Commercial

1093 Blender) was used for this purpose. The CNC suspension was blended at 4000 rpm for 60 seconds
1094 twice. When the concrete truck arrived at the construction site, the CNC suspension was added to
1095 the concrete ready-mix truck from the hopper (Figure 31). The concrete was then mixed at the
1096 maximum speed (14-16 rpm) for five minutes.

1097

1098   Figure 31. Addition of the CNC suspension to the ready-mix truck at the construction site

1099 ## 5.4. Experimental Methods

1100 Fresh concrete mixtures were tested for consistency by measuring slump following ASTM
1101 C143/C143M-20, temperature following ASTM C1064/C1064M-17, air content using the
1102 pressure method following ASTM C231/C231M-17, and unit weight following ASTM
1103 C138/C138M-17. In addition, setting time of the concrete was measured following ASTM C403.
1104 Three specimens per mixture were tested for the setting time measurement.

1105 The concrete specimens were prepared with mixture sampled from the corresponding read-mix
1106 truck during the slabs construction. The specimens were cured in wooden boxes or covered with
1107 wet burlap, in the either case inside a room, until 24 hours (Figure 32). Then they were demolded
1108 and stored in lime water at 23°C until testing. The laboratory testing included several properties
1109 evaluated at different times as shown in Table 7. Three specimens were tested for each property
1110 measurement.
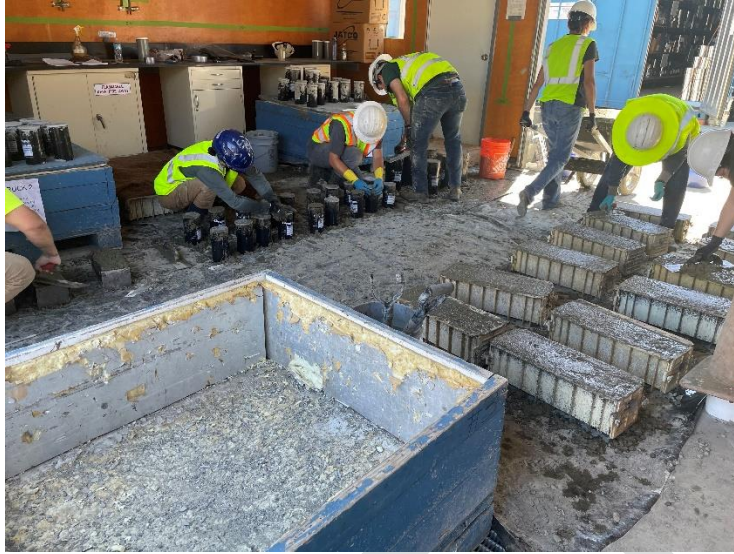
1111

1112   Figure 32. Specimen preparation and wooden boxes

1113   Table 7. List of hardened properties tested

Property	Standard	Specimen size (in.)	Testing times [1]
Flexural strength	ASTM C78	6×6×20 beams	10 days, 28 days, and 4 months
Compressive strength	ASTM C39	4×8 cylinders	10 days, 28 days, and 4 months
Modulus of elasticity	ASTM C469	6×12 cylinders	10 days, 28 days, and 4 months
Bulk electrical resistivity	ASTM C1876	4×8 cylinders	10 days, 28 days, and 4 months
Coefficient of thermal expansion (CTE)	AASHTO T 336	4×7 cylinders	42 days
Drying shrinkage	ASTM C157 [2]	4×4×11 prims	Up to 4 months

1114   [1] A fourth set of specimens was prepared for testing at 1 year age. Testing results not included in this report.
1115   [2] Except for the water immersion period; in this research, the specimens were subjected to drying at 7-day
1116   age.

1117 5.5. Experimental Results

1118 5.5.1. Fresh properties

1119 Fresh concrete testing results are presented in Table 8.

1120   Table 8. Fresh concrete testing results

Mixture	Slump (in.)	Temp	Air Content (%)	Unit Weight (lb/ft³)
PLC	6.50	88.2 °F (31.2 °C)	2.2	146.6
CNC	5.75	85.5 °F (29.7 °C)	1.9	147.8
OPC	7.75	88.9 °F (31.6 °C)	1.9	149.8

1121

1122   The slump of the mixtures with Type IL cement (PLC and CNC) was slightly lower than the slump
1123   of the mixture with Type II/V cement (OPC) with similar water content, indicating a higher water
1124   demand of the Type IL cement versus the Type II/V, for the same consistency. Most likely, this
1125   outcome is due to the higher fineness of the Type IL cement (Blaine 5470 cm²/g) compared to the
1126   Type II/V cement (Blaine 4184 cm²/g) used in this experiment (Blaine fineness from Cemex
1127   cement mill test reports).

1128   The small temperature differences between mixtures are most likely due to the different time of
1129   the day when each mixture was placed (CNC at approximately 1:00 pm, PLC at approximately
1130   2:00 pm, and finally OPC at approximately 3:00 pm).

1131   The construction workers and industry experts present at the construction site commented on the
1132   "creamy" consistency of the two mixtures with Type IL cement (CNC and PLC) compared to the
1133   mixture with Type II/V (OPC). The creamy consistency, based on construction workers and
1134   industry experts' opinion, would improve the constructability and reduce the segregation of the
1135   mixture. Most likely, this outcome is also due to the higher fineness of Type IL compared to the
1136   Type II/V cement used in this experiment.

1137   Construction workers and industry experts did not observe consistency or workability differences
1138   between the two mixtures with Type IL cement (CNC versus PLC).

1139   5.5.2. Setting time

1140   The setting time of the concrete was measured following ASTM C403. Three specimens were
1141   tested per mixture type. Penetration resistance evolution and set times are shown in Figure 33 and
1142   Table 9, respectively.
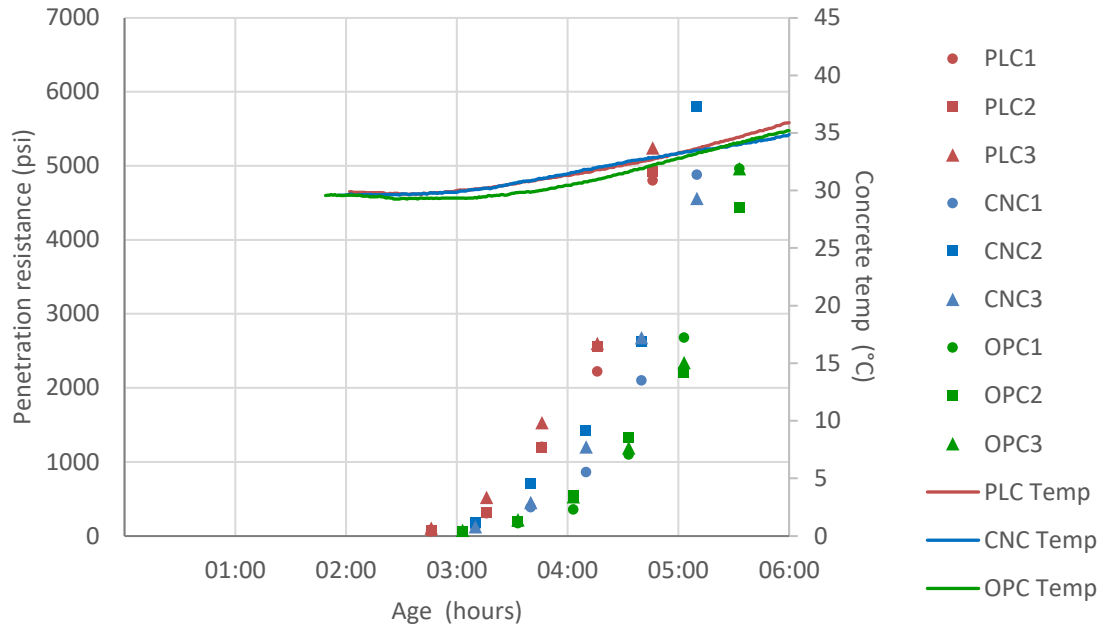
1143

1144 Figure 33. Penetration resistance (ASTM C403); temperature in the plot is measured in a dummy
1145 penetration resistance specimen

1146 Table 9. Setting time results (ASTM C403)

Mixture	Initial Set (∗) (500 psi)	Final Set (∗) (4000 psi)
PLC	3:25	4:30
CNC	3:45	4:55
OPC	4:05	5:25

1147 (∗) Set time is measured from the ready-mix truck batching time. For example, 4:30 means 4.5
1148 hours after the ready-mix truck batching.

1149 The OPC mixture's initial and final setting times were longer than the setting times of the two
1150 mixtures with Type IL, most like due to the lower fineness of the Type II/V compared to the Type
1151 IL. The setting time of the mixture with CNC was slightly delayed compared to the PLC mixture
1152 without CNC. It has been shown previously that CNC delays the set time of the cement, most
1153 likely by electrostatic dispersion of the cement [103] or the coating of clinker (primarily aluminate
1154 phases with CNC [6].

1155 **5.5.3. Hardened properties**

1156 The testing results are included in Figure 34 to Figure 39. Overall, the two mixtures with Type IL
1157 cement (CNC and PLC) were similar to each other for all properties (strength, modulus of

1158   elasticity, electrical resistivity, CTE, and shrinkage), with differences being either approximately
1159   10% or less (flexural and compressive strength) or not statistically significant at the 5%
1160   significance level (modulus of elasticity, electrical resistivity, CTE, and drying shrinkage).

1161   The two mixtures with Type IL (CNC and PLC) presented approximately 10-15% higher strength
1162   than the mixture with Type II/V (OPC). The resistivity of these two mixtures was also considerably
1163   better (higher) than the resistivity of the mixture with Type II/V. On the contrary, the mixtures
1164   with Type IL presented higher CTE than the mixture with Type II/V. Regarding drying shrinkage,
1165   the Type IL resulted higher strains in the short term (6 days drying) which is consistent with a
1166   more rapid hydration but lower strains after 4 months of drying, compared to the mixture with
1167   Type II/V. Overall, the differences between the two mixtures with Type IL versus the mixture with
1168   Type II/V were statistically significant.
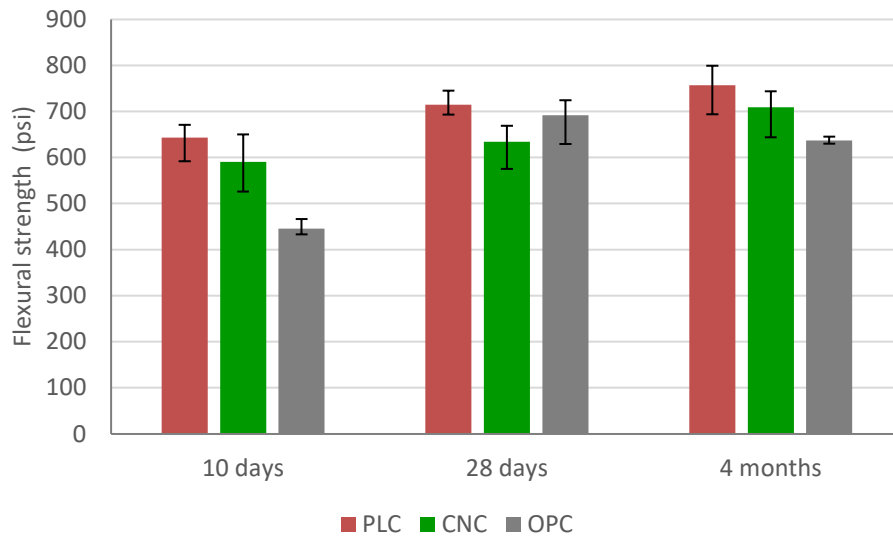
1169

1170   Figure 34. Flexural strength of the different mixtures
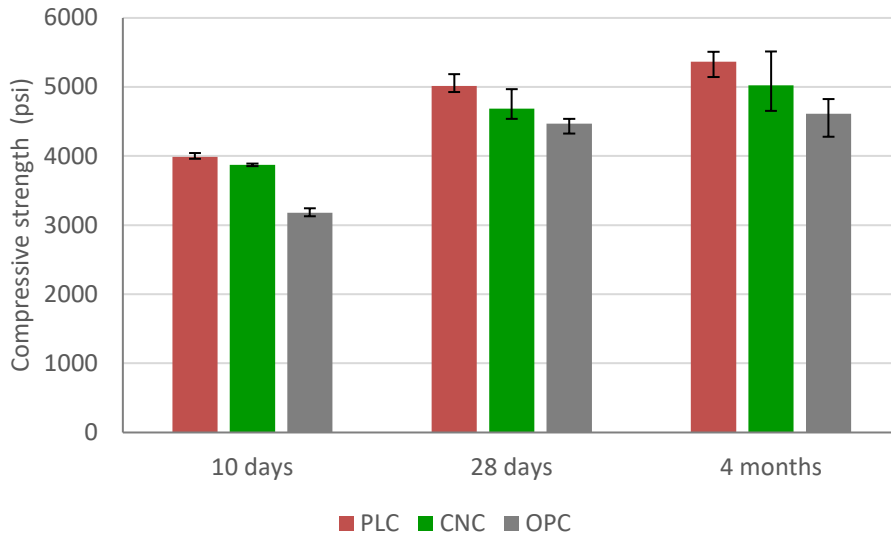
1171

Figure 35. Compressive strength of the different mixtures.

1173
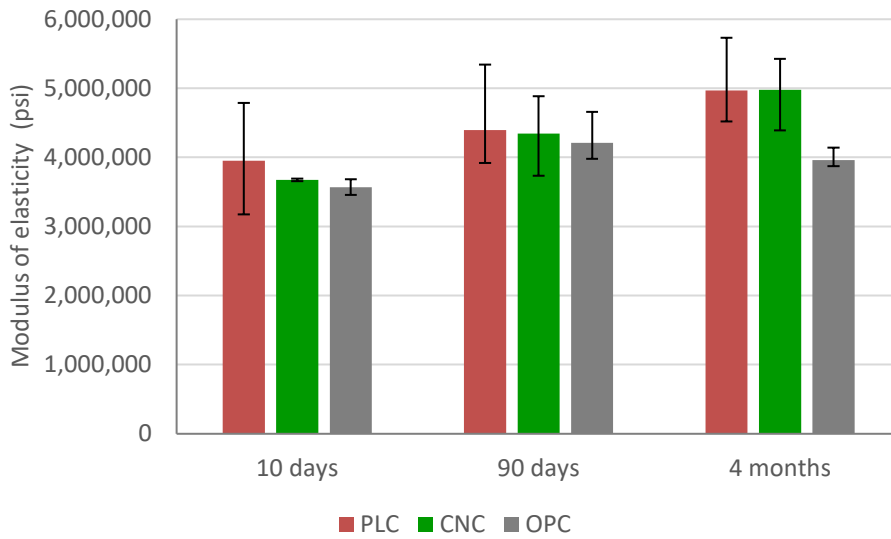
1174

1175   Figure 36. Modulus of elasticity of the different mixtures.

1176
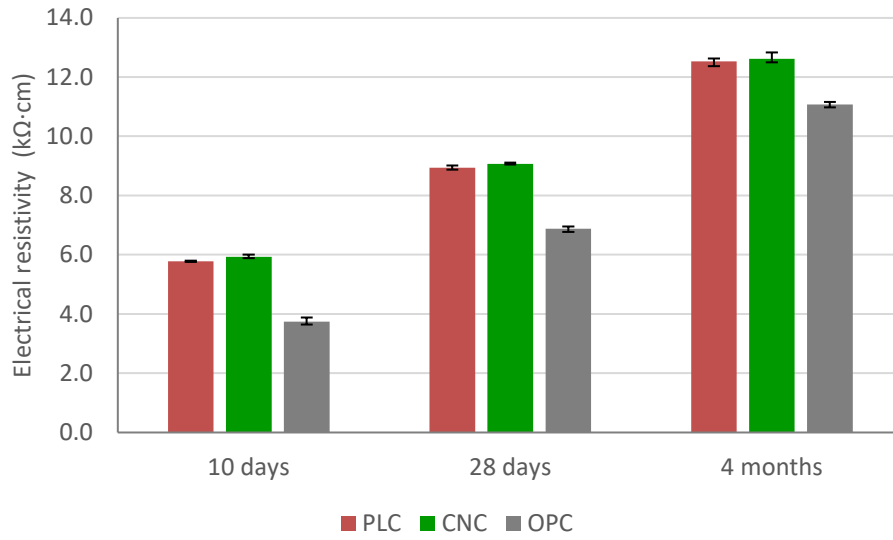
1177

Figure 37. Bulk electrical resistivity of the different mixtures.

1179
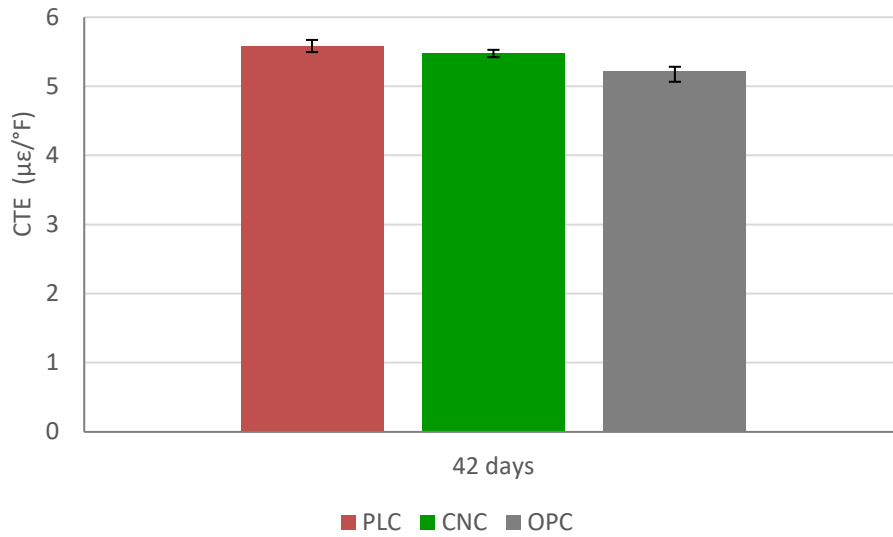
1180

Figure 38. CTE of the different mixtures.

1182
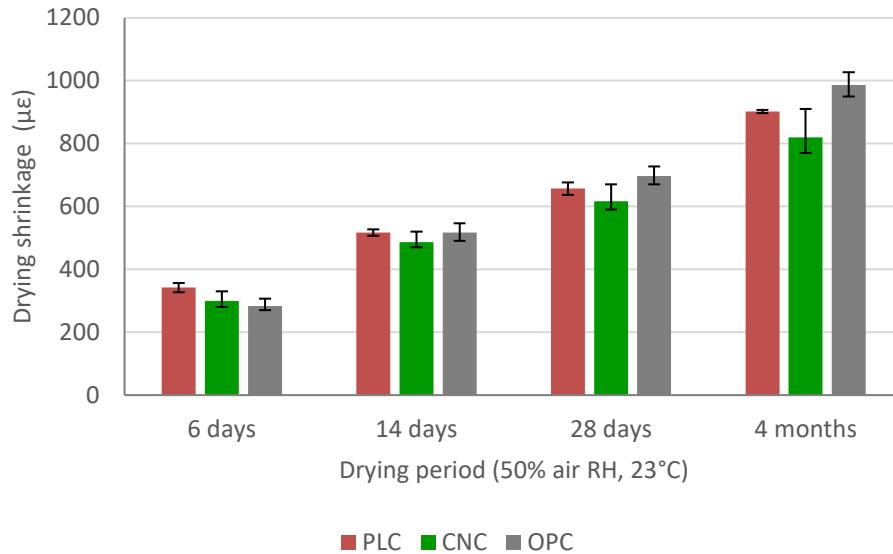
Figure 39. Drying shrinkage of the different mixtures.

5.5.4. Hygrothermal deformation of the slabs

One of the goals of the experiment is to evaluate the impact of the CNC addition on the moisture-related shrinkage and thermal deformations of the concrete. This evaluation was based on the strains measured with VWSGs in the two corresponding sets of slabs (CNC versus PLC sections). A secondary goal is to compare the mixture with Type IL cement versus the mixture with Type II/V cement (PLC versus OPC sections).

The strains measured with VWSGs in the three sections are presented in Figure 40 (ε_{MEAN}: mean strain, i.e. average of top and bottom of the slab) and Figure 41 (ε_{DIFF}: differential strain, i.e. top versus bottom of the slab). In all sections, a "field setting time" of 5 hours has been adopted as reference for strain calculation (ε is set to zero at the "field setting time"). The adoption of 5 hours is based on the setting time testing results presented in Table 9. The strain measured in the unrestrained shrinkage prisms is presented in Figure 42.

Note that there are two periods with missing data in Figure 40 and Figure 41: Aug-22 to Aug-30, and Sep-16 to Sep-30. In both cases, the problem was a failure in the data acquisition system electrical supply.

The average of all sensors per mixture type is shown In Figure 40 to Figure 42: the average of two pairs of VWSGs (located at each of the two instrumented corners in each section) in Figure 40 and Figure 41 and the average of three unrestrained shrinkage prisms per mixture type in Figure 42.

1204 Figure *43* shows an example of variability of strain measured within pairs of VWSGs. In this
1205 figure, the diurnal variations of the strain and temperature can be also observed.
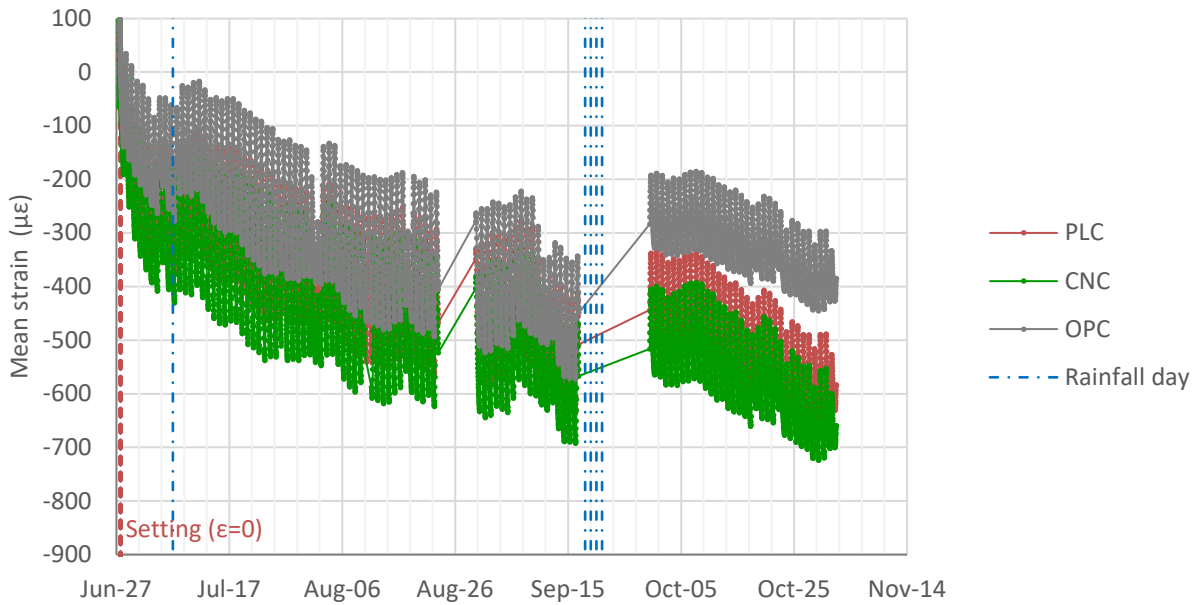
1206

1207 Figure 40. Mean strain measured in the slabs (average of top and bottom VWSGs; for each
1208 section, the average of two pairs of VWSGs is shown)

1209
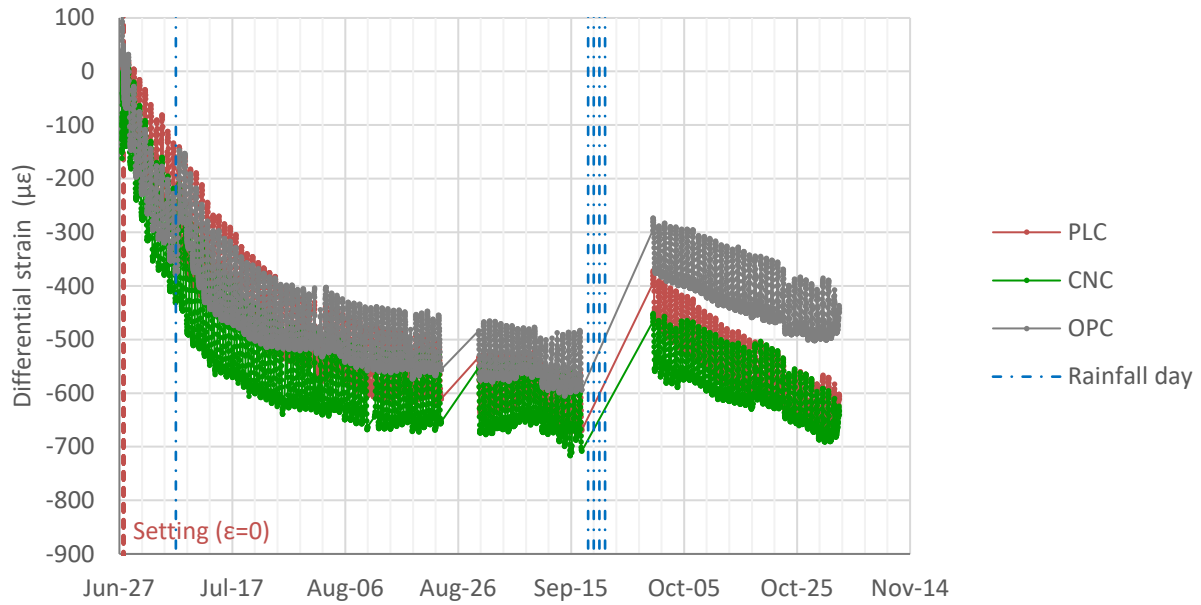
1210

1211   Figure 41. Differential strain measured in the slabs (difference between top and bottom VWSGs
1212   multiplied by H/D, where H is slab thickness [4 in.] and D is distance between VWSGs [2.4 in.];
1213   for each section, the average of two pairs of VWSGs is shown)

1214
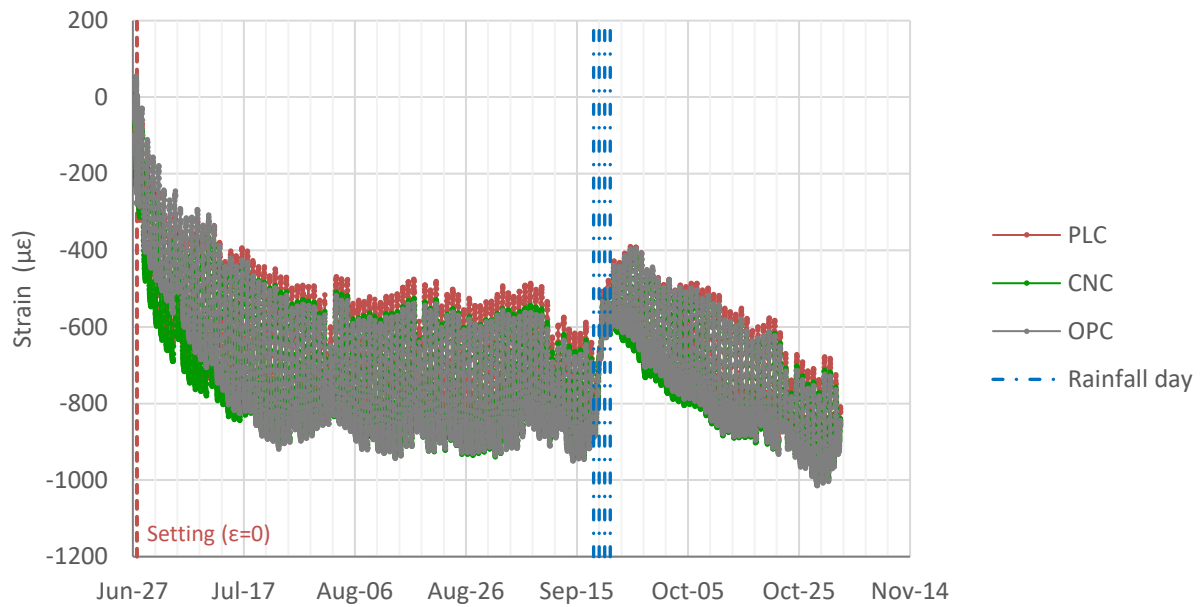
1215

1216   Figure 42. Strain measured in the unrestrained shrinkage prisms (for each mixture, the average of
1217   three unrestrained shrinkage prisms shown; one of the PLC prisms was regarded an outlier and
1218   discarded)

1219
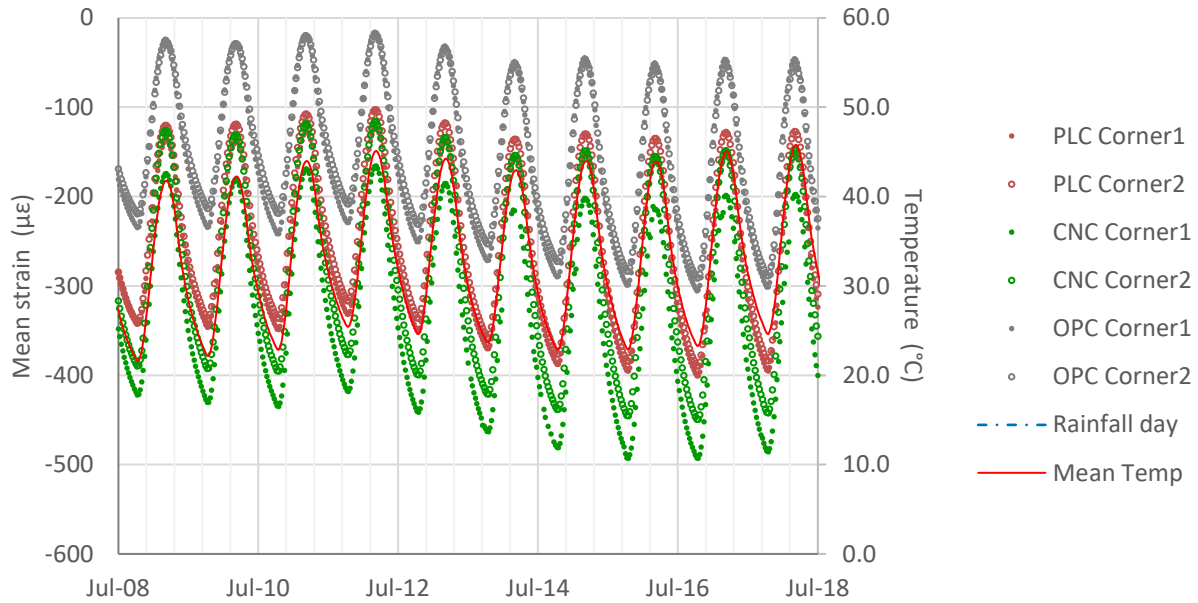
1220

1221 Figure 43. Example of diurnal variation of mean strain measured in the slabs (average of top and
1222   bottom VWSGs; Corner1 and Corner2 correspond to each of the two instrumented corners in
1223   each section; Mean Temp is the mean temperature of the slabs)

1224

1225 Based on the strains measured in the sections (Figure 40 and Figure 41) and in the unrestrained
1226 shrinkage prisms (Figure 42), it is evident that the CNC and PLC mixtures have similar
1227 hydrothermal deformations (moisture-related shrinkage and thermal strains).

1228 Further analysis of the strains measured in the sections and unrestrained shrinkage prisms was
1229 conducted to determine which part of the measured strain is related to the moisture-related
1230 shrinkage and which part is related to the thermal action. The strain data were fitted with the
1231 models shown in equations 11 and 12 below, following the methodology described in reference
1232 [104].

$$\Delta\varepsilon_{MEAN} \ = \ \Delta\varepsilon_{MEAN,Hyg} + \alpha \cdot CTE1(t) \cdot \Delta T_{MEAN} \qquad \text{(Eq. 11)}$$

1233 where: $\varepsilon_{MEAN,Hyg}$ is the component of ε_{MEAN} that is caused by the hygral action (Mean drying shrinkage
1234   shown in Figure 44)
1235 α is a coefficient that accounts for the restriction to slab expansion-contraction due to
1236   slab weight and slab interaction with its base; it can be assumed to be 1 for the
1237   VWSGs configuration used in this experiment
1238   CTE1(t) is time-dependent equivalent CTE of the concrete slab in terms of mean expansion-
1239   contraction
1240   t   is time
1241 T_{MEAN} is the mean slab temperature
1242

69

$$\Delta\varepsilon_{DIFF} \;=\; \Delta\varepsilon_{DIFF,Hyg} + \beta \cdot CTE2(t) \cdot \Delta ELTD \qquad \text{(Eq. 12)}$$

1243 where: $\varepsilon_{DIFF,Hyg}$ is the component of ε_{DIFF} that is caused by the hygral action (Differential drying
1244   shrinkage shown in Figure 45)
1245 β is a coefficient that accounts for the restriction to slab bending due to slab weight, slab
1246   interaction with its base, and transverse joint locking or lack of deployment; it can be
1247   assumed to be 1 for the VWSGs configuration used in this experiment
1248   CTE2(t)   is time-dependent equivalent CTE of the concrete slab in terms of bending
1249   t   is time
1250   ELTD   is the equivalent linear temperature difference in the slab (for a given temperature
1251   profile, the ELTD is the temperature difference between the top and bottom of the slab
1252   for the "equivalent linear temperature profile"; the "equivalent linear temperature
1253   profile" is the temperature profile that is linear versus depth and produces the same
1254   slab curvature produced by the actual vertical temperature profile)

1255 The moisture-related shrinkage estimated in the sections, based on equations 11 and 12, is
1256 presented in Figure *44* (mean strain: average of top and bottom of the slab), Figure *45* (differential
1257 strain: top versus bottom of the slab), and Figure *46* (unrestrained shrinkage prisms). Note that the
1258 estimated moisture-related strain is referred to as "drying shrinkage" rather than "moisture-related
1259 shrinkage" as it is due to external drying and wetting of the concrete rather than internal
1260 desiccation. Internal desiccation and the consequent autogenous shrinkage are minimal in this
1261 experiment due to the relatively high water to cementitious materials ratio of the mixtures.
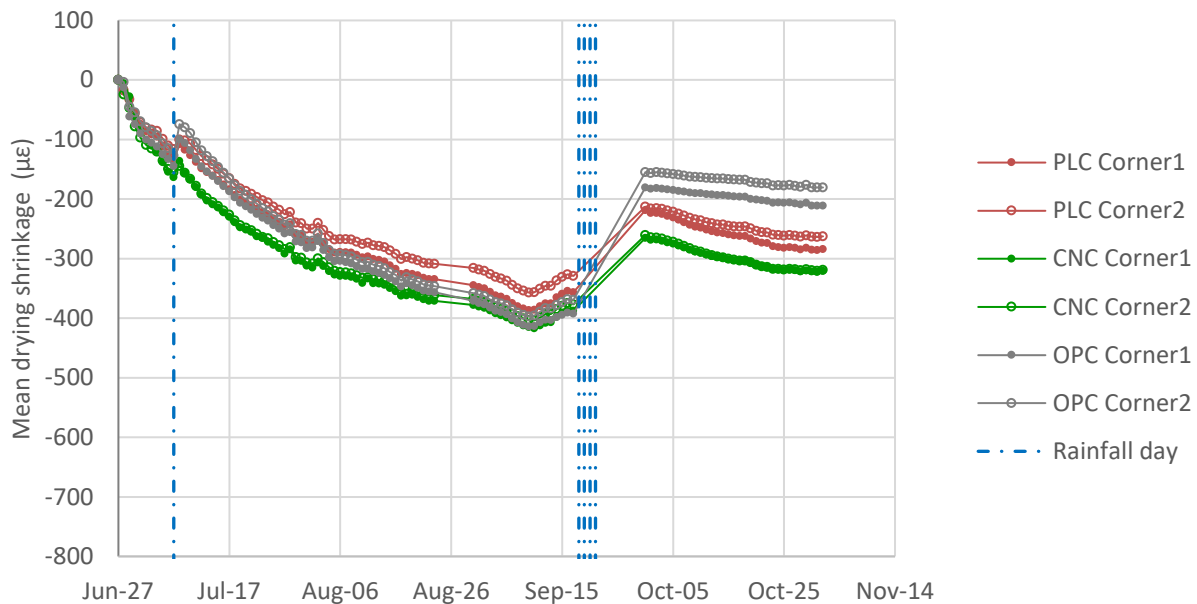
1262

1263 Figure 44. Mean drying shrinkage estimated in the slabs (Corner1 and Corner2 are each of the
1264 two instrumented corners in each section)

1265
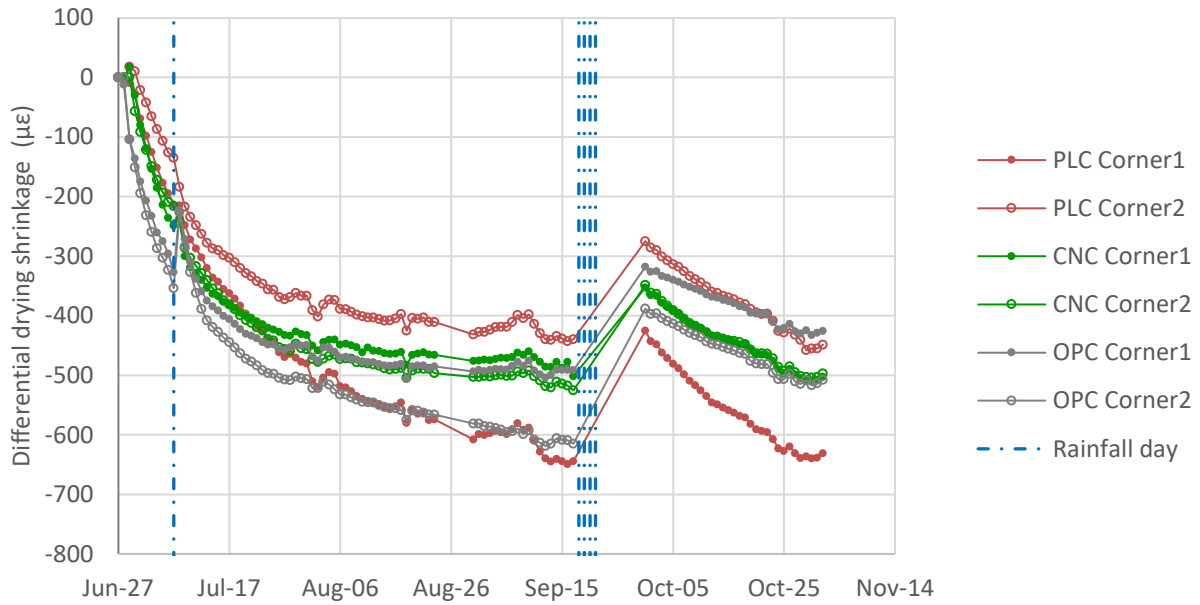
1266

1267   Figure 45. Differential drying shrinkage estimated in the slabs (Corner1 and Corner2 are each of
1268   the two instrumented corners in each section)

1269
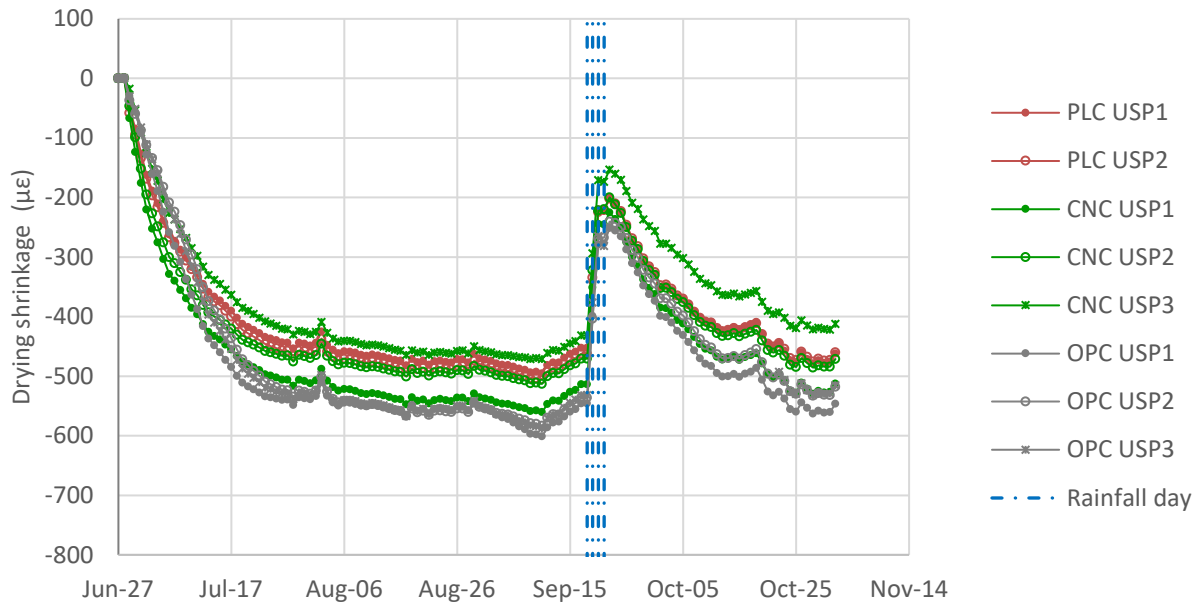
1270

1271   Figure 46. Drying shrinkage estimated in the unrestrained shrinkage prisms (USP1, USP2, and
1272   USP3 are the three prisms for each of the mixtures; PLC USP3 was regarded an outlier and
1273   discarded)

1274

1275 Based on the estimated drying shrinkage of the sections and the unrestrained shrinkage prisms,
1276 shown in Figure 44, Figure 45, and Figure 46, the CNC and PLC mixtures have similar
1277 performance. Also, these two mixtures present drying shrinkage similar to that of the OPC mixture.

1278 The thermal deformations of the CNC and PLC mixtures are similar to each other. As an example,
1279 the apparent CTE of the slabs in terms of expansion and contraction is shown in Figure *47*. In this
1280 figure, the increase in CTE as the concrete dries and the drop in CTE after rainfall are evident. In
1281 the CNC and PLC sections, because of drying, the apparent CTE of the slabs reached values up to
1282 40% higher than the CTE determined in the laboratory under saturated conditions (following
1283 AASHTO T 336); the CTE increase is somewhat smaller in the OPC section. Similar changes in
1284 CTE have been measured in other field experiments by UCPRC [104].

1285
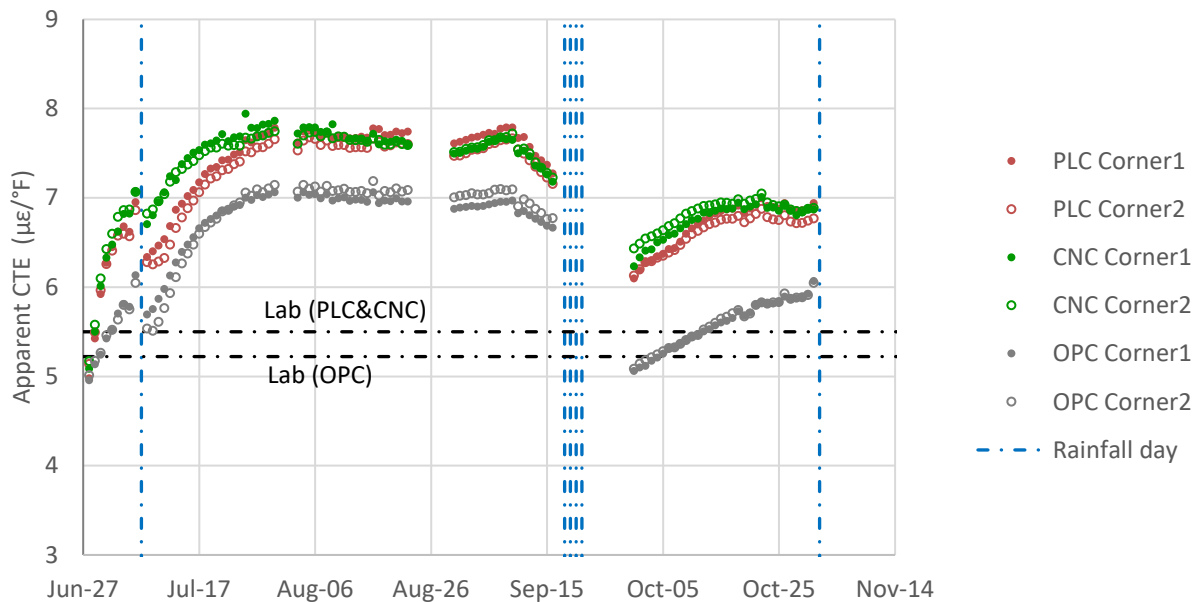
1286

1287   Figure 47. Apparent CTE of the slabs in terms of expansion-contraction (Corner1 and Corner2
1288   are each of the two instrumented corners in each section); for a given day, the apparent CTE can
1289   be defined as the ratio between changes in slab's horizontal strain and slab's mean temperature

1290 The RH measured at 0.8 inch depth in the sections can be also used to evaluate the effect of the
1291 CNC addition on RH. The measured RH data are presented in Figure *48*. While some CNC versus
1292 PLC differences are observed in this figure, the differences are within the sensor-to-sensor
1293 variability. Overall, the concrete internal RH was not affected much by the CNC addition. The RH
1294 measured in these two mixtures is somewhat different from the RH measured in the OPC mixture.
1295 Due to the dry and warm weather conditions of the summer, the RH in the OPC mixture dropped
1296 faster than in the CNC and PLC mixtures. This outcome might be related to a greater porosity of
1297 the OPC mixture compared to the other two mixtures, which needs to be confirmed.

The diurnal variations of the concrete internal RH (variations within a day, mainly related to temperature changes) in the CNC and PLC mixtures are also similar to each other. Interestingly, the variations are somewhat higher for these two mixtures than for the OPC mixture (Figure 48 and Figure 49). This outcome is believed to be the reason why the apparent CTE of the CNC and PLC mixtures increased upon drying somewhat more than the CTE of the OPC mixture (further investigation and explanation of this outcome is outside the scope of this report).
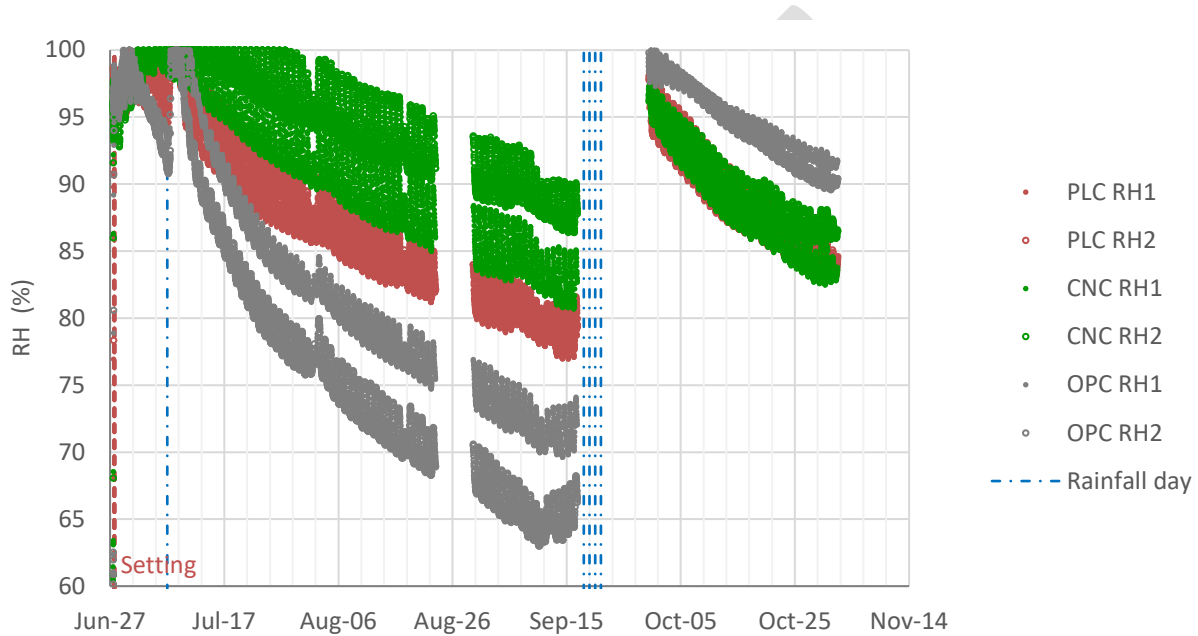
Figure 48. RH measured in the concrete, at 0.8 in. depth (RH1 and RH2 are each of the two RH sensors embedded in each of the sections)
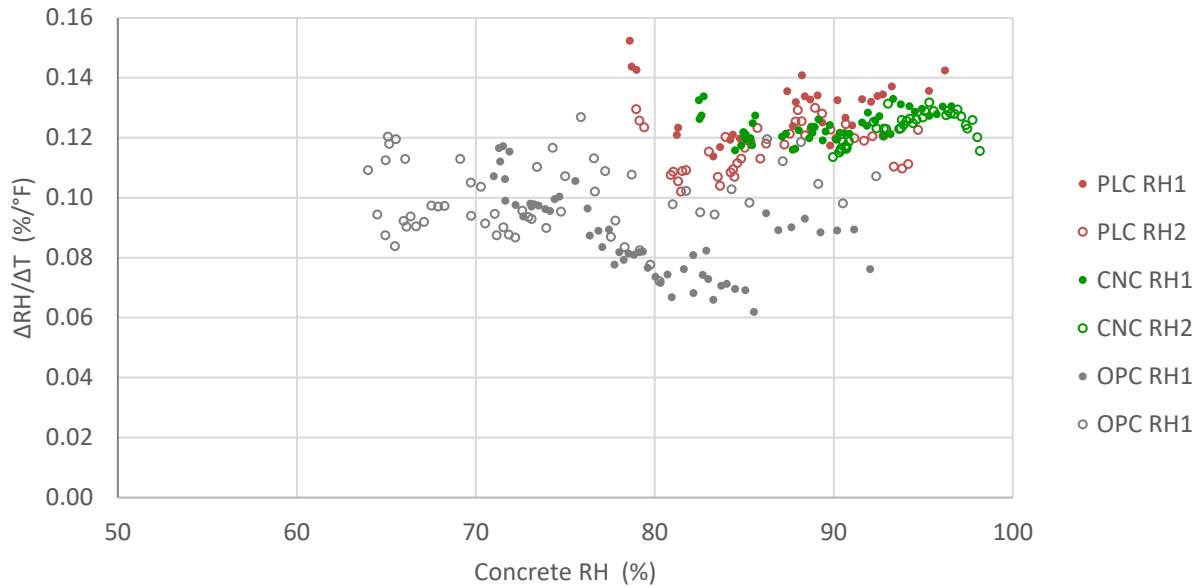
1309

1310   Figure 49. Diurnal variation of RH versus temperature (for a given day, the ratio ΔRH/ΔT
1311   indicates how much concrete internal RH changes versus temperature while the moisture of the
1312   concrete remains essentially constant)

5.6. Discussion of Test Sections Experimental Results

1314   The experiment presented in this chapter of the report was designed to evaluate the effects of the
1315   addition of CNC on the constructability and properties of the portland-limestone cement concrete.
1316   A secondary goal of the experiment was to compare the constructability and properties of the
1317   portland-limestone cement concrete versus concrete made with Type II/V ordinary portland
1318   cement. The control mixture, made with Type II/V cement, represents a typical concrete paving
1319   mixture used in the Caltrans road network.

1320   The experiment includes the construction and monitoring of a set of slabs and the testing of the
1321   mixtures sampled during the construction. Based on the collected experimental data, a number of
1322   conclusions can be drawn regarding mixtures constructability, including fresh concrete properties,
1323   hardened concrete mechanical properties, and concrete hygrothermal deformations (i.e., response
1324   under ambient environmental actions).

5.6.1. Effects of the CNC addition

1326   The effect of the CNC addition can be established by comparing the initial properties,
1327   constructability, and several months of hydrothermal performance under the hot, dry
1328   environmental conditions of the test section location of the CNC and PLC mixtures. The only
1329   difference between the CNC and PLC mixtures is that the former includes 0.1% cellulose
1330   nanocrystals (CNC solids by weight of total cementitious materials).

1331 Based on the collected experimental data, no important differences were found between the CNC
1332 and PLC mixtures:

1333 • Fresh concrete properties (slump, air content, and unit weight) were similar in the two
1334   mixtures.

1335 • The setting time was similar for the two mixtures, and the same applies to the concrete
1336   temperature recorded during the setting time experiment, which indicates similar early-age
1337   heat of hydration release.

1338 • Based on construction workers and Industry expert's observations, there were no
1339   consistency or workability differences between the two mixtures.

1340 • Mechanical properties of the two mixtures, based on laboratory testing of the hardened
1341   concrete, were similar for all properties (strength, modulus of elasticity, electrical
1342   resistivity, CTE, and shrinkage), with differences being either approximately 10% or less
1343   (flexural and compressive strength) or not statistically significant at the 5% significance
1344   level (modulus of elasticity, electrical resistivity, CTE, and drying shrinkage).

1345 • The hygrothermal responses of the slabs made with each of the two mixtures were very
1346   similar. The two groups of slabs presented similar drying shrinkage during the 4-month
1347   evaluation period and similar thermal deformations.

1348 Based on these results, it can be concluded that the CNC addition did not produce any significant
1349 effect on the fresh concrete properties, including constructability, and neither on the properties of
1350 the hardened-concrete.

1351 **5.6.2. Comparison of OPC and PLC**

1352 The effect of the substitution of the Type II/V ordinary portland cement by Type IL portland-
1353 limestone cement can be established by comparing the properties and performance of the PLC and
1354 OPC mixtures. The only difference between the PLC and OPC mixtures is that the former includes
1355 substituting Type IL instead of Type II/V cement. The cement content of both mixtures was the
1356 same.

1357 Based on the collected experimental data, some differences were found between the PLC and OPC
1358 mixtures:

1359 • The slump of the OPC mixture was slightly higher than the slump of the PLC mixture (7.75
1360   versus 6.50 in.), with similar water content. This outcome suggests a higher water demand

1361   of the Type IL cement versus the Type II/V, for the same consistency. The other fresh
1362   concrete properties (air content and unit weight) were similar for the two mixtures.

1363   • The PLC mixture set faster than the OPC mixture. Initial and final setting times of the OPC
1364   mixture, based on penetrating resistance, were 4:05 and 5:25 hours, respectively. The
1365   setting times of the PLC mixture were approximately 15% shorter (3:25 and 4:30 hours for
1366   the initial and final set, respectively). The temperature recorded during the setting time
1367   experiment was slightly higher, up to 2°F (1°C) higher, in the PLC than in the OPC mixture.

1368   • The construction workers and industry experts present at the construction site indicated a
1369   "creamy" consistency of the PLC mixture compared to the OPC mixture, which would
1370   improve the constructability and reduce the segregation of the PLC mixture compared to
1371   the OPC.

1372   • The PLC mixture presented around 10-15% higher strength than the OPC mixture
1373   regardless of the testing age (between 10 days and 4 months). The PLC mixture also
1374   presented higher electrical resistivity than the OPC mixture (around 50% higher after 10
1375   days and around 15% higher after 4 months). On the contrary, the CTE of the PLC mixture
1376   was 0.7 µε/°C higher than the CTE of the OPC mixture.

1377   • The PLC mixture presented 20% higher laboratory drying shrinkage (73°F (23°C), 50%
1378   air RH) than the OPC mixture in the short term (6 days drying) but 10% lower drying
1379   shrinkage after 4 months of drying.

1380   • The hygrothermal response of the slabs made with each of the two mixtures were similar
1381   to each other. The two groups of slabs presented similar drying shrinkage during the 4-
1382   month evaluation period and similar thermal deformations.

1383 Overall, the results indicate that PLC can be used interchangeably with OPC; however, the effect
1384 of differences in fineness of PLC and OPC should be noted. The mixtures with Type IL had better
1385 performance in terms of workability, mechanical, and durability properties than the mixture with
1386 Type II/V, mainly due to higher surface area of Type IL cement and synergistic behavior between
1387 the limestone and alumina. The mixtures with Type IL were observed to have higher water demand
1388 and somewhat higher CTE (0.7 µε/°C) when compared to the mixture with Type II/V due to higher
1389 fineness of Type IL cement.

1390

6. CHAPTER 5: Conclusions

A comprehensive plan was undertaken to evaluate CNCs as a value-based additive for low-carbon footprint concrete. This project was aimed at evaluating the performance of mixtures with limestone and CNC to develop mixtures with a lower embodied carbon footprint. In addition, the project included the implementation of the use of CNC in a set of pilot slabs built on the research site of the University of California Pavement Research Center (UCPRC) in Davis, California.

OPC-LS-CNC mixtures were evaluated for various limestone additions ranging from 0 – 30% by weight and various CNC dosages ranging from 0 – 1% of CNC solids per volume of cementitious materials. The heat of hydration using isothermal calorimetry, B3B flexural strength, CH content, non-evaporable water content, porosity, pore connectivity, and bulk resistivity of the mixtures were determined. GHG emissions of the mixtures were calculated using the life cycle inventory (LCI) calculation tool.

The addition of CNCs to the OPC-LS mixtures resulted in slight retardation by approximately 2-3 hours, depending on the CNC dosage. When CNCs are added, there was an increase in heat release measured at seven days by about 2-3% for OPC-LS mixtures due to increased clinker hydration. The increase in the degree of hydration at early ages was due to the combined effect of LS and CNCs. When the degree of hydration at later ages (28 days) was determined by measuring non-evaporable water content, it was found that mixtures with CNCs at lower dosages up to 0.5% had a higher degree of hydration, which was mainly attributed to CNCs.

CNCs addition to OPC-LS mixtures did not have a significant impact on the porosity of the paste samples. B3B flexural strength of the OPC-LS-CNC mixtures measured at 28 days was within $\pm$15% of the flexural strength of the OPC-LS mixtures. Also, CNCs did not have a significant impact on the drying shrinkage strain of mortar samples. The drying shrinkage strain of the mortar mixtures with CNC was statistically similar or slightly higher (~5%) than mixtures without CNCs after 90 days of exposure to a drying environment.

The addition of CNCs to OPC-LS mixtures had an impact on pore connectivity (β). Lower dosages of CNC addition resulted in a decrease in pore connectivity by up to 29% and improved bulk resistivity by up to 38%. The addition of 20% LS and 0.2% CNC resulted in similar mechanical and transport properties to the conventional mixture; this resulted in the development of an OPC-LS-CNC mixture with 19.4% lower GHG emissions than 100% OPC mixture without compromising on the strength and transport properties.

The performance of OPC-SCM and PLC-SCM mixtures with CNC were evaluated. The 7-day heat of hydration, 28- and 56-day B3B flexural strength, 28- and 56-day porosity, 28- and 56-day pore connectivity, and 28- and 56-day bulk resistivity were determined. The addition of CNC to SCM mixtures resulted in slight retardation due to the CNC covering the clinker, primarily aluminate phase. The 7-day heat release of the SCM mixtures with CNCs were within $\pm$5% of the heat release

1427   of the mixtures without CNC. Overall porosity and B3B flexural strength did not vary significantly
1428   with the CNC dosage. Unlike what was observed for the plain and limestone mixtures, the CNC
1429   addition at low dosages resulted in an increase in pore connectivity and a decrease in bulk
1430   resistivity for the majority of the SCM mixtures. Additional research is needed to understand the
1431   role of the CNCs on the performance when SCMs are used. Specifically, research is needed to
1432   understand what surfaces the CNC are absorbed on. Work is underway to evaluate the long-term
1433   transport properties.

1434   The demonstration of the use of CNCs and PLCs was successfully done in field trials in California
1435   at the UC Davis Pavement Research Center. With the addition of CNCs, no significant difference
1436   in fresh concrete properties, including constructability, was observed. In addition, the compression
1437   and flexural strength of the mixtures with and without CNC were similar. CNCs addition had no
1438   statistically significant effect on the measured modulus of elasticity, electrical resistivity, and
1439   drying shrinkage. The hygrothermal responses of the slabs with and without CNC were very
1440   similar as well. The results indicated that PLC could be used alternative to OPC.

1441   Overall, in this project, comprehensive testing was done to evaluate CNCs as a value-based
1442   additive to mixtures with limestone to lower GHG emissions. Through this project, it was
1443   demonstrated that designing lower embodied carbon footprint mixtures with limestone and CNCs
1444   is possible without compromising on the mechanical and transport properties of concrete.

7. References

1.   Moon, R.J., et al., *Cellulose nanomaterials review: structure, properties and nanocomposites.* Chemical Society Reviews, 2011. **40**(7): p. 3941-3994.
2.   Moon, R.J., G.T. Schueneman, and J. Simonsen, *Overview of cellulose nanomaterials, their capabilities and applications.* Jom, 2016. **68**(9): p. 2383-2394.
3.   Fu, T., et al., *Cellulose nanomaterials as additives for cementitious materials*, in *Cellulose-Reinforced Nanofibre Composites*. 2017, Elsevier. p. 455-482.
4.   Cuenca, E., et al., *Concept of ultra high durability concrete for improved durability in chemical environments: preliminary results.* 2019.
5.   Aziz, M.A., M. Zubair, and M. Saleem, *Development and testing of cellulose nanocrystal-based concrete.* Case Studies in Construction Materials, 2021. **15**: p. e00761.
6.   Cao, Y., *Nano-modification for high performance cement composites with cellulose nanocrystals and carbon nanotubes*. 2014: Purdue University.
7.   Peters, S.J., et al., *Nanocellulose and microcellulose fibers for concrete.* Transportation Research Record, 2010. **2142**(1): p. 25-28.
8.   Sun, X., et al., *Cellulose nanofibers as a modifier for rheology, curing and mechanical performance of oil well cement.* Scientific reports, 2016. **6**(1): p. 1-9.
9.   da Costa Correia, V., et al., *Nanofibrillated cellulose and cellulosic pulp for reinforcement of the extruded cement based materials.* Construction and Building Materials, 2018. **160**: p. 376-384.
10.   Haddad Kolour, H., et al., *An investigation on the effects of cellulose nanofibrils on the performance of cement paste and concrete.* Advances in Civil Engineering Materials, 2018. **7**(1): p. 15.
11.   Lee, H.-J. and W. Kim, *Long-term durability evaluation of fiber-reinforced ECC using wood-based cellulose nanocrystals.* Construction and Building Materials, 2020. **238**: p. 117754.
12.   Montes, F., et al., *Rheological impact of using cellulose nanocrystals (CNC) in cement pastes.* Construction and Building Materials, 2020. **235**: p. 117497.
13.   Santos, R.F., et al., *Nanofibrillated cellulose and its applications in cement-based composites: A review.* Construction and Building Materials, 2021. **288**: p. 123122.
14.   Cuenca, E., A. Mezzena, and L. Ferrara, *Synergy between crystalline admixtures and nano-constituents in enhancing autogenous healing capacity of cementitious composites under cracking and healing cycles in aggressive waters.* Construction and Building Materials, 2021. **266**: p. 121447.
15.   Kamasamudram, K.S., W. Ashraf, and E.N. Landis, *Cellulose nanofibrils with and without nanosilica for the performance enhancement of Portland cement systems.* Construction and Building Materials, 2021. **285**: p. 121547.
16.   Kamasamudram, K.S., et al., *Effects of ligno–and delignified–cellulose nanofibrils on the performance of cement-based materials.* Journal of Materials Research and Technology, 2021. **13**: p. 321-335.
17.   Cao, Y., et al., *The influence of cellulose nanocrystal additions on the performance of cement paste.* Cement and Concrete Composites, 2015. **56**: p. 73-83.
18.   Cao, Y., et al., *Performance-enhanced cementitious materials by cellulose nanocrystal additions.* Production and Applications of Cellulose Nanomaterials, 2013. **2**.

19. Cao, Y., et al., *The relationship between cellulose nanocrystal dispersion and strength.* Construction and Building Materials, 2016. **119**: p. 71-79.

20. Dousti, M.R., Y. Boluk, and V. Bindiganavile, *The effect of cellulose nanocrystal (CNC) particles on the porosity and strength development in oil well cement paste.* Construction and Building Materials, 2019. **205**: p. 456-462.

21. Deze, E., et al., *Nanocellulose enriched mortars: Evaluation of nanocellulose properties affecting microstructure, strength and development of mixing protocols.* Materials Today: Proceedings, 2021.

22. Haque, M.I., et al., *A comparative investigation on the effects of nanocellulose from bacteria and plant-based sources for cementitious composites.* Cement and Concrete Composites, 2022. **125**: p. 104316.

23. Fu, T., et al., *The influence of cellulose nanocrystals on the hydration and flexural strength of Portland cement pastes.* Polymers, 2017. **9**(9): p. 424.

24. Flores, J., M. Kamali, and A. Ghahremaninezhad, *An investigation into the properties and microstructure of cement mixtures modified with cellulose nanocrystal.* Materials, 2017. **10**(5): p. 498.

25. Claramunt, J., et al., *Effect of nanocelluloses on the microstructure and mechanical performance of CAC cementitious matrices.* Cement and Concrete Research, 2019. **119**: p. 64-76.

26. Cao, Y., et al., *The influence of cellulose nanocrystals on the microstructure of cement paste.* Cement and Concrete Composites, 2016. **74**: p. 164-173.

27. Bu, Y., et al., *The influence of accelerated curing on the properties used in the prediction of chloride ingress in concrete using a Nernst–Planck approach.* Construction and Building Materials, 2014. **66**: p. 752-759.

28. Bu, Y., R. Spragg, and W. Weiss, *Comparison of the pore volume in concrete as determined using ASTM C642 and vacuum saturation.* Advances in Civil Engineering Materials, 2014. **3**(1): p. 308-315.

29. Becerril, A.P., *The Influence of Cellulose Nanocrystals on Performance and Transport Properties of Cementitious Materials and Gypsum.* 2020, Purdue University Graduate School.

30. Barnat-Hunek, D., et al., *Effect of eco-friendly cellulose nanocrystals on physical properties of cement mortars.* Polymers, 2019. **11**(12): p. 2088.

31. Washington, T., W.J. Weiss, and J. Youngblood, *Construction of full-scale concrete elements containing cellulose nanocrystals (CNCs) in bridge decks and pavements*, R.t.U.E.f.F.a. Communities, Editor. 2021.

32. Ramanathan, S., et al., *Cellulose Nanocrystals as an Additive for Prestressed Box Girders* in *ASPIRE - The Concrete Bridge Magazine*. 2023 (In Press): www.aspirebridge.org.

33. Lothenbach, B., K. Scrivener, and R. Hooton, *Supplementary cementitious materials.* Cement and concrete research, 2011. **41**(12): p. 1244-1256.

34. Juenger, M.C. and R. Siddique, *Recent advances in understanding the role of supplementary cementitious materials in concrete.* Cement and Concrete Research, 2015. **78**: p. 71-80.

35. Environment, U., et al., *Eco-efficient cements: Potential economically viable solutions for a low-CO2 cement-based materials industry.* Cement and Concrete Research, 2018. **114**: p. 2-26.

1534 36. Hawkins, P., P.D. Tennis, and R.J. Detwiler, *The use of limestone in Portland cement: a*
1535 *state-of-the-art review*. 1996: Portland Cement Association.
1536 37. Thomas, M.D. and R.D. Hooton, *The durability of concrete produced with portland-*
1537 *limestone cement: Canadian studies*. PCA R&D SN3142, Portland Cement Association,
1538 Skokie, IL, 2010: p. 28.
1539 38. Tennis, P., M. Thomas, and W. Weiss, *State-of-the-Art Report on Use of Limestone in*
1540 *Cements at Levels of up to 15%*. PCA R&D SN3148, Portland Cement Association, Skokie,
1541 IL, 2011.
1542 39. Barrett, T.J., *Performance of portland limestone cements: Cements designed to be more*
1543 *sustainable that include up to 15% limestone addition*. 2013, Purdue University.
1544 40. Hooton, R. and M. Thomas, *Sulfate resistance of mortar and concrete produced with*
1545 *portland-limestone cement and supplementary cementing materials*, in *Recommendation*
1546 *for ASTM C595/AASHTO M 240, PCA R&D SN3285a*. 2016, Portland Cement
1547 Association.
1548 41. Bharadwaj, K., et al., *CALTRANS: Impact of the Use of Portland-Limestone Cement on*
1549 *Concrete Performance as Plain or Reinforced Material - Final Report*. 2021.
1550 42. Bharadwaj, K., et al., *Predicting pore volume, compressive strength, pore connectivity, and*
1551 *formation factor in cementitious pastes containing fly ash*. Cement and Concrete
1552 Composites, 2021: p. 104113.
1553 43. Bentz, D.P., et al., *Limestone fillers conserve cement; Part 1: an analysis based on Powers'*
1554 *model*. Concrete international, 2009. **31**(11): p. 41-46.
1555 44. Berodier, E. and K. Scrivener, *Understanding the Filler Effect on the Nucleation and*
1556 *Growth of C-S-H*. Journal of the American Ceramic Society, 2014. **97**(12): p. 3764-3773.
1557 45. Zajac, M., et al., *Influence of limestone and anhydrite on the hydration of Portland*
1558 *cements*. Cement and Concrete Composites, 2014. **46**: p. 99-108.
1559 46. Ramanathan, S., M. Croly, and P. Suraneni, *Comparison of the effects that supplementary*
1560 *cementitious materials replacement levels have on cementitious paste properties*. Cement
1561 and Concrete Composites, 2020. **112**: p. 103678.
1562 47. Association, P.C., *Roadmap to Carbon Neutrality*. 2021.
1563 48. Bharadwaj, K., *Towards the Development of Performance-Based Concrete Mixtures Made*
1564 *with Modern Cementitious Materials Using Thermodynamic Modeling*, in *Civil*
1565 *Engineering*. 2022, Oregon State University: Corvallis, OR. p. 327.
1566 49. Bharadwaj, K., et al., *Predicting Pore Volume, Compressive Strength, Pore Connectivity,*
1567 *and Formation Factor in Cementitious Pastes Containing Fly Ash*. Cement and Concrete
1568 Composites, 2021. **122**: p. 104113.
1569 50. Bharadwaj, K., et al., *Toward the Prediction of Pore Volumes and Freeze-Thaw*
1570 *Performance of Concrete Using Thermodynamic Modelling*. Cement and Concrete
1571 Research, 2019. **124**: p. 105820.
1572 51. Bharadwaj, K., B.O. Isgor, and J.W. Weiss, *Pozzolanic reactivity of SCMs from a*
1573 *thermodynamic perspective*. ACI Materials Journal, 2022. **In Review**.
1574 52. Bharadwaj, K., B.O. Isgor, and J.W. Weiss, *A Simplified Approach to determine the*
1575 *Pozzolanic Reactivity of Commercial Supplementary Cementitious Materials*. Concrete
1576 International, 2022. **44**(1): p. 27-32.
1577 53. Choudhary, A., et al., *Pozzolanic Reactivity Test of Supplementary Cementitious*
1578 *Materials*. ACI Mater J, 2022. **119**(2): p. 255-268.

| 1579 | 54. | Glosser, D., et al., *Investigation of Reactivity of Fly Ash and Its Effect on Mixture Properties*. ACI Materials Journal, 2019. **116**(4): p. 193-200. |

1579   54.   Glosser, D., et al., *Investigation of Reactivity of Fly Ash and Its Effect on Mixture*
1580   *Properties*. ACI Materials Journal, 2019. **116**(4): p. 193-200.

1581   55.   Glosser, D., O.B. Isgor, and W.J. Weiss, *Non-Equilibrium Thermodynamic Modeling*
1582   *Framework for Ordinary Portland Cement/Supplementary Cementitious Material Systems*.
1583   ACI Materials Journal, 2020. **117**(6): p. 111-123.

1584   56.   Lothenbach, B. and M. Zajac, *Application of thermodynamic modelling to hydrated*
1585   *cements*. Cement and Concrete Research, 2019. **123**.

1586   57.   Kulik, D.A., et al., *GEM-Selektor geochemical modeling package: revised algorithm and*
1587   *GEMS3K numerical kernel for coupled simulation codes*. Computational Geosciences,
1588   2013. **17**(1): p. 1-24.

1589   58.   Wagner, T., et al., *Gem-Selektor geochemical modeling package: TSolmod library and*
1590   *data interface for multicomponent phase models*. Canadian Mineralogist, 2012. **50**(5): p.
1591   1173-1195.

1592   59.   Lothenbach, B., et al., *Cemdata 18: A chemical thermodynamic database for hydrated*
1593   *Portland cements and alkali-activated materials*. Cement and Concrete Research, 2019.
1594   **115**: p. 472-506.

1595   60.   Lothenbach, B., et al., *Thermodynamic modelling of the effect of temperature on the*
1596   *hydration and porosity of Portland cement*. Cement and Concrete Research, 2008. **38**(1):
1597   p. 1-18.

1598   61.   Lothenbach, B. and F. Winnefeld, *Thermodynamic modelling of the hydration of Portland*
1599   *cement*. Cement and Concrete Research, 2006. **36**(2): p. 209-226.

1600   62.   Lothenbach, B., et al., *Effect of temperature on the pore solution, microstructure and*
1601   *hydration products of Portland cement pastes*. Cement and Concrete Research, 2007.
1602   **37**(4): p. 483-491.

1603   63.   Myers, R.J., S.A. Bernal, and J.L. Provis, *A thermodynamic model for C-(N-) ASH gel:*
1604   *CNASH_ss. Derivation and validation*. Cement and Concrete Research, 2014. **66**: p. 27-
1605   47.

1606   64.   Myers, R.J., et al., *Thermodynamic modelling of alkali-activated slag cements*. Applied
1607   Geochemistry, 2015. **61**: p. 233-247.

1608   65.   Lothenbach, B., K. Scrivener, and R.D. Hooton, *Supplementary cementitious materials*.
1609   Cement and Concrete Research, 2011. **41**(12): p. 1244-1256.

1610   66.   Zajac, M., et al., *Impact of microstructure on the performance of composite cements: Why*
1611   *higher total porosity can result in higher strength*. Cement and Concrete Composites, 2018.
1612   **90**: p. 178-192.

1613   67.   Azad, V.J., et al., *Interpreting the pore structure of hydrating cement phases through a*
1614   *synergistic use of the Powers-Brownyard model, hydration kinetics, and thermodynamic*
1615   *calculations*. Advances in Civil Engineering Materials, 2017. **6**(1): p. 1-16.

1616   68.   Glosser, D., et al., *An extension of the Powers-Brownyard model to pastes containing SCM*.
1617   ACI Materials Journal, 2019. **116**(5): p. 205-216.

1618   69.   Bharadwaj, K., et al., *A New Mixture Proportioning Method for Performance-Based*
1619   *Concrete*. ACI Materials Journal, 2022. **119**(2): p. 207-220.

1620   70.   Bharadwaj, K., et al., *CALTRANS: Impact of the Use of Portland-Limestone Cement on*
1621   *Concrete Performance as Plain or Reinforced Material - Final Report*. 2021, Oregon State
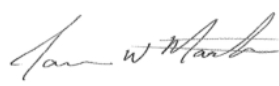1622   University: Corvallis. p. 320.

71. Isgor, B., et al., *Development of a performance-based mixture proportioning procedure for concrete incorporating off-spec fly ash*. 2020, Energy Power Research Institute (EPRI): Palo Alto, CA. p. 78.

72. Ramanathan, S., et al., *Reducing GHG Emission Using Cellulose Nanocrystals, OPC, and Limestone.* ACI Materials Journal.

73. Han, D. and R.D. Ferron, *Effect of mixing method on microstructure and rheology of cement paste.* Construction and Building Materials, 2015. **93**: p. 278-288.

74. Oguz, O., et al., *Poly (lactide)/cellulose nanocrystal nanocomposites by high-shear mixing.* Polymer Engineering & Science, 2021. **61**(4): p. 1028-1040.

75. Barger, G.S., *A Fusion Method for the X-Ray Fluorescence Analysis of Portland Cements, Clinker and Raw Materials Utilizing Cerium (IV) Oxide in Lithium Borate Fluxes.* Advances in X-ray Analysis, 1985. **29**: p. 581-585.

76. Tsui Chang, M., *The Evaluation of Cementitious Pore Solution Composition and Electrical Resistivity Using X-ray Fluorescence (XRF).* 2017, Oregon State University.

77. Castro, J., I.D.l. Varga, and J. Weiss, *Using isothermal calorimetry to assess the water absorbed by fine LWA during mixing.* Journal of materials in civil engineering, 2012. **24**(8): p. 996-1005.

78. Zaw, M., *Automated Chemical Acidification Testing of Cementitious Materials*. 2021, Oregon State University.

79. Fu, T. and W.J. Weiss, *The Ball-on-Three-Ball (B3B) Test–Application to Cement Paste and Mortar.* Advances in Civil Engineering Materials, 2020. **9**(1): p. 128-142.

80. Börger, A., P. Supancic, and R. Danzer, *The ball on three balls test for strength testing of brittle discs: stress distribution in the disc.* Journal of the European Ceramic Society, 2002. **22**(9-10): p. 1425-1436.

81. Kim, T. and J. Olek, *Effects of sample preparation and interpretation of thermogravimetric curves on calcium hydroxide in hydrated pastes and mortars.* Transportation research record, 2012. **2290**(1): p. 10-18.

82. AASHTO, *AASHTO TP 119—Standard Method of Test for Electrical Resistivity of a Concrete Cylinder Tested in a Uniaxial Resistance Test*, in *AASHTO, Washington, DC*. 2021.

83. Spragg, R., et al., *Factors that influence electrical resistivity measurements in cementitious systems.* Transportation research record, 2013. **2342**(1): p. 90-98.

84. Coyle, A.T., et al., *Activation energy of conduction for use in temperature corrections on electrical measurements of concrete.* Advances in Civil Engineering Materials, 2019. **8**(1): p. 158-170.

85. AASHTO, *AASHTO TP 135—Standard Method of Test for Determining the Total Pore Volume in Hardened Concrete Using Vacuum Saturation*, in *AASHTO, Washington, DC*. 2020.

86. Barrett, E.P., L.G. Joyner, and P.P. Halenda, *The Determination of Pore Volume and Area Distributions in Porous Substances. I. Computations from Nitrogen Isotherms.* Journal of the American Chemical Society, 1951. **73**: p. 373-380.

87. Rajabipour, F. and W.J. Weiss, *Electrical conductivity of drying cement paste.* Materials and Structures, 2007. **40**: p. 1143-1160.

88. Leao, T.P. and M. Tuller, *Relating soil specific surface area, water film thickness, and water vapor adsorption.* Water Resources Research, 2014. **50**(7873-7885).

89. Parrot, L.J. and D.C. Killoh, *Prediction of cement hydration.* British Ceramic Proceedings, 1984. **35**: p. 41-53.

90. Glosser, D., et al., *Estimating reaction kinetics of cementitious pastes containing fly ash.* Cement and Concrete Composites, 2020. **112**: p. 103655.

91. Palacios, M., et al., *Effect of PCs superplasticizers on the rheological properties and hydration process of slag-blended cement pastes.* Journal of Materials Science, 2009. **44**(10): p. 2714-2723.

92. Lerch, W., *The influence of gypsum on the hydration and properties of Portland cement pastes*. 2008.

93. Niemuth, M.D., *Effect of fly ash on the optimum sulfate of Portland Cement*. 2012: Purdue University.

94. Ramanathan, S., *Reactivity of Supplementary Cementitious Materials in Model Systems and Cementitious Pastes*. 2021, University of Miami.

95. Valadez-Carranza, Y., et al., *Report - Working Group for Advancement of Cellulose Nano-Materials Use in Cement-Based Materials*. 2022, US Endowment.

96. Haddad Kolour, H., W. Ashraf, and E.N. Landis, *Hydration and early age properties of cement pastes modified with cellulose nanofibrils.* Transportation Research Record, 2021. **2675**(9): p. 38-46.

97. Matschei, T., B. Lothenbach, and F.P. Glasser, *The role of calcium carbonate in cement hydration.* Cement and concrete research, 2007. **37**(4): p. 551-558.

98. Bharadwaj, K., O. Isgor, and W. Weiss, *Supplementary Cementitious Materials in Portland Limestone Cements.* ACI Materials Journal, 2022. **119**(2).

99. Matschei, T., et al. *Relationships of Cement Paste Mineralogy to Porosity and Mechanical Properties*. in *International Conference on Modelling of Heterogeneous Materials with Applications in Construction and Biomedical Engineering*. 2007.

100. Hisseine, O.A., et al., *Nanocellulose for improved concrete performance: A macro-to-micro investigation for disclosing the effects of cellulose filaments on strength of cement systems.* Construction and Building Materials, 2019. **206**: p. 84-96.

101. Miller, S.A., et al., *Carbon dioxide reduction potential in the global cement industry by 2050.* Cement and Concrete Research, 2018. **114**: p. 115-124.

102. Bradford, K. and F. Lolli, *CONOMIC AND ENVIRONMENTAL IMPACT OF NANOCELLULOSE ADDITIVES IN PORTLAND CEMENT*, in *18th International Conference on Non-conventional Materials and Technologies (NOCMAT 2022)*. 2022.

103. Nassiri, S., et al., *Comparison of unique effects of two contrasting types of cellulose nanomaterials on setting time, rheology, and compressive strength of cement paste.* Cement and Concrete Composites, 2021. **123**: p. 104201.

104. Mateos, A., et al., *Structural Response of Concrete Pavement Slabs under Hygrothermal Actions.* Construction and Building Materials, 2020. **243**.

1707 **8. Appendix**

1708 In this section, the mill certificates of the OPC, PLC, and Slag used for the field trials are attached.

	CEMEX	4200 E Jurupa St. Suite 312 Ontario, CA 91761 Telephone (909) 974-5469 FAX (909) 974-5525			CEMENT MILL TEST REPORT	

Cement Identified as: Date: 6/17/2022

Plant: Cemex Construction Materials Pacific LLC

Location: Victorville, CA   Prod dates: Beginning: 6/3/2022

Ending: 6/9/2022   Ref . No   44729

STANDARD CHEMICAL REQUIREMENTS (ASTM C114)	ASTM C150 / AASHTO M 85 SPECIFICATIONS	TYPE I	TYPE II	TYPE V	TEST RESULTS
Silicon Dioxide (SiO2), %	Minimum	----	----	----	20.3
Aluminum Oxide (Al2O3), %	Maximum	----	6.0	----	4.1
Ferric Oxide (Fe2O3), %	Maximum	----	6.0	----	3.9
Calcium Oxide (CaO), %		----	----	----	62.4
Magnesium Oxide (MgO), %	Maximum	6.0	6.0	6.0	4.9
Sulfur Trioxide (SO3), % **	Maximum	3.0	3.0	2.3	3.1
Loss on Ignition (LOI), %	Maximum	3.5	3.5	3.5	2.6
Insoluble Residue, %	Maximum	1.5	1.5	1.5	1.07
Sodium Oxide (Na2O), %		----	----	----	0.19
Potassium Oxide (K2O), %		----	----	----	0.41
Equivalent Alkalies (Na2O+.658K2O), %	Maximum	0.60	0.60	0.60	0.46
CO2(%)		----	----	----	1.7
Limestone (%)	Maximum	5.0	5.0	5.0	3.4
CaCO3 in limestone	Minimum	70.0	70.0	70.0	74.7
Inorganic addition	Maximum	5.0	5.0	5.0	2.1
Tricalcium Silicate (C3S), %	Maximum	----	----	----	54
Dicalcium Silicate (C2S), %		----	----	----	16
Tricalcium Aluminate (C3A), %	Maximum	----	8	5	4
Tetracalcium Aluminoferrite (C4AF), %		----	----	----	11
Heat Index (C3S + 4.75C3A)	Maximum		100		73
(C4AF + 2C3A) or (C4AF + C2F), %	Maximum	----	----	25	19
PHYSICAL REQUIREMENTS					
Heat of Hydration (ASTM C1702)	Informational data only				
7 days, kj/kg (cal/g)	Most recent value				301(72.4)
(ASTM C204) Blaine Fineness, cm²/gm	Minimum	2600	2600	2600	4184
(ASTM C430) -325 Mesh, %		----	----	----	98
(ASTM C191) Time of Setting (Vicat)					
Initial Set, minutes	Minimum / Maximum	45 / 375	45 / 375	45 / 375	108
Final Set, minutes		---	---	---	266
(ASTM C451) False Set, %	Minimum	50	50	50	89
(ASTM C185) Air Content, %	Maximum	12	12	12	6.1
(ASTM C151) Autoclave Expansion, %	Maximum	0.80	0.80	0.80	0.01
(ASTM C87) Normal Consistency, %		----	----	----	26
(ASTM C1038) Expansion in Water %	Maximum	0.020	0.020	0.020	0.008
(ASTM C109) Compressive Strength, psi (MPa)					
1 Day		----	----	----	2140(14.8)
3 Day	Minimum	1740(12.0)	1450(10.0)	1160(8.0)	3670(25.3)
7 Day		2760(19.0)	2470(17.0)	2180(15.0)	4600(31.7)
28 Day (strength for Ref. No. 44701)	Minimum			3050(21.0)	5850(40.3)

** *The performance of CEMEX Type II, Type V has proven to be improved with sulfur trioxide levels in excess of the 2.3% limit for Type V.*
    Note D in ASTM C150 allows for additional sulfate, provided expansion as measured by ASTM C1038 does not exceed 0.020%.

CEMEX hereby certifies that this cement meets or exceeds the chemical
and physical Specifications of:

ASTM C150-21 Type I, Type II, and Type V Low Alkali portland cements
ASTM C1157-20 Type GU Hydraulic Cement
AASHTO M 85-20 Type I, Type II, and Type V Low Alkali portland cements
CalTrans, Section 90-2.01 T II Modified and Type V (2006)
CalTrans, Section 90-1.02B (2) (2010-2020)
Arizona DOT Standard Specification 1006-2.01 Hydraulic Cement
Nevada DOT Specification 701.03.01
C465 qualification data will be made available upon request

By: _____
Quality Control Manager
CEMEX - Victorville Cement Plant
16888 North "E" St., 'Victorville, CA 92394

1709

85

CEMEX

4200 E Jurupa St
Suit 312
Ontario, Ca 91764
Telephone (909) 974-5469
Fax (909) 974-5525

CEMENT MILL TEST REPORT

Cement Identified as:

Plant: **CEMEX Construction Materials Pacific LLC**   **TYPE IL (15)**   Date: **10/30/2021**
Location: Victorville, Ca
Production Dates:

Beginning: **October 20, 2021**
Ending: **October 25, 2021**

STANDARD CHEMICAL REQUIREMENTS (ASTM C114)	TEST RESULTS		ASTM C595 Spec.	Type IL
Sulfur Trioxide (SO3), % **	3.6		Maximum	3.0
Loss on Ignition (LOI), %	5.6		Maximum	10
CO_2, %	5.0			
Limestone, %	14		Min. - Max.	5 - 15
$CaCO_3$ in Limestone, %	85		Minimum	70
PHYSICAL REQUIREMENTS				
(ASTM C 204) Blaine Fineness, cm^2/gm	5470			----
(ASTM C 188) Density	3.06			----
(ASTM C 430) -325 Mesh, %	97.5			----
(ASTM C 191) Time of Setting (Vicat)				
Initial Set, minutes	135		Min. - Max.	45 - 420
Final Set, minutes	315			----
(ASTM C 185) Air Content, %	8		Maximum	12
(ASTM C 151) Autoclave Expansion, %	0.01		Contraction	0.2
			Expansion	0.8

(ASTM C 109) Compressive Strength, psi (MPa)	psi	MPa		
1 Day	2650	18.3		
3 Day	3970	27.4	Minimum	1890 (13.0)
7 Day	4790	33.0	Minimum	2900 (20.0)
28 Day	5820	40.1	Minimum	3620 (25.0)

CEMEX hereby certifies that this cement meets or
exceeds the chemical and physical Specifications of:

ASTM C595 - 19 for Type IL Cement

[signature]

James Martin
Quality Control Manager
CEMEX - Victorville Cement Plant

1710

Slag Cement Test Report

CTC ID: 607	
Slag Source: Rizhao	Cemex Technical Center
Vessel: Monthly sample- Redwood City	6725 78th St, Riverview, FL, 33578
Sample Date: April 2022	Phone: (813) 671-2266
Report Date: 5/27/2022	Fax: (813) 677-7597
Sample Log CTC ID: 2022-227	

Specifications: ASTM C 989 Grades 100 & 120

Chemical and Physical Requirements	Test Result	Specifications	
Sulfur Trioxide (SO_3) (ASTM C114), %	2.46	---	
Sulfide Sulfur (S) (ASTM C114), %	0.32	2.5 Max	
Chloride (Cl) (ASTM C114), %	0.013	---	
Aluminum Oxide (Al_2O_3) (ASTM C114), %	17.5	---	
Blaine Fineness (ASTM C204), m^2/kg	478	---	
Fineness Retained - 45 Micron (ASTM C430), %	0.3	20 Max	
Specific Gravity (ASTM C188)	2.91	---	
Air Content (ASTM C185), %	3	12 Max	
Mortar Expansion (ASTM C1038) 14-day ,%	0.018	0.020 Max	
Total Equivalent Alkalies ($Na_2O+0.685 K_2O$), (ASTM C114), %	0.45	---	

Slag Activity Index (ASTM C109)		Grade 100	Grade 120
7 Day - Individual, %	119	---	---
7 Day - Average of last 5, %	108	---	---
28 Day - Individual, %	133	90 Min	110 Min
28 Day - Average of last 5, %	123	95 Min	115 Min

Compressive Strength (ASTM C109)		Specifications	
7 Day - Reference Cement, psi	4126	---	
28 Day - Reference Cement, psi	5397	5,000 Min	
7 Day Slag and Cement Reference, psi	4906	---	
28 Day Slag and Cement Reference, psi	7164	---	

Reference Cement (ASTM C114 & C150)		Specifications	
Cement Type	Type I/II	Type I-Type II	
Total Equivalent Alkalies ($Na_2O+0.685 K_2O$), %	0.79	0.6 Min/ 0.9 Max	

This GGBFS meets requirements of ASTM C 989-18a and AASHTO M 302-19

☐ Grade 100 ASTM C989
☐ Grade 100 AASHTO M302
☑ Grade 120 ASTM C989
☑ Grade 120 AASHTO M302

Chemical testing completed by: YR
Physical testing completed by: YR

Jose M. Dominguez
Director at Cemex Technical Center USA

1711